NTNU – Trondheim
Norwegian University of
Science and Technology

Implementation of a Critical State Soft Soil Creep Model with Shear Stiffness

Mohammad Ali Haji Ashrafi

Geotechnics and Geohazards
Submission date: June 2014
Supervisor: Gustav Grimstad, BAT

Norwegian University of Science and Technology
Department of Civil and Transport Engineering

NORWEGIAN UNIVERSITY OF SCIENCE AND TECHNOLOGY
DEPARTMENT OF CIVIL AND TRANSPORT ENGINEERING

Report Title:

Implementation of a Critical State Soft Soil Creep Model with Shear Stiffness

Date: June 6, 2014

Number of pages (incl. appendices): 120

Master Thesis	x	Project Work	

Name: **Mohammad Ali Haji Ashrafi**

Professor in charge/supervisor: **Professor Gustav Grimstad**

Other external professional contacts/supervisors: -

Abstract

The existing creep constitutive models do not include directly shear stiffness of the soil that can be easily obtained by standard geotechnical tests. These models do not account for high shear stiffness of the soil at small mobilisation degree. In this respect, they do not distinguish between soil elements that undergo lower mobilisation in the far field and the ones that undergo higher mobilisation close to the embankment. This may result in overprediction of horizontal displacements under the field and the result of the finite element analysis is sensitive to the extension of the model boundary. To address this model deficiency, a new critical state soft soil creep model with shear stiffness (CS-SSCG) is implemented. In the CS-SSCG model, shear stiffness of the soil will be explicitly given by the engineer instead of commonly used Poisson's ratio. Results from the simulation of the MIT-MDPW embankment show that horizontal displacement has been improved significantly using the CS-SSCG model compared to Plaxis Soft Soil Creep (SSC) standard model.

Keywords:

1. creep
2. constitutive soil model
3. shear stiffness
4. numerical analysis
5. MIT embankment

Mohammad Ali Haji Ashrafi

MASTER DEGREE THESIS

Spring 2014
for

Student: Mohammad Ali Haji Ashrafi

Implementation of a Critical State Soft Soil Creep Model with Shear Stiffness

BACKGROUND

In 1967 a test embankment (MIT-MDPW) was constructed in relation to the construction of a highway north of Boston, USA. The embankment was heavily instrumented and documented for more than 2000 days after start of construction. Back calculations of the embankment, with different soil models, are found several places in literature. However, there seems to be difficult to match all the field measurements simultaneously. In his project, Haji Ashrafi examined the embankment with focus on the proper selection of OCR. The vertical displacements improved significantly both at the deeper and shallower levels and at the center and toe of the embankment. However, the simulated horizontal displacement under the embankment remained unsatisfactory, as before. The Plaxis soft soil creep model predicted the horizontal displacements that were considerably higher than the field measurements, particularly at the beginning of creep settlement.

The existing creep constitutive models do not include directly shear stiffness of the soil that can be easily obtained by standard geotechnical tests. These models do not account for high shear stiffness of the soil at small mobilization degree. This may result in over prediction of horizontal displacements under the field and the result of the finite element analysis is dependent on the extension of the boundary. To address this model deficiency, a new creep model with shear stiffness is to be implemented in this thesis.

TASK

This Master thesis primarily deals with model implementation. The task in this thesis is as follows:

- Perform a literature study on creep in soft soil (clay).
- Implement a user defined creep model in Plaxis. The model performance should be similar to Plaxis soft soil creep model under the odometer condition.
- Implement a new soft soil creep model that includes mobilized shear stiffness of the soil. In this model shear stiffness of the soil will be given as input parameter instead of Poisson's ratio.
- Validate the performance of the implemented models in MIT-MDPW embankment with a simplified Boston Blue Clay profile. The vertical settlement, pore pressure and horizontal displacement of the embankment are to be back calculated. Finally, try to investigate if the prediction of the horizontal displacement has been improved with the new implemented model while the vertical displacement and the pore pressure response are predicted well enough.

Part of this master thesis will be a paper for an International Conference.

General about content, work and presentation

The text for the master thesis is meant as a framework for the work of the candidate. Adjustments might be done as the work progresses. Tentative changes must be done in cooperation and agreement with the professor in charge at the Department.

In the evaluation thoroughness in the work will be emphasized, as will be documentation of independence in assessments and conclusions. Furthermore the presentation (report) should be well organized and edited; providing clear, precise and orderly descriptions without being unnecessary voluminous.

The report shall include:
- Standard report front page (from DAIM, http://daim.idi.ntnu.no/)
- Title page with abstract and keywords.(template on: http://www.ntnu.no/bat/skjemabank)
- Preface
- Summary and acknowledgement. The summary shall include the objectives of the work, explain how the work has been conducted, present the main results achieved and give the main conclusions of the work.
- The main text.
- Text of the Thesis (these pages) signed by professor in charge.

The thesis can as an alternative be made as a scientific article for international publication, when this is agreed upon by the Professor in charge. Such a report will include the same points as given above, but where the main text includes both the scientific article and a process report.

Advice and guidelines for writing of the report is given in “Writing Reports” by Øivind Arntsen, and in the departments “Råd og retningslinjer for rapportskriving ved prosjekt og masteroppgave” (In Norwegian) located at http://www.ntnu.no/bat/studier/oppgaver.

Submission procedure

Procedures relating to the submission of the thesis are described in DAIM (http://daim.idi.ntnu.no/). Printing of the thesis is ordered through DAIM directly to Skipnes Printing delivering the printed paper to the department office 2-4 days later. The department will pay for 3 copies, of which the institute retains two copies. Additional copies must be paid for by the candidate / external partner.

On submission of the thesis the candidate shall submit a CD with the paper in digital form in pdf and Word version, the underlying material (such as data collection) in digital form (e.g. Excel). Students must submit the submission form (from DAIM) where both the Ark-Bibl in SBI and Public Services (Building Safety) of SB II has signed the form. The submission form including the appropriate signatures must be signed by the department office before the form is delivered Faculty Office.

Documentation collected during the work, with support from the Department, shall be handed in to the Department together with the report.

According to the current laws and regulations at NTNU, the report is the property of NTNU. The report and associated results can only be used following approval from NTNU (and external cooperation partner if applicable). The Department has the right to make use of the results from the work as if conducted by a Department employee, as long as other arrangements are not agreed upon beforehand.

Tentative agreement on external supervision, work outside NTNU, economic support etc.
Separate description is to be developed, if and when applicable. See http://www.ntnu.no/bat/skjemabank for agreement forms.

Health, environment and safety (HSE) http://www.ntnu.edu/hse
NTNU emphasizes the safety for the individual employee and student. The individual safety shall be in the forefront and no one shall take unnecessary chances in carrying out the work. In particular, if the student is to participate in field work, visits, field courses, excursions etc. during the Master Thesis work, he/she shall make himself/herself familiar with "Fieldwork HSE Guidelines". The document is found on the NTNU HMS-pages at http://www.ntnu.no/hms/retningslinjer/HMSR07E.pdf

The students do not have a full insurance coverage as a student at NTNU. If you as a student want the same insurance coverage as the employees at the university, you must take out individual travel and personal injury insurance.

Startup and submission deadlines
Startup for this thesis is January 15th 2014. The thesis should be submitted electronically in DAIM before June 11th 2014.

Professor in charge: Gustav Grimstad

Department of Civil and Transport Engineering, NTNU
Date: 15.01.2014, (revised: 06.06.2014)

Gustav Grimstad

Professor Gustav Grimstad

Preface

This thesis is submitted in partial fulfilment of the requirements for the Degree of Master of Science in Geotechnics and Geohazards.

The study was supervised by Professor Gustav Grimstad. The work is presented as a literature review of creep in clay followed by development and implementation of a critical state soft soil creep model with mobilised shear stiffness (CS-SSCG) in Fortran code. The computer code is tested and verified at the element level. The CS-SSCG model is also validated in a boundary value problem.

This work was carried out at the Geotechnical Division, Department of Civil and Transport Engineering, Norwegian University of Science and Technology (NTNU) from January 14 to June 9, 2014.

Trondheim/ June 9, 2014
Mohammad Ali Haji Ashrafi

Acknowledgements

I would like to thank Professor Gustav Grimstad for giving me the opportunity to do this work, and for his invaluable advice and extensive support throughout the course of this thesis.

I would like to thank all the staff and students for making the Geotechnical division at NTNU such a pleasant place. I would like to thank in particular Professor Lars Grande, Assistant Professor Arnfinn Emdal, Professor Gudmund Reidar Eiksund, Professor Thomas Benz, Professor Steinar Nordal and PhD candidates Jon A. Rønningen and Ivan Depina.

Lastly, I would like to thank my family for all the support and encouragement they have given me.

Trondheim/ June 9, 2014
Mohammad Ali Haji Ashrafi

Summary

The stress range in which a soil element can be considered as elastic is very limited. The initial shear stiffness decays non-linearly in the well-known S-shaped stress strain curve from laboratory tests (see e.g. Atkinson and Sällfors (1991) and Benz (2007)). This thesis concerns primarily on the development and implementation of a creep model to reflect this behaviour of soil. MIT-MDPW embankment (see Karlsrud (1969) and Whittle (1974)) is studied to validate the model in a boundary value problem.

The Soft Soil Creep model (SSC) (Stolle et al., 1999a) in Plaxis does not account for high shear stiffness that soil exhibits at small mobilisation degree. In this respect, SSC does not distinguish between soil elements that undergo lower mobilisation in the far field and the ones that undergo higher mobilisation close to the embankment. This may result in overprediction of horizontal displacements in the field. Usually, in practical analysis of settlements this model deficiency should be taken into account by limiting the extension of the finite element mesh. The existing creep constitutive models e.g. Anisotropic Creep Model (ACM) (Leoni et al., 2009), non-Associated Creep Model for Structured Anisotropic Clay (n-SAC) Grimstad and Degago (2010), and Structured Anisotropic Creep Model (Creep-SCLAY1S) Sivasithanparam (2012) do not include directly shear stiffness of the soil that can be easily obtained by standard geotechnical tests e.g. triaxial test or direct simple shear test. Instead, they use the Poisson's ratio as an input parameter. In this new implementation, shear stiffness of the soil will be explicitly given by the engineer instead of commonly used Poisson's ratio.

Several researchers have been studied numerical analysis of MIT-MDPW embankment. Neher et al. (2001) and Fatahi et al. (2012) use Plaxis SSC for their simulation. They are able to show a good agreement for vertical settlement under the centre of the embankment but they overestimate the vertical settlements under the toe and also at the deep layers. The main reason is that they do not reflect on the importance of the selection of OCR when using creep rate models in settlement problems. Haji Ashrafi (2013) and Grimstad et al. (2013) addressed this issue and examined the embankment with focus on the 'proper' selection of OCR. The vertical displacements improved significantly both at the deeper and shallower levels and at the centre and toe of the embankment. However, prediction of the horizontal deformation under the embankment remained unsatisfactory as before. The Plaxis SSC model simulated

the horizontal displacements that were considerably higher than the field measurements - the problem yet to be resolved. In this regard, this thesis is one plausible solution to the problem by implementing a creep model that accounts for high shear stiffness of soil in low mobilisation degree, i.e. the lower the mobilisation, the higher the shear stiffness.

In doing so, first a Critical State Soft Soil Creep model (CS-SSC) is implemented and verified against the Plaxis SSC model. The model performance is very similar to Plaxis SSC in a settlement problem. Secondly, CS-SSC was used as a basis to develop and implement a new Critical State Soft Soil Creep model with mobilised Shear Stiffness (CS-SSCG). Initial high shear stiffness of the soil will be degraded with respect to the shear mobilisation. Results from the simulation of the MIT embankment show that horizontal displacement has been improved significantly using the CS-SSCG model.

Chapter 1 gives literature review of creep in soft soil (clay). Chapter 2 gives a brief introduction to soil modelling and some of the existing creep constitutive models (the focus is primarily on the Plaxis SSC model). In Chapter 3, firstly an introduction to Plaxis User Defined Soil Models (UDSM) will be presented. Secondly, mathematical formulation and numerical implementation of the CS-SSC model will be given. Lastly, the CS-SSC model will be verified against Plaxis SSC at element level. In Chapter 4 the CS-SSCG model is developed and implemented. All the models used in this study (Plaxis SSC, CS-SSC and CS-SSCG) will be tested at element level. Finally, MIT-MDPW embankment is simulated using these models and the results are compared to the field measurements. Finally, Chapter 5 gives conclusions and recommendations for further work.

Contents

Preface . . . i
Acknowledgements . . . iii
Summary . . . v
List of Figures . . . xii
List of Tables . . . xiii

1 Literature Study of Creep in Soft Soil (Clay) 1
1.1 Introduction . . . 1
1.2 Compressibility of soft soil . . . 5
  1.2.1 Ageing effect and delayed compression . . . 7
  1.2.2 Time resistance . . . 8
1.3 Rate dependency . . . 9
  1.3.1 Creep rheological models . . . 9
  1.3.2 Effect of sample disturbance . . . 13
  1.3.3 Clay strength anisotropy . . . 14
1.4 Objectives . . . 14
1.5 Limitations . . . 15
1.6 Approach . . . 15

2 Soil Modelling and Creep Constitutive Models 17
2.1 Introduction to soil modelling . . . 18
  2.1.1 Stress and Strain . . . 19
  2.1.2 Theory of elastoplasticity . . . 20
2.2 Existing creep constitutive models . . . 22
  2.2.1 Soft soil creep (SSC) . . . 22
  2.2.2 Other existing creep models . . . 25

3 Implementation and Verification CS-SSC Model 27
3.1 Plaxis user defined soil model 27
3.2 Model development and implementation 28
3.2.1 Model parameters 28
3.2.2 Mathematical formulation 30
3.2.3 Numerical implementation 32
3.2.4 Numerical aspects 37
3.3 Model verification at element level 38
3.3.1 Simulation of oedometer test 38
3.3.2 Simulation of triaxial test 41

4 Implementation and Verification CS-SSCG Model 43
4.1 Model development and implementation 43
4.1.1 Model parameters 43
4.1.2 Mathematical formulation 45
4.1.3 Numerical implementation 49
4.2 MIT-MDPW embankment 49
4.2.1 Background 51
4.2.2 Selection of parameters 52
4.3 Model verification and validation at element level 55
4.3.1 Simulation of oedometer tests 56
4.3.2 Simulation of triaxial tests 57
4.4 MIT-MDPW embankment case study 62
4.4.1 Vertical displacements 63
4.4.2 Horizontal displacements 64
4.4.3 Pore pressure 67
4.4.4 Mobilised shear stiffness 67

5 Concluding Remarks 71
5.1 Conclusions and discussion 71
5.2 Recommendations for further work 74

Bibliography 76

A List of Symbols **85**

B CS-SSCG Fortran Pseudo Code **91**

C Paper Abstract **97**

D Curriculum Vitae **99**

List of Figures

1.1 Primary and secondary compression (Gray, 1936) 1

1.2 Hypotheses A and B after (Ladd et al., 1977), from (Leroueil, 2006) 2

1.3 The reinterpreted results by Leroueil (1996) for special one-dimensional consolidation test carried out by Mesri et al. (1995) on Saint-Hilaire clay. from (Leroueil, 2006) 3

1.4 Comparison of strain rates between laboratory tests and in-situ (Leroueil, 2006) 4

1.5 Comparison between stress – strain relationships observed in-situ and laboratory tests at similar depth. after Kabbaj et al. (1988) from Leroueil (2006) 5

1.6 Better representation of soil compressibility (Wesley, 2013) 6

1.7 Representation of one-dimensional compression of ideal clay (Benz, 2010) . . . 6

1.8 Ageing effect and delayed compression concept: (left) ageing effect; (right) delayed compression concept (Bjerrum, 1967) 7

1.9 Time resistance: (left) typical representation of an IL oedometer test at a load step based on Janbu's resistance concept, vertical strain versus time (upper), and resistance versus time (lower) after (Havel, 2004); (right) resistance concept used for creep modelling in Plaxis (Neher et al., 2001) 9

1.10 Isotache concept: isotaches for lacustrine chalk sample (Šuklje, 1957) 11

1.11 CRS oedometer tests on Batiscan clay (Leroueil et al., 1985) 12

1.12 Preconsolidation stress as a linear function of log strain rate (Leroueil et al., 1985) 12

1.13 Effect of sample disturbance in IL oedometer tests on Väsby clay from depth of 4-4.3 m (Leroueil and Kabbaj, 1987) 13

1.14 Gloucester clay anisotropy during CIU triaxial compression tests: (a) stress-strain response; (b) corresponding ESPs (Hinchberger et al., 2010) 15

2.1 The isotache concept as used in SSC (Degago, 2011) 23

2.2 Plaxis SSC's reference surface and quivalent mean stress in $p-q$ stress space (Stolle et al., 1999b) . . . 24

3.1 CS-SSC & Plaxis SSC (normalised) difference [%] in IL oedometer test . . . 40
3.2 CS-SSC & Plaxis SSC normalised difference [%] in UK_0TC test . . . 42

4.1 The CS-SSCG model input parameters window in Plaxis . . . 44
4.2 Characteristic shear stiffness of soil with typical strain ranges for laboratory tests and structures; after Atkinson and Sällfors (1991) and Mair (1993), from Benz (2007) . . . 45
4.3 Increasing initial shear stiffness with depth . . . 46
4.4 Degradation of initial shear stiffness with degree of mobilisation . . . 47
4.5 MIT-MDPW embankment with instrumentation (Ladd et al., 1994) . . . 51
4.6 OCR and POP as defined in Plaxis (Plaxis2DManual, 2012) . . . 52
4.7 Selection of POP for BBC1 layer based on test data after (Ladd et al., 1994) . . . 53
4.8 G_0 used in CS-SSCG and G_0 back-calculated from Plaxis SSC . . . 55
4.9 Degradation of initial shear stiffness . . . 56
4.10 Oedometer simulation for soil elements from BBC1 (EL -10 m) and BBC2 (EL -28 m) . . . 58
4.11 Triaxial Undrained Compression and Extension tests for a soil element from BBC1 Layer at EL -10 m . . . 60
4.12 Triaxial Undrained Compression and Extension tests for a soil element from BBC2 Layer at EL -28 m . . . 61
4.13 Plaxis finite element model of two-layer embankment studied in this work . . . 62
4.14 Construction sequence of MIT-MDPW embankment; after Whittle (1974), from Fatahi et al. (2012) . . . 63
4.15 Calculated and measured vertical displacements . . . 65
4.16 Calculated and measured horizontal displacements at day 620 and 2053 . . . 66
4.17 Calculated and measured excess pore pressure at day 620 and 2053 . . . 68
4.18 Mobilised shear stiffness contours at day 620 and 2053 . . . 69

5.1 The ratio of shear stiffness to bulk modulus with varying Poisson's ratio . . . 72
5.2 Inclination of stress path in oedometer test in p-q plot . . . 73

List of Tables

1.1 Most commonly-used soil compression parameters in literature 6

2.1 Plaxis SSC input parameters 23
2.2 Comparison of creep constitutive models 25

3.1 CS-SSC input parameters 29
3.2 Initial stress for the two soil elements BBC1 and BBC2 38
3.3 BBC1 and BBC2 clay parameters 38
3.4 IL oedometer test simulation as defined in Plaxis General Soil Test 39

4.1 CS-SSCG input parameters 44
4.2 Clay parameters for 12-layer model 53
4.3 Clay parameters used in this study for two-layer model 53
4.4 Mohr-Coulomb (MC) parameters used for peat and till 54
4.5 Hardening soil (HS) parameters used for sand 54
4.6 Shear stiffness parameters used for CS-SSCG 54
4.7 Back-calculated shear stiffness from Plaxis SSC 54
4.8 Initial stress for the two soil elements BBC1 and BBC2 55
4.9 Incremental oedometer test simulation defined in Plaxis General Soil Test . . . 57
4.10 Construction sequence of the embankment as defined in Plaxis 63

Chapter 1

Literature Study of Creep in Soft Soil (Clay)

1.1 Introduction

When using the term 'soft' soil, it is usually included near-normally consolidated clays, clayey silts and peats. In this work, however, the main focus will be on soft clay. After Terzaghi's well-known theory of one-dimensional consolidation (Terzaghi, 1923), laboratory tests and also field observations revealed that soft soil settlement would continue even after the dissipation of excess pore pressure. In order to distinguish between the two type deformations, the term 'primary' consolidation and 'secondary' consolidation or 'creep' has been used. The former is used to describe the time dependent deformation because of the volume change due to the dissipation of excess pore pressure whereas the latter is used to describe the deformation under 'constant' effective stress, see Figure 1.1.

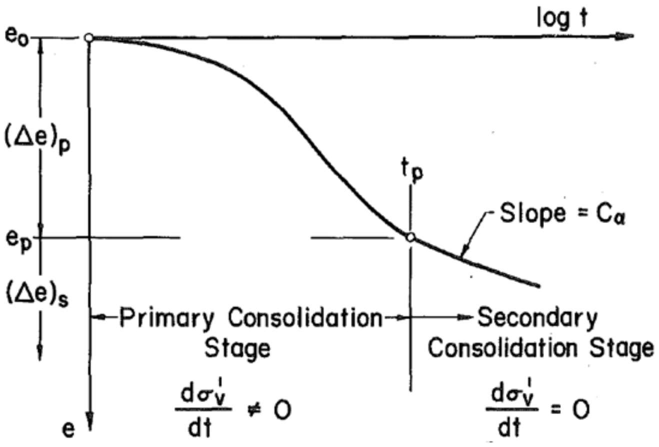

Figure 1.1: Primary and secondary compression (Gray, 1936)

As indicated by Ladd et al. (1977) and Jamiolkowski et al. (1985) two hypotheses A and B were used as a basis for discussion on how to extrapolate creep from short time observations in laboratory tests to long term predictions in field, see Figure 1.2. Opposing views can be found in selected works that support hypothesis A e.g. Ladd (1973), Mesri (1974) and hypothesis B e.g. Taylor (1942), Brinch Hansen (1969), Barden (1969), and Degago (2011). Hypothesis A implies a unique end of primary (EOP) strain (or void ratio) that is valid for both laboratory and in-situ primary consolidation. This means that for a given effective stress increment from the same initial effective stress, the EOP strain is independent of primary consolidation duration (t_{final}). Thus, Hypothesis A predicts the same EOP preconsolidation stress for both laboratory and in-situ. Hypothesis B, on the other hand, predicts a different in-situ EOP strain than the laboratory thin sample. Hypothesis B implies that creep occurs also during pore pressure dissipation. Accordingly, EOP increases with sample thickness due to the higher time required for primary consolidation. As can be seen from Figure 1.2, the EOP calculated based on the two hypotheses may differ significantly - hypothesis A predicts lower EOP than hypothesis B. After reaching EOP both hypotheses predict similar creep deformation.

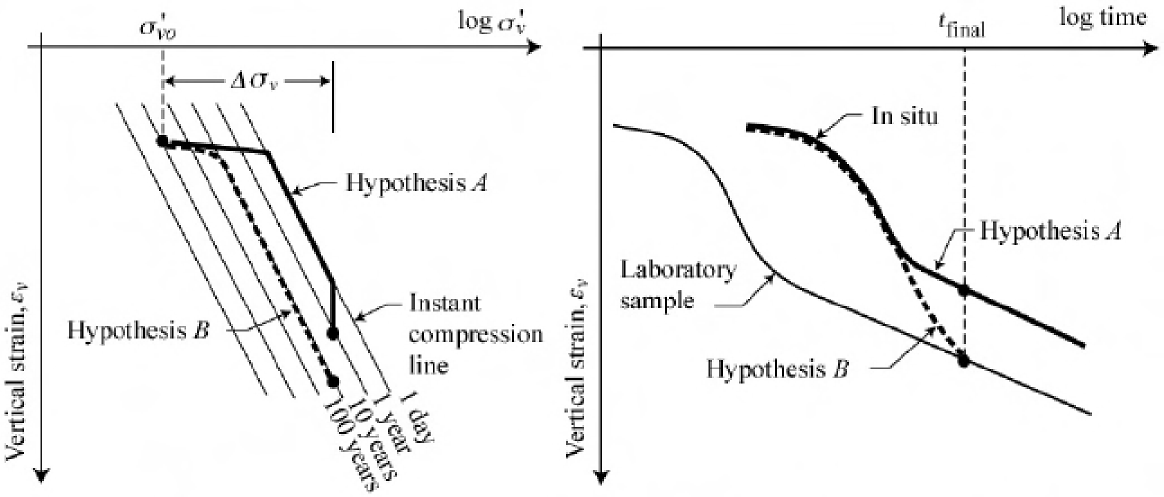

Figure 1.2: Hypotheses A and B after (Ladd et al., 1977), from (Leroueil, 2006)

Mesri (1986) and Mesri et al. (1995) performed special one-dimensional consolidation tests on Saint-Hilaire clay. They formed a 500 mm thick sample by connecting four 125 mm sub-specimens in series. The sample was isotropically consolidated with one-dimensional drainage at the top. The axial strain of the sub-specimens and the pore pressure in between were measured. The results from these tests were reinterpreted by leroueil et al. (1986) and

Leroueil (1996) to define the compression curves followed in the different sub-elements.

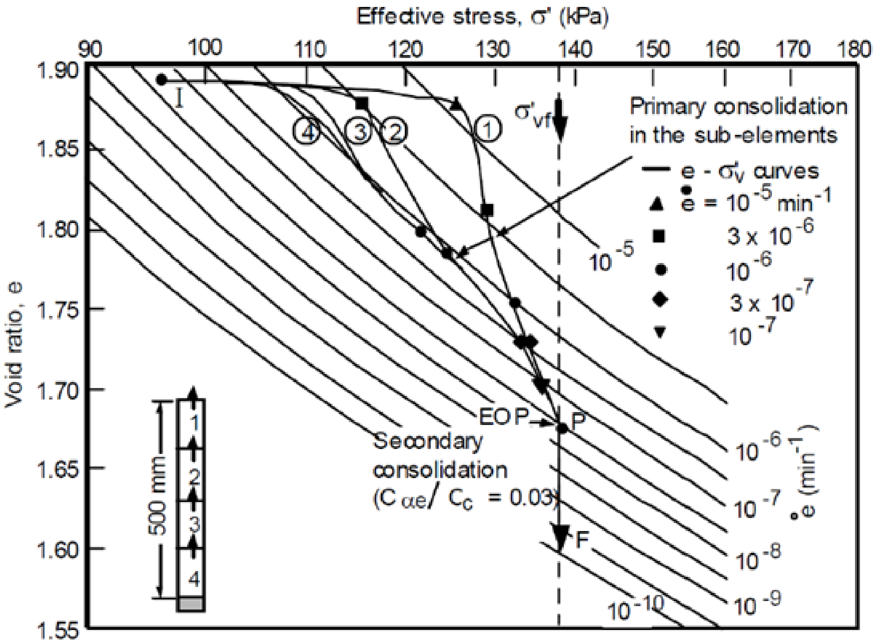

Figure 1.3: The reinterpreted results by Leroueil (1996) for special one-dimensional consolidation test carried out by Mesri et al. (1995) on Saint-Hilaire clay. from (Leroueil, 2006)

Figure 1.3 presents an example of reinterpreted compression curves obtained from consolidation of Saint-Hilaire clay. The compression curves are drawn from initial condition (point I) to the end-of-primary (EOP) consolidation (point P). Also drawn on the figure is a hypothetical secondary consolidation phase from point P to F. It can be seen that the compression curve followed during primary consolidation varies with the location of the sub-specimens in the sample. Near the drainage boundary (sub-specimen 1), the strain rate is the highest during the early stages of consolidation due to rapid dissipation of excess pore pressure. The vertical effective stress near the drainage boundary therefore reached isotaches with highest strain rate. On the other hand, for the sub-specimens that are far from the drainage boundary (sub-specimens 3 and 4), the strain rates are much smaller during the same period and the effective stress remains close to isotaches with lower strain rates. However, when the soil is approaching the end of primary consolidation (point P), the compression curves of the sub-specimens converge. After the EOP consolidation, the entire sample would be in secondary consolidation and would settle from P to F.

Imai and Tang (1992) observed similar behaviour in a consolidating clay with 7 sub-specimens connected in series. These reinterpreted results by Leroueil, which were originally used to justify hypothesis A, demonstrate that clay behaviour is strain rate dependent during both primary and secondary consolidation (hypothesis B). Note that hypothesis A implies that a soil element at the drainage boundary will 'wait' for the EOP of a soil element at the bottom sub-layer to start its secondary consolidation (Jostad, 2006), which seems quite doubtful. The tests carried out by Aboshi (1973) on remoulded clay shows EOP between the predictions given by hypotheses A and B. It implies that the strain rate dependency of soil compression is different during primary and secondary consolidation. However, most of the soil elements in the field will never experience 'secondary' phase during the lifetime of the embankment.

It should also be noted that laboratory tests provide compression curves with strain rates that are generally larger than 5×10^{-8} s^{-1} while strain rates measured in the field are usually lower than 10^{-9} s^{-1}, see Figure 1.4. Thus if the isotache model (hypothesis B) is valid, the vertical effective stress-strain curve followed in-situ should be below the end-of-primary compression curve obtained in the laboratory, as schematised earlier in Figure 1.2 (right part). In order to validate this, Kabbaj et al. (1988) examined the performance of four well-documented embankments built on clay deposits. Figure 1.5 shows comparison between in-situ compression curve (dotted curve) and laboratory compression curve for these 4 test embankments. In all four cases, at a given effective stress, the in-situ vertical strain is larger than vertical strain from the end of primary laboratory compression curve. This indicates that hypothesis B is valid.

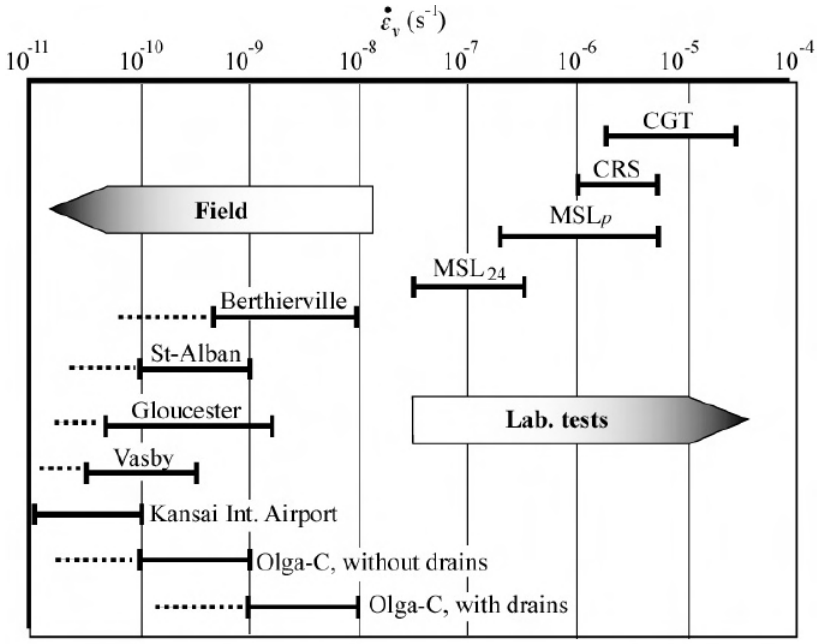

Figure 1.4: Comparison of strain rates between laboratory tests and in-situ (Leroueil, 2006)

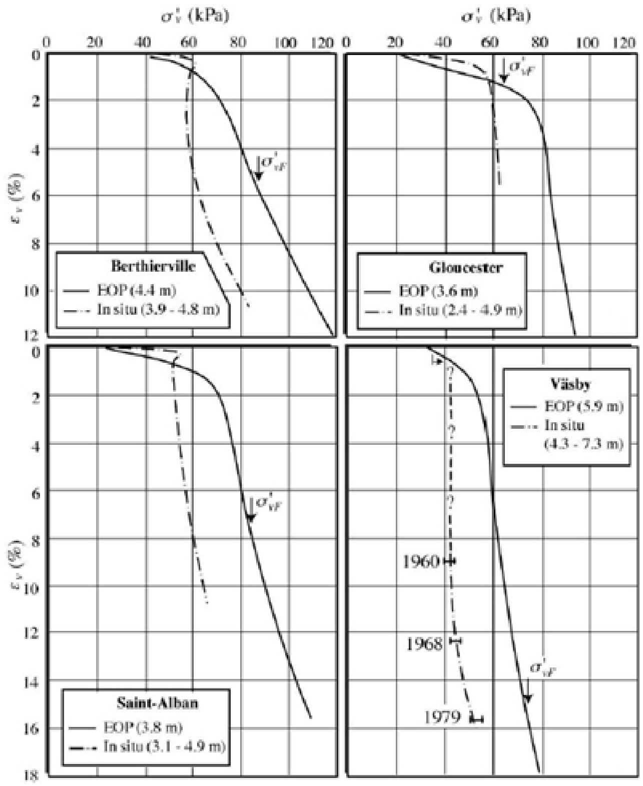

Figure 1.5: Comparison between stress – strain relationships observed in-situ and laboratory tests at similar depth. after Kabbaj et al. (1988) from Leroueil (2006)

1.2 Compressibility of soft soil

In literature one-dimensional logarithmic compression 'law' of soft soils has been represented by different compression curves e.g. void ratio versus vertical stress ($e - \sigma_v$) or specific volume ($v = 1 + e$) versus vertical natural logarithmic mean stress ($v - ln\sigma_p$). Figure 1.7 and Table 1.1 summarise the well-known compressibility parameters of soft soils. It may also be beneficial that the geotechnical society pays more attention to the message from Janbu (1998): 'it remains a mystery why the international profession still uses the awkward $e - log$ plots, and the incomplete and useless coefficient C_c which is not even determined from the measured data, but from a constructed line outside the measurements.' Figure 1.7 shows a better graphical representation of soil compressibility valid for different soils based on Janbu's message ($\varepsilon_v - \sigma_v$).

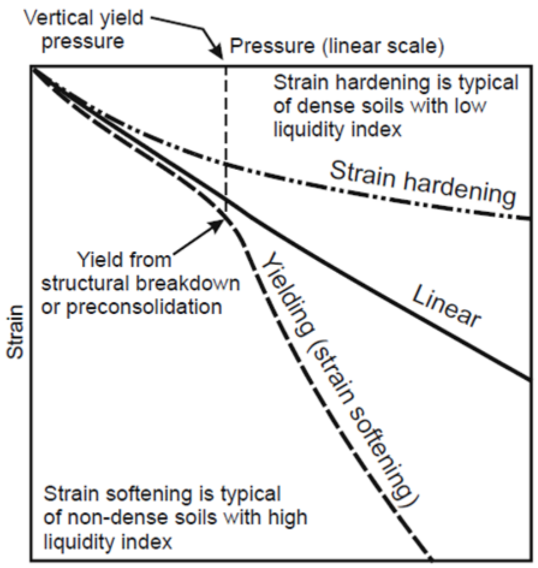
Vertical yield pressure
Pressure (linear scale)
Strain hardening is typical of dense soils with low liquidity index
Strain hardening
Yield from structural breakdown or preconsolidation
Linear
Yielding (strain softening)
Strain
Strain softening is typical of non-dense soils with high liquidity index

Figure 1.6: Better representation of soil compressibility (Wesley, 2013)

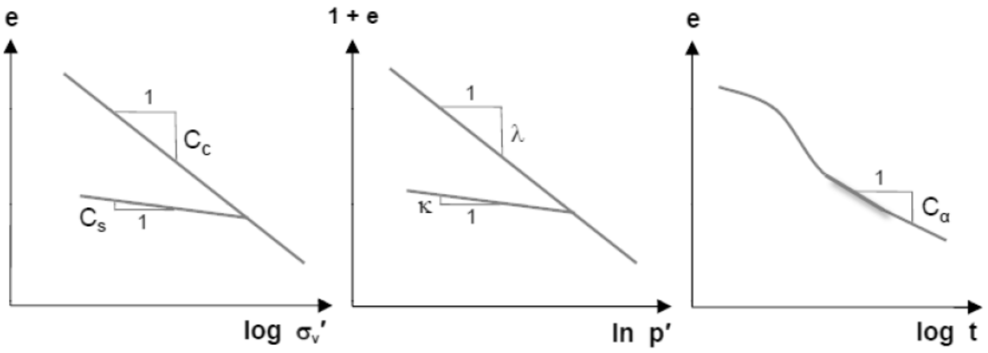
e
1
Cc
Cs
1
log σv'
1 + e
1
λ
κ
1
ln p'
e
1
Cα
log t

Figure 1.7: Representation of one-dimensional compression of ideal clay (Benz, 2010)

Table 1.1: Most commonly-used soil compression parameters in literature

Origination	Compression index	Recompression index or swelling index	Secondary compression index or creep index
International	C_c	C_r or C_s	C_α or $C_{\alpha e}$
Cam-Clay	$\lambda = \frac{C_c}{\ln 10}$	$\kappa \approx \frac{3}{\ln 10} \frac{(1-\nu_{ur})}{\nu_{ur}} C_s$	$\mu = \frac{C_\alpha}{\ln 10}$
Plaxis	$\lambda^* = \frac{\lambda}{1+e}$	$\kappa^* = \frac{\kappa}{1+e}$	$\mu^* = \frac{\mu}{1+e}$
Norway	$m_{nc} = \frac{1}{\lambda^*}$	$m_{oc} = \frac{\ln 10(1+e)}{C_s}$	$r = \frac{1}{\mu^*}$

1.2.1 Ageing effect and delayed compression

Bjerrum (1967) introduced two new terms ‘instant’ and ‘delayed’ compression. The former is to describe the strains occurring simultaneously with the effective stress increase while the latter is for strains under constant effective stress, see Figure 1.8 (right part). The two new terms, instant and delayed compression, were contrary to the ‘primary’ and ‘secondary’ compression introduced by Gray (1936). The dotted curve shows the response of the soil that would occur if the pore water in the clay were absolutely compressible. Thus, the applied pressure would be transferred instantaneously to the clay structure as effective pressure. However, due to the low permeability of the clay and also creep the effective stress will increase gradually as the excess pore pressures dissipate and compression will occur along the bold curve. Time required for dissipation of the excess pore pressures is dependent on the following factors : (1) thickness of the clay layer; (2) soil permeability; and (3) drainage type. Therefore, separation of the compression into a primary and a secondary part is rather arbitrary and may not be the best approach to describe the soil compression response. Figure 1.8 (left part) shows how the compression of a clay layer would develop if loaded with different time duration in an incremental loading (IL) test with time step e.g. 24-h, 0.1 years, 1 year, 10 years, etc. Soft soil may show an apparent overconsolidation stress in contrast to

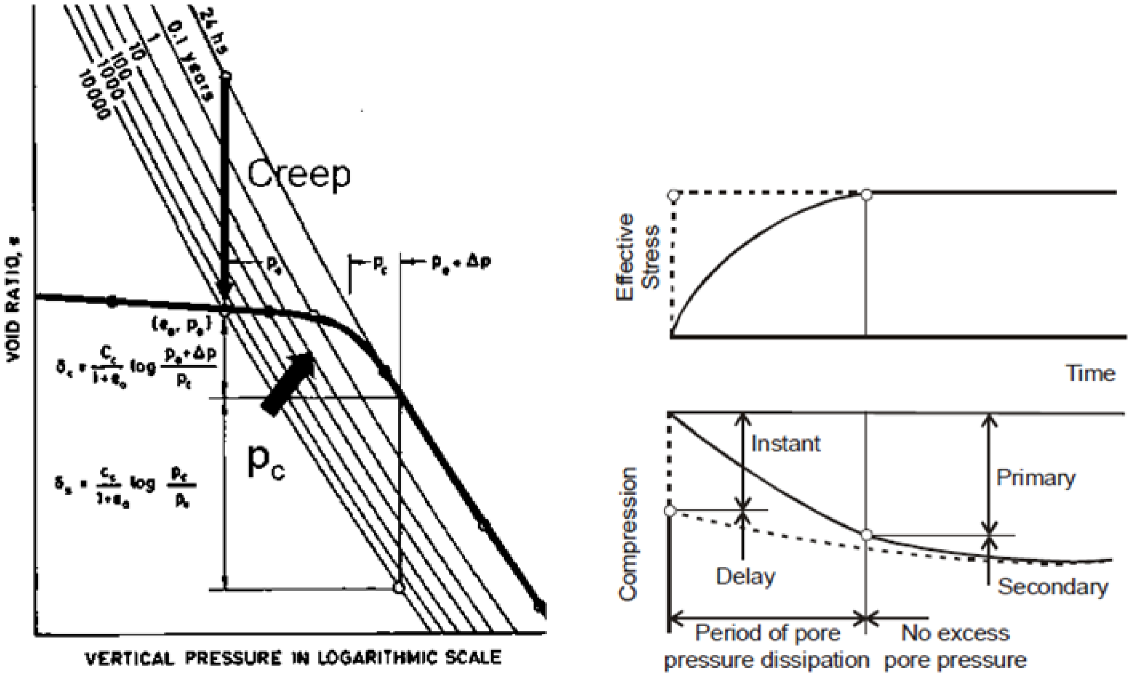
VOID RATIO, e
24 hs
0.1 years
1
10
100
1000
10000
Creep
p_0
p_c
$p_0 + \Delta p$
(e_0, p_0)
$\delta_c = \frac{C_c}{1+e_0} \log \frac{p_0+\Delta p}{p_c}$
$\delta_s = \frac{C_s}{1+e_0} \log \frac{p_c}{p_0}$
p_c
VERTICAL PRESSURE IN LOGARITHMIC SCALE
Effective Stress
Time
Compression
Instant
Delay
Primary
Secondary
Period of pore pressure dissipation
No excess pore pressure

Figure 1.8: Ageing effect and delayed compression concept: (left) ageing effect; (right) delayed compression concept (Bjerrum, 1967)

the conventional overconsolidation stress introduced by Casagrande (1936). The latter is related to the geological loading history while the former is associated to 'ageing' effect (creep). As shown in figure, a 10,000-year old clay sample when loaded in IL 24-hr test would show an apparent preconsolidation stress (P_c) controlled by the combination of its current void ratio and loading rate (similar to the isotache concept). The reason is that clay will adjust to the 24-hr compression curve which has a higher strain rate. In doing so, clay exhibits higher preconsolidation stress than in-situ P_c which is solely due to the loading history. Therefore overconsolidation state can be reached by loading history and/or 'ageing' effect (creep).

1.2.2 Time resistance

The resistance concept is commonly used in physics e.g. thermal or electrical resistance. Janbu (1969) applied this concept into geotechnical engineering based on experimental observations, see Equation (1.1). When plotting resistance R versus time t, a 'linear' relationship between R and t is observed after the intrinsic time (t_r or t_c), see Figure 1.9. The slope of the line defines resistance or creep number (r_s). Typical values of the resistance number for normally consolidated clays are estimated in the range of 100-500 with natural water content 30-60 (Havel, 2004).

$$R = \frac{dt}{d\varepsilon} \tag{1.1}$$

Figure 1.9 (left part) illustrates Janbu's time resistance for a one-load increment (load step) in IL test. The region before intrinsic time is not following the straight line, see Figure 1.9 (lower left part). This is due to the domination of excess pore pressure in this region. However, after t_r soil shows a linear increase of resistance over time under approximately constant effective stress. This implies that creep strain rate will decrease linearly with time. Time (t) can be set to 0.0 and time frame (t') can be introduced, Figure 1.9 (lower right part). The idea of Soft Soil Creep (SSC) constitutive model Stolle et al. (1999a) is primarily based on time resistance and isotache concept. Further discussions on the SSC model will be presented in Chapter 2.

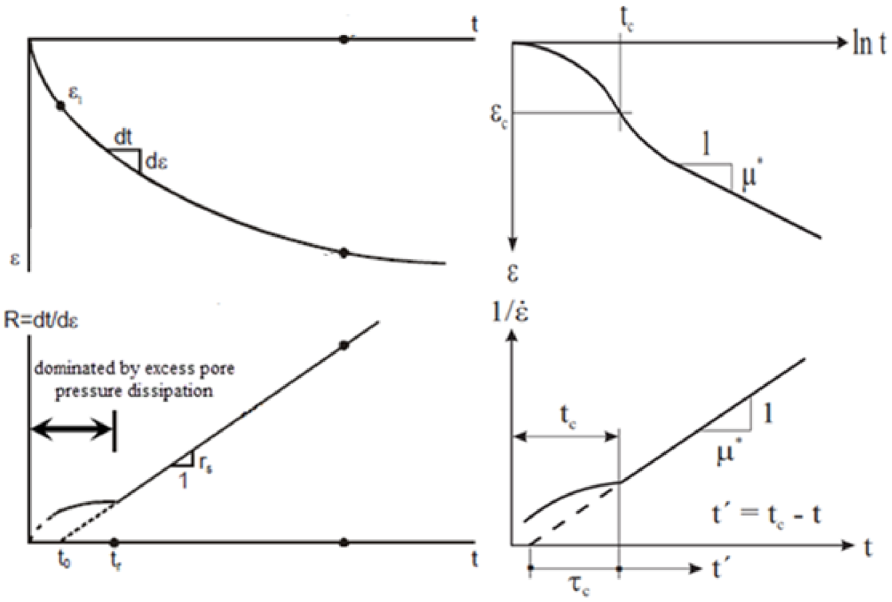

Figure 1.9: Time resistance: (left) typical representation of an IL oedometer test at a load step based on Janbu's resistance concept, vertical strain versus time (upper), and resistance versus time (lower) after (Havel, 2004); (right) resistance concept used for creep modelling in Plaxis (Neher et al., 2001)

1.3 Rate dependency

Rate dependency of soft soil compressibility, i.e. the effect(s) of strain rate on soft soil compression, is a very important (or even the most important) concept for better understanding the viscous behaviour of soft soil (creep). Accordingly, many researchers have contributed to this topic.

1.3.1 Creep rheological models

There are mainly four types of creep rheological models that describe one-dimensional compressibility of soft soils, see Equation (1.2) to (1.5). These equations can also be expressed in terms of void ratio or specific volume. Equation (1.2) represents the case for classical consolidation theory of Terzaghi in which the effective stress-strain relationship is independent of time or strain rate.

$$\Gamma_1(\sigma'_v, \varepsilon) = 0 \tag{1.2}$$

$$\Gamma_2(\sigma'_v, \varepsilon, t) = 0 \tag{1.3}$$

$$\Gamma_3(\sigma'_v, \dot{\sigma}'_v, \varepsilon, \dot{\varepsilon}) = 0 \tag{1.4}$$

$$\Gamma_4(\sigma'_v, \varepsilon, \dot{\varepsilon}) = 0 \tag{1.5}$$

$$z_t = \alpha_s + \alpha_p \log_{10} t \tag{1.6}$$

Several researchers have studied the time dependent behaviour of soft soils under the constant effective stress (creep). Buisman (1936) was probably the first who proposed a creep model based on Equation (1.3). He is best known for his $log(t)$ compression 'law' - that is linear strain increase with respect to the logarithm of time, Equation (1.6). He used the term 'secular' in the sense of a period spanning approximately a human lifetime and he used the word 'direct' in the sense of instant compression. The subscript 'p' signifies the direct influence of effective stress, and p was the symbol for effective stress at that time (den Haan, 2014). Note that the subscript p and s do not stand for primary and secondary. Also, Koppejan (1948) and Bjerrum (1967) and Hansen (1969) proposed models based on Equation (1.3) where strain is function of effective stress and time. The drawback of the models based on this type of equation is that the time origin must be defined. Time is implicitly deleted from the models corresponding to Equation (1.4) and Equation (1.5) since soil response may be expressed by its current state. Taylor and Merchant (1940) were the first to suggest a model of the type represented by Equation (1.4) where the rate of change in void ratio is a function of the effective stress, the void ratio and the rate of change in effective stress. This suggestion has been followed by several researchers e.g. (Gibson, 1961).

Later on, it was shown that soil response is not dependent on stress rate. Rate dependent creep models corresponding to Equation (1.5) show a unique relationship between the effective stress, the void ratio and the rate of change in void ratio. Figure 1.10 (lower part) illustrates the isotache model (Šuklje, 1957). An isotache is defined as a contour of constant void ratio rate (or constant strain rate). As can be seen from figure a unique relationship can be obtained between the vertical effective stress, void ratio and void ratio rate. Figure 1.10 (upper right part) are the vertical effective stress versus void ratio curves for samples with a thickness n times larger than the thickness of a reference sample. It indicates the influence of sample thickness on obtained compression curves. The isotache concept clearly corresponds to hypothesis B and at the same time may contradict hypothesis A. In this model, void ratio and effective stress relation continuously changes with the rate of deformation and there is no distinguish between primary and secondary consolidation. It means that creep deformation is not a process that starts immediately after primary consolidation but rather occurs simultaneously during the dissipation of excess pore pressure as well.

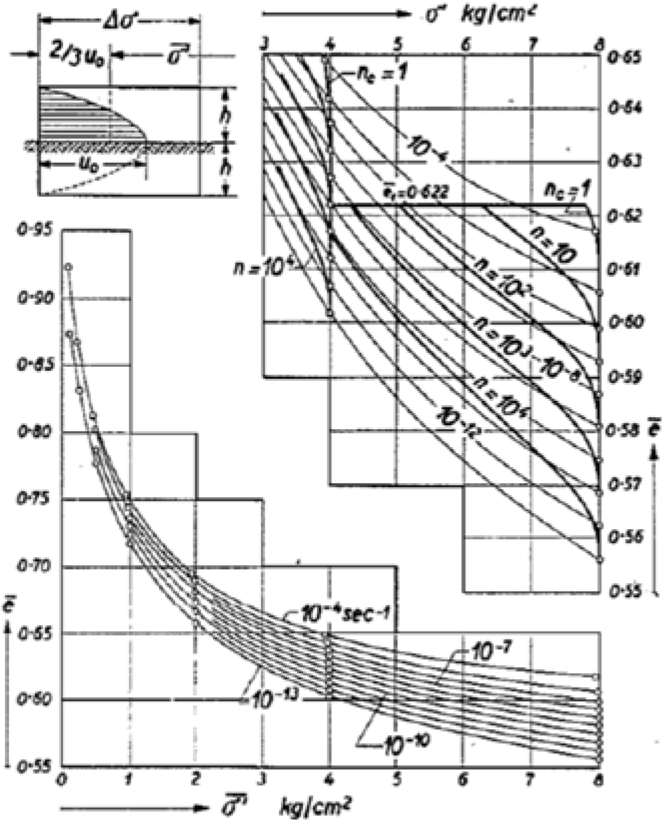

Figure 1.10: Isotache concept: isotaches for lacustrine chalk sample (Šuklje, 1957)

Figure 1.11 illustrates typical results from 18 CRS tests performed on Batiscan clay with strain rate varying from $1.69 \times 10^{-8} s^{-1}$ (lowest strain rate) to $1.43 \times 10^{-5} s^{-1}$(highest strain rate). It can be seen that: (1) the higher the strain rate, the higher the vertical preconsolidation stress; (2) the higher the strain rate, the higher the pore pressure increase at the base of the sample; (3) for the lowest strain rate, the soil response is not obeying the same pattern as observed in the higher strain rates. This latter aspect may be explained by test deficiently. In order to perform a CRS test with such a low strain rate, there is a possibility that apparatus cannot push the sample well enough due to the induced friction between the thrust piston and oedometer ring. This different pattern obtained at very low strain rates can also be explained with microstructuration, i.e. bonding between soil particles within time Leroueil and Vaughan (1990). Thus, more investigations on this aspect may be advantageous. The general trend in these tests is very similar to the one observed by e.g. Sällfors (1975) on Swedish clays. It can be concluded that the compression curve is strain rate dependent even during primary consolidation. This may contradict hypothesis A again. It has also found that there is a 'linear' variation of vertical preconsolidation stress versus strain rate for a given soil when plotted in a log scale as shown in Figure 1.12 for Batiscan clay. Several other researchers have reported the similar behaviour e.g. Adachi et al. (1982), Vermeer (1999), and Kim (2001).

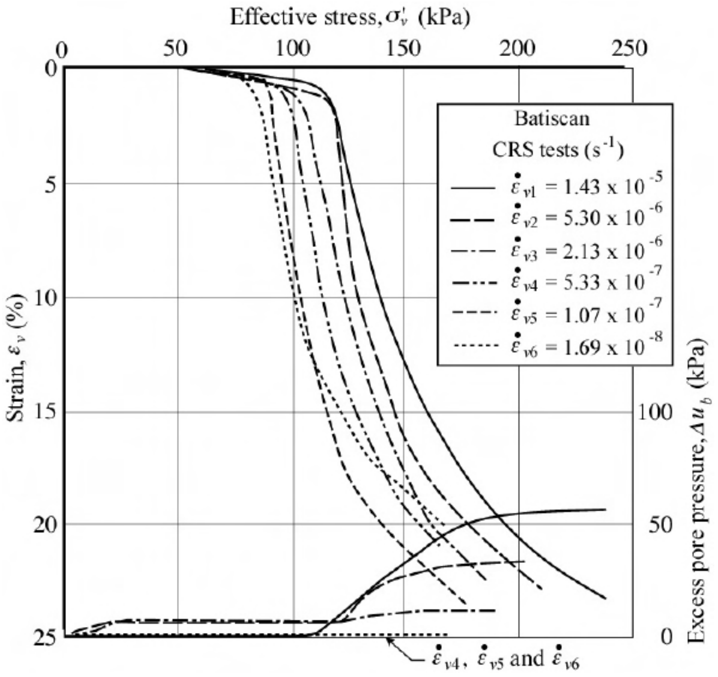

Figure 1.11: CRS oedometer tests on Batiscan clay (Leroueil et al., 1985)

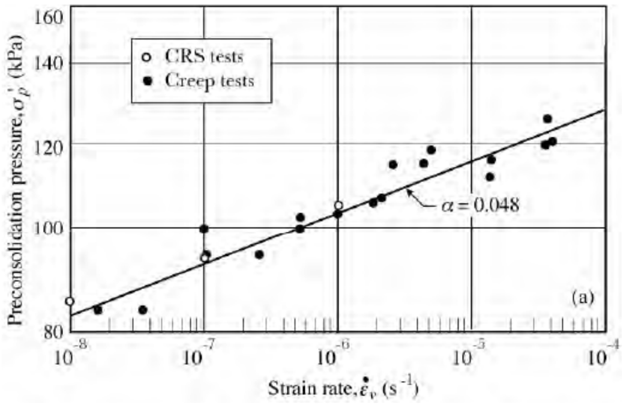

Figure 1.12: Preconsolidation stress as a linear function of log strain rate (Leroueil et al., 1985)

1.3.2 Effect of sample disturbance

Figure 1.13 shows typical IL oedometer test results. The curves are obtained from samples taken from the depth 4-4.3 m from Väsby clay with the 50 and 200 mm sampler. The effect of sample disturbance is evident. The specimen taken with 200 mm high quality sampler (Laval sampler or block sampler) shows a sharp break when passing vertical preconsolidation stress whereas the sample taken with the Swedish standard 50 mm piston sampler shows a significantly more rounded curve. Mesri and Choi (1985) estimated preconsolidation stress of 7 kPa on the basis of 50 mm samples compared to 20 kPa on the basis of 200 mm high quality samples. They further found a good agreement using hypothesis A based on the selection of preconsolidation stress from disturbed samples. It is believed that the good agreement was achieved because of: (1) underestimating the preconsolidation stress, and (2) using the laboratory EOP which is smaller than in-situ EOP. It is also to be emphasized that when using soft soil model based on hypothesis B (creep rate dependent models) e.g. the Soft Soil Creep model (SSC) sample quality is of great importance.

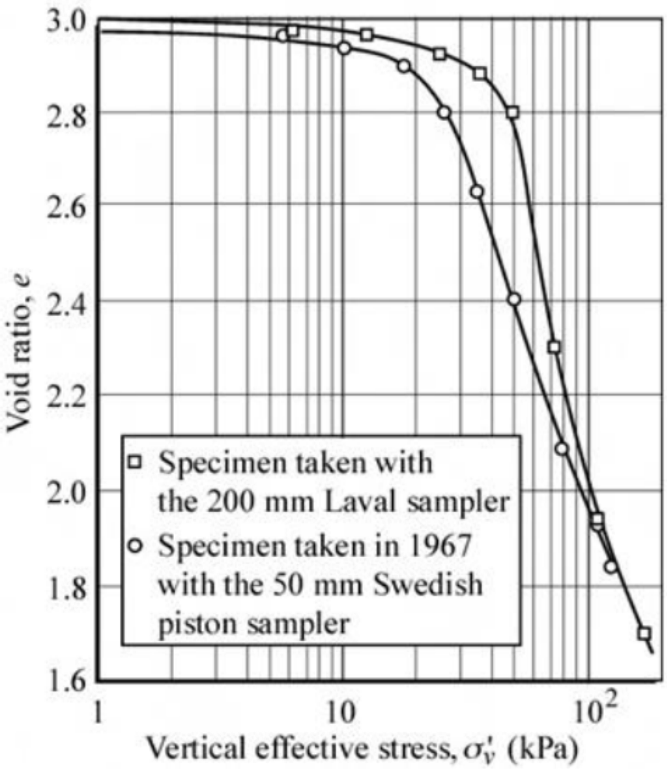

Figure 1.13: Effect of sample disturbance in IL oedometer tests on Väsby clay from depth of 4-4.3 m (Leroueil and Kabbaj, 1987)

1.3.3 Clay strength anisotropy

Material is anisotropic if its properties are direction dependent. Natural soft clay tends to have a considerable degree of anisotropic fabric which is developed during the deposition and sedimentation. Casagrande and Carillo (1944) were probably the first to model strength anisotropy in soils by introducing: (1) inherent anisotropy which refers to intrinsic physical characteristic related to the material and entirely independent of applied stress; (2) initial anisotropy (K_0-consolidation) which refers to anisotropy related to the soil sedimentation and (3) induced anisotropy which is exclusively due to the strains associated to the applied stress. Anisotropy can be induced in soil when experiencing subsequent strains, re-orientation of particles and changes in particle contacts.

Anisotropy influences the compression behaviour of soil regarding both elastic and plastic strains (Wheeler et al., 2003). In soft soils which exhibit significant plastic deformations, plastic anisotropy is of more importance in engineering practice than elastic anisotropy. Both empirical and numerical investigations show that plastic anisotropy has significant influence on the soil stiffness and its strength, see e.g. (Tavenas and Leroueil, 1977), (Burland, 1990) and (Wheeler et al., 2003). Figure 1.14 a shows stress-strain response of Gloucester clay in undrained triaxial compression test (CIU) where different samples trimmed at various angles (i) relative to the vertical direction. Figure illustrates that the peak undrained strength of Gloucester clay varies with the sample orientation. Figure 1.14 b shows the corresponding effective stress paths (ESPs) for the samples. It indicates that all samples may reach the same critical state line (M_c) at large-strain, which is independent of the sample orientation. However, ESP is clearly anisotropic before reaching to failure state. Similar behaviour has been reported for other clays e.g. St. Vallier clay (Lo and Morin, 1972).

1.4 Objectives

After literature review on the topic, the two main objectives of this Master's thesis are:

1. Implementation and verification of a critical state creep model similar to Plaxis SSC
2. Implementation and validation of a critical state creep model with shear stiffness to improve horizontal displacement in a settlement problem

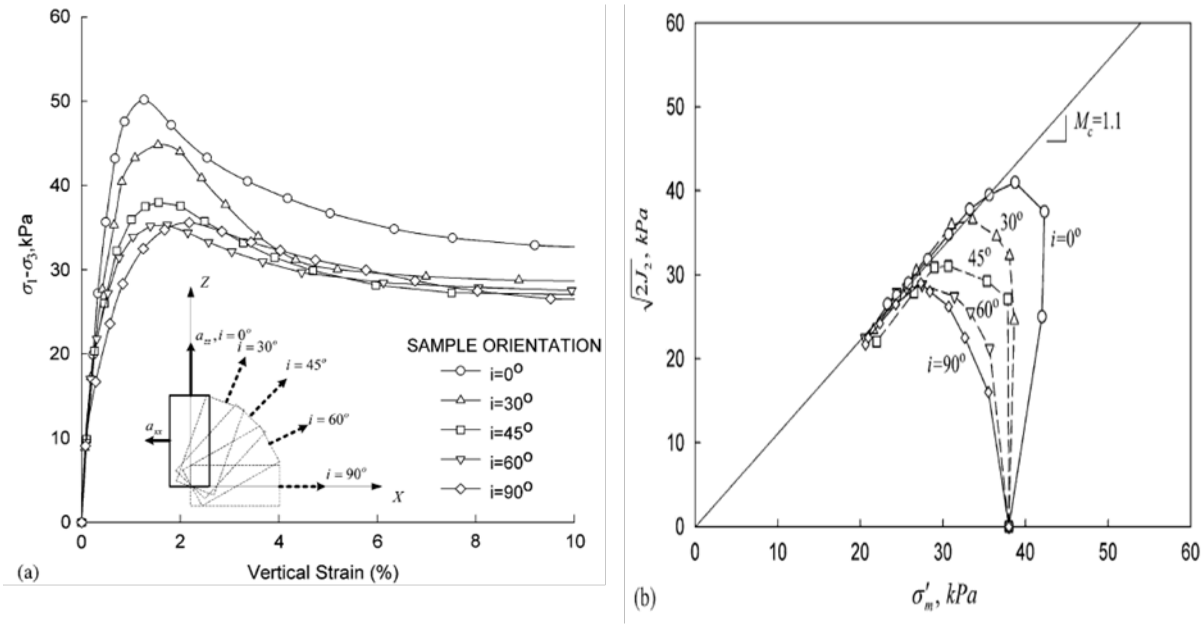

Figure 1.14: Gloucester clay anisotropy during CIU triaxial compression tests: (a) stress-strain response; (b) corresponding ESPs (Hinchberger et al., 2010)

1.5 Limitations

For implementation of a constitutive model the first step is to understand the soil behaviour (here creep). The second step is to find and understand a theoretical framework to model the soil behaviour (here mainly theory of elastoplasticity and continuum mechanics). The final step is to implement the model in a computer code (here Fortran). This procedure and in particular the final step is time demanding. Sometimes it may take up to a couple of days or more to fix a problem in the computer code. The amount of time for doing this thesis was quite limited though.

1.6 Approach

The isotache and resistance concept will be used to implement two user defined creep models within the framework of elastoplasticity. Firstly, a critical state soft soil creep model (CS-SSC) will be formulated and implemented in Plaxis. The model will be validated against built-in Plaxis SSC to ensure that it will reproduce the similar soil response. Secondly, CS-SSC will be extended to a new critical state soft soil creep model with shear stiffness (CS-SSCG). Finally, the model performance will be validated in MIT-MDPW embankment and results from Plaxis SSC, CS-SSC and CS-SSCG will be compared.

Chapter 2

Introduction to Soil Modelling and Creep Constitutive Models

Constitutive models for clays are often based on the modified Cam-Clay model (MCCM) (Roscoe and Burland, 1968). MCCM was originally developed to model simple elastoplastic behaviour of reconstituted soils under triaxial condition. Various features and modifications are later applied to MCCM in order to account for different aspects of natural clays such as anisotropy, destructuration and creep (Grimstad et al., 2013):

1. Rotating the yield/reference surface to account for anisotropy, e.g. Dafalias (1986)
2. Accounting for unstable structure by associating the yield/reference surface with a destructuration formulation by Gens and Nova (1993)
3. Modelling creep and rate dependency by controlling the size of the reference surface using concepts developed by Šuklje (1957) or Janbu (1969)

Adding these features to MCCM demands the increased level of mathematical complexity, and also the need for extra soil parameters that may require special laboratory tests. Occasionally the application of a 'simpler' model could facilitate a better understanding of the problem in hand than a more 'advanced' model. One can focus on certain aspect of the soil behaviour and try to understand the influence of it by freezing the other features. In doing so, name it 'simple' or 'advanced', Plaxis Soft Soil Creep model (Plaxis SSC) is used as a basis to develop a new model with focus on influence of shear stiffness. Therefore, the models used in this study do not incorporate rotated ellipse and destructuration.

In this chapter some theoretical components from soil modelling that will be needed in the following chapters will be introduced: stress and strain definitions, notations and some invariants. For more comprehensive overview of this topic reader can refer to e.g. Nordal (2010). Moreover, an overview of some of the existing creep constitutive models will be presented. The focus will be on the Plaxis SSC model.

2.1 Introduction to soil modelling

Probably the most innovative invention of the human is 'number'. Later on equations came into the picture to describe the relations between the numbers in a mathematical way. It has been understood that many of the problems in physics can be expressed by differential equations, e.g. the motion of a mass body. Usually in soil constitutive modelling a set of governing partial differential equations is used to model the problem. Finding an analytical solution to the equations, however, is not always guaranteed and therefore computational or numerical procedure is commonly used to solve these type of equations. One can divide the procedure for implementing a soil constitutive model into four parts:

1. Soil behaviour: understanding the behaviour of the soil in hand
2. Mathematical model: finding the governing equations that capture the overall behaviour of the soil within an appropriate theoretical framework
3. Numerical model: implementation of the mathematical model in a computer code
4. Code verification and model validation: debugging and verifying the computer code and testing the model against laboratory tests and/or field measurements

Note that if the model fails to fulfil the last part it should not be accepted regardless how complex it is mathematically formulated or how many advanced features it possesses. It is also to be noted that there should be a balance between the practicality of the model and its ability to capture the soil behaviour. Adding more features usually comes with more parameters, i.e. less 'engineer-friendly' model. Therefore it is advantageous to to capture the soil behaviour with minimised number of input parameters used in the model. Moreover, these parameters should be easily quantified based on standard geotechnical laboratory tests.

2.1.1 Stress and Strain

We apply continuum mechanics in modelling macro behaviour of soil, even though soil is obviously not a continuous material. The two most important variables from continuum mechanics in soil modelling are stress and strain tensors. In the mathematical formulation all the stresses are effective even though they are not denoted by prime superscript ($'$). In mathematical development of the model, compressive stress is treated as positive whereas tensile stress is negative. For model implementation, however, the Plaxis sign convection must be used; that is compression (-) and extension(+). **Vectors** and **matrices** are denoted by **boldface letters**. Cauchy symmetric stress tensor of a soil element in 3D-Cartesian space can be expressed by Equation (2.1). Corresponding to the stress vector the strain vector is established by Equation (2.2). The deviatoric stress $\boldsymbol{\sigma_d}$ is defined with Equation (2.3).

$$\boldsymbol{\sigma} = \begin{pmatrix} \sigma_{\text{xx}} \\ \sigma_{\text{yy}} \\ \sigma_{\text{zz}} \\ \sigma_{\text{xy}} \\ \sigma_{\text{yz}} \\ \sigma_{\text{zx}} \end{pmatrix} \tag{2.1}$$

$$\boldsymbol{\varepsilon} = \begin{pmatrix} \varepsilon_{\text{xx}} \\ \varepsilon_{\text{yy}} \\ \varepsilon_{\text{zz}} \\ \varepsilon_{\text{xy}} \\ \varepsilon_{\text{yz}} \\ \varepsilon_{\text{zx}} \end{pmatrix} \tag{2.2}$$

$$\boldsymbol{\sigma_d} = \begin{pmatrix} \sigma_{\text{xx}} - p \\ \sigma_{\text{yy}} - p \\ \sigma_{\text{zz}} - p \\ \sqrt{2}\sigma_{\text{xy}} \\ \sqrt{2}\sigma_{\text{yz}} \\ \sqrt{2}\sigma_{\text{zx}} \end{pmatrix} \tag{2.3}$$

The principal stresses ($\sigma_1 \geq \sigma_2 \geq \sigma_3$) and strains ($\varepsilon_1 \geq \varepsilon_2 \geq \varepsilon_3$) are eigenvalues of stress and strain tensors, respectively. Stress invariants are stress quantities that their value are not dependent on the selected reference system. In soil modelling it is occasionally beneficial to use the invariants e.g. mean stress p, see Equation (2.4) and deviatoric stress q, see Equation (2.5). In triaxial test condition (triaxial compression $\sigma_1 = \sigma_a$ and $\sigma_2 = \sigma_3 = \sigma_r$; and triaxial extension: $\sigma_3 = \sigma_a$ and $\sigma_2 = \sigma_1 = \sigma_r$) the deviatoric stress will simplify to Equation (2.6). The third deviatoric stress invariant J_3 can be calculated from Equation (2.7).

$$p = \frac{\sigma_{xx} + \sigma_{yy} + \sigma_{zz}}{3} \tag{2.4}$$

$$q = \sqrt{\frac{3}{2}\left(\boldsymbol{\sigma}_{\boldsymbol{d}}^{T} \cdot \boldsymbol{\sigma}_{\boldsymbol{d}}\right)} \tag{2.5}$$

$$q = \sigma_1 - \sigma_3 \tag{2.6}$$

$$J_3 = (\sigma_{xx} - p)(\sigma_{yy} - p)(\sigma_{zz} - p) - \left[\sigma_{yz}^2(\sigma_{yy} - p) + \sigma_{zx}^2(\sigma_{yy} - p) + \sigma_{xy}^2(\sigma_{yy} - p)\right] + 2\sigma_{xy}\sigma_{yz}\sigma_{zx} \tag{2.7}$$

2.1.2 Theory of elastoplasticity

In elastoplasticity strains are commonly divided into elastic (recoverable) and plastic (irrecoverable) part. In this work plastic strain is viscous strain (creep strain) that is time dependent irrecoverable strain under ‘constant’ stress. Thus, total strain increment in an elastoviscoplastic material can be decomposed into elastic and viscoplastic strain increment as shown by Equation (2.8):

$$\Delta\boldsymbol{\varepsilon} = \Delta\boldsymbol{\varepsilon}^{e} + \Delta\boldsymbol{\varepsilon}^{vp} \tag{2.8}$$

Constitutive Equation (2.9) relates stress increment to strain increment by Hooke’s law. Where $\boldsymbol{D}$ is elastic stiffness matrix. In this work $\boldsymbol{D}$ is isotropic.

$$\Delta\boldsymbol{\sigma} = \boldsymbol{D}(\Delta\boldsymbol{\varepsilon} - \Delta\boldsymbol{\varepsilon}^{vp}) \tag{2.9}$$

Elasticity

Isotropic elastic stiffness matrix in 3D-Cartesian space is a symmetric matrix that can be expressed by different sets of two independent elastic parameters, e.g the bulk modulus K

and the shear modulus G as shown in Equation (2.13), or K and the Poisson's ratio ν. In this work the bulk modulus is mean stress dependent, see Equation (2.12), where κ^* is modified swelling index.

$$F_1 = K + \frac{4G}{3} \tag{2.10}$$

$$F_2 = K - \frac{2G}{3} \tag{2.11}$$

$$K = \frac{p}{\kappa^*} \tag{2.12}$$

$$\boldsymbol{D} = \begin{pmatrix} F_1 & F_2 & F_2 & & & \\ & F_1 & F_2 & & \mathbf{0} & \\ & & F_1 & & & \\ & & & G & 0 & 0 \\ & SYM & & & G & 0 \\ & & & & & G \end{pmatrix} \tag{2.13}$$

In formulation of the Plaxis SSC model, ν and κ^* are elastic input parameters. Therefore, G in elastic matrix is replaced with Equation (2.14).

$$G = \frac{3(1-2\nu)}{2(1+\nu)} K \tag{2.14}$$

Thermodynamically, K and G must be positive numbers. This means that theoretically from Equations (2.15) and (2.16) the upper limit and lower limit for Poisson's ratio is 0.5 and -1, respectively ($-1 < \nu < 0.5$).

$$K = \frac{E}{3(1-2\nu)} \tag{2.15}$$

$$G = \frac{E}{2(1+\nu)} \tag{2.16}$$

Plasticity

The following concepts from plasticity are summarised:

- yield surface (f): when stress increment touches the yield surface plastic strain increment will occur. Note that occasionally yield surface, yield criteria, and yield function are used interchangeably. This can be a fixed surface as in e.g. Mohr Coulomb model (MC model) or a non-fixed surface that will be expanded or contracted as in e.g. hardening soil model (HS model). However, in elastoviscoplastic soft soil creep model (SSC) there is no such a yield surface. Instead viscoplastic strains will occur always with time and creep rate will be controlled by a non-fixed reference surface evolving with preconsolidation stress state.

- Potential surface (g): In associated flow rule potential and yield surface are equal ($f = g$) , whereas in non-associated flow rule ($f \neq g$). Viscoplastic strain increment vector is gradient of potential surface with respect to stress vector times plastic multiplier. In SSC potential function is equivalent isotropic pressure ($g = p^{eq}$) which is a function of stress state and inclination of critical state line M. The parameter M determines top of the ellipse and consequently shape of cap in the ellipse. For a constant state of stress p^{eq} the ellipse represents a contour of constant volumetric creep strain rate.
- Hardening: It can be expressed by equation(s) describing the evolution of hardening sate variable(s) e.g. degree of mobilisation, kinematic hardening in anisotropy, or void ratio. The hardening parameter in SSC is the equivalent isotropic preconsolidation pressure that is a function of accumulated volumetric creep strain with time.
- Failure surface (F): determines the ultimate yield surface e.g Mohr Coulomb failure criteria.

2.2 Existing creep constitutive models

2.2.1 Soft soil creep (SSC)

The soft soil creep model (SSC) is the standard creep model in Plaxis that is being used to simulate the soft soil response for monotonic compression problems. As an 'advanced' soil model, SSC possesses several features: (1) stress-dependent stiffness (logarithmic compression 'law'); (2) distinction between primary loading and unloading-reloading; (3) time-dependent compression; (4) memory of preconsolidation stress; (5) soil strength following the Mohr-Coulomb (MC) failure criteria; (6) yield surface adapted from the Modified Cam-Clay model (MCCM); (7) associated flow rule for plastic strains (PLAXIS, 2012). Table 2.1 shows the model input parameters.

Table 2.1: Plaxis SSC input parameters

Parameter	Description	Unit
λ^*	modified compression index	[-]
κ^*	modified swelling index	[-]
μ^*	modified creep index	[-]
ν_{ur}	Poisson's ratio for unloading-reloading	[-]
K_0^{NC}	horizontal to vertical stress ratio at NC region	[-]
OCR	overconsolidation ratio	[-]
POP	preoverburden stress	[kPa]
K_0	horizontal to vertical stress ratio at rest	[-]
c	cohesion	[kPa]
ϕ	friction angle	[°]
ψ	dilatancy angle	[°]

Figure 2.1 illustrates how the isotache concept is used in Plaxis SSC. The initial soil state is given by point A and EOP consolidation by point B. In order to reach point B the SSC model assumes that the elastic strain will occur at time equal to zero and the viscoplastic strain will develop during the entire period.

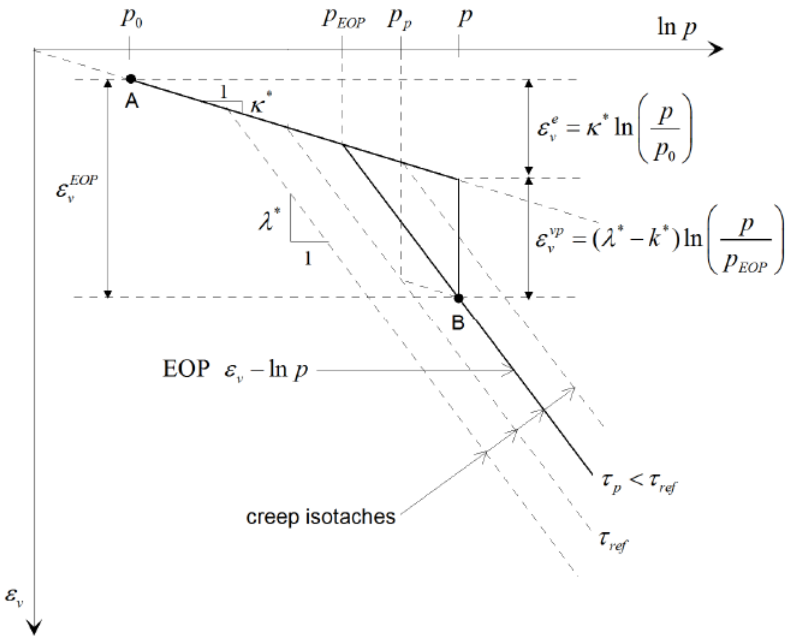
p_0
p_{EOP}
p_p
p
$\ln p$
A
1
κ^*
ε_v^{EOP}
λ^*
1
$\varepsilon_v^e = \kappa^* \ln\left(\frac{p}{p_0}\right)$
$\varepsilon_v^{vp} = (\lambda^* - k^*)\ln\left(\frac{p}{p_{EOP}}\right)$
B
EOP $\varepsilon_v - \ln p$
$\tau_p < \tau_{ref}$
creep isotaches
τ_{ref}
ε_v

Figure 2.1: The isotache concept as used in SSC (Degago, 2011)

The SSC model (Stolle et al., 1999a) uses the creep time dependent stain rate as expressed by Equation (2.17). Creep strain rate as a function of time is defined with Equation (2.17). Where $\dot{\varepsilon}$ is the strain rate, t is time and μ^* is the modified creep index parameter. The Plaxis SSC model uniquely relates the effective stress state (p^{eq}) and the equivalent preconsolidation stress (p_p^{eq}), see Equation (2.18). Where τ is the reference time corresponding to the OCR. Note that OCR is not an intrinsic soil parameter, rather it is dependent on time interval used between each load increments in the oedometer test. Reference time τ is set to one day (24-h) in the SSC model and therefore OCR should be determined with standard incremental oedometer tests with one day load steps. As can be seen from Equation (2.18), modified creep index μ^*, creep ratio $\frac{\lambda^*-\kappa^*}{\mu^*}$ and overconsolidation ratio OCR are governing soil parameters for calculation of creep strain rates. For p^{eq} less than p_p^{eq} creep rate is negligible and for p^{eq} greater than p_p^{eq} time dependent deformation is of more significance.

$$\dot{\varepsilon} = \frac{\mu^*}{t} \tag{2.17}$$

$$\dot{\varepsilon}_{vol}^{vp} = \frac{\mu^*}{\tau}\left(\frac{p^{eq}}{p_p^{eq}}\right)^{\frac{\lambda^*-\kappa^*}{\mu^*}} = \frac{\mu^*}{\tau}\left(\frac{1}{OCR^*}\right)^{\frac{\lambda^*-\kappa^*}{\mu^*}} \tag{2.18}$$

Figure 2.2 shows the Plaxis SSC model reference surface and equivalent mean stress in $p-q$ space. As can be seen from figure, MCCM's elliptical yield surface is cut off by Mohr-Coulomb failure line. The inclination of critical state (CS) line M_{cs} is determined by soil friction angle (ϕ). Plaxis SSC does not allow the stress state to reach CS. Top of the extended ellipse in SSC is controlled by an internal model parameter M that is dependent primarily on K_0^{NC}. In the next chapter a critical state soft soil creep model will be implemented and it will be validated against the Plaxis SSC model.

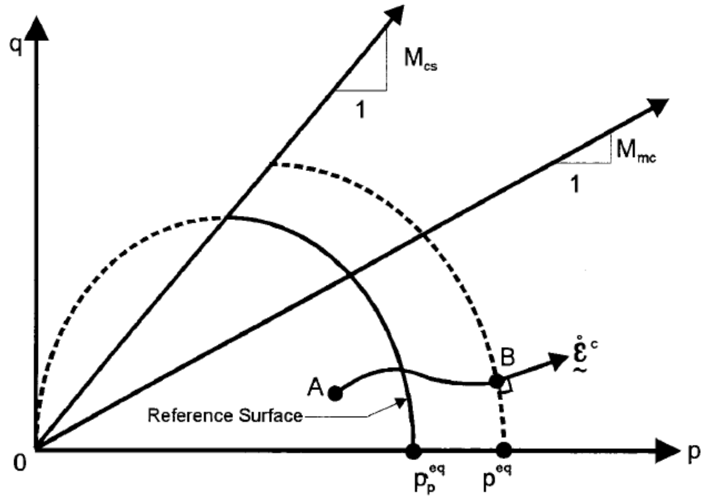

Figure 2.2: Plaxis SSC's reference surface and quivalent mean stress in $p-q$ stress space (Stolle et al., 1999b)

2.2.2 Other existing creep models

Creep user defined soil models (UDSMs) that include more plasticity features compared to SSC can be found in literature e.g. (1) Anisotropic Creep Model (ACM) (Leoni et al., 2009), (2) non-Associated Creep Model for Structured Anisotropic Clay (n-SAC) (Grimstad and Degago, 2010), and (3) Structured Anisotropic Creep Model (Creep-SCLAY1S) (Sivasithanparam, 2012). The purpose of this work is not to go to the details or equations for these models.

Table 2.2 shows the comparison of creep constitutive models used in this study (Plaxis SSC, and two implemented models CS-SSC and CS-SSCG) and other creep models (ACM, n-SAC, Creep-SCLAY1S). Creep modelling started with the assumption of contours of constant creep strain rates for constant equivalent mean stress. This assumption is used in e.g. Plaxis SSC and ACM. This approach, applying creep term on volumetric creep strain rate, gives creep strain rates that are always positive. Consequently, this does not allow the stress path to reach to the left side of the Cam-Clay ellipse regardless whether it is cut off by a failure criteria or not. Therefore, swelling behaviour cannot be simulated. This issue resolved by applying the creep term on the plastic multiplier (Grimstad, 2009), i.e. the assumption of constant rate of plastic multiplier. This idea is used in development of creep models e.g. n-SAC, Creep-SCLAY1S, and also the two implemented models in this study (CS-SSC and CS-SSCG).

Table 2.2: Comparison of creep constitutive models

Model	Plasticity					Elasticity	
	Creep		Anisotropy	destruc.	Lode angle	Poisson's ratio	Shear stiffness
	Vol. creep	Pl. multiplier					
Plaxis SSC	✓	-	-	-	-	✓	-
ACM	✓	-	✓	-	-	✓	-
Creep-SCLAY1S	-	✓	✓	✓	✓	✓	-
n-SAC	-	✓	✓	✓	✓	✓	-
CS-SSC	-	✓	-	-	✓	✓	-
CS-SSCG	-	✓	-	-	✓	-	✓

Models with destructuration, n-SAC and Creep-SCLAY1S, can simulate the post peak strain softening of the soil. However, the numerical analysis of strain softening problems by means of the conventional finite element method is well known to suffer from severe mesh dependency (Schädlich and Schweiger, 2012). Models with anisotropy use the rotated ellipse while isotropic creep models used in this study have non-rotated ellipse. Note that the elasticity formulation is identical for all the models except for the CS-SSCG model - all the models need Poisson's ratio as an input elastic parameter whereas CS-SSCG needs shear stiffness.

Chapter 3

Implementation and Verification of a Critical State Soft Soil Creep Model (CS-SSC)

In this chapter implementation of a critical state soft soil creep model (CS-SSC) will be demonstrated. The performance of the model is similar to Plaxis SSC. The CS-SSC model will be verified against Plaxis SSC at element level using Plaxis soil test. CS-SSC is a basis to implement a new critical state soft soil creep model with shear stiffness (CS-SSCG) in the next chapter.

3.1 Plaxis user defined soil model

The development of stress state in Plaxis finite element package (`http://www.plaxis.nl/`) is treated as an incremental procedure within steps (discretisation in time), also in quasi static time independent problems in which full load can be considered to be applied instantaneously. Discretisation in space will be obtained by generating a mesh with a finite number of elements. In a nutshell, real problems with infinite degrees of freedom (DOF) will simplify to mathematical models with finite DOF. In Plaxis 15-node triangular elements are commonly used with 12 stress (integration, gauss) points. Each phase will be divided into load steps. For each load step and each integration point, Plaxis will provide a strain increment that satisfies the difference between external load and internal reactions. For each step this is done iteratively (global iterative procedure) since the stiffness matrix is usually not constant. In doing so constitutive soil models are responsible for the local integration. It means that for each global iteration and each integration point, local iterative procedure will calculate the stress increment and update the state variables. This can be formulated either explicitly or implicitly which will be discussed in this chapter.

Plaxis has a facility that allows to implement a user defined soil model (UDSM). This requires a Fortran subroutine 'User_Mod' that is compiled as a Dynamic Link Library (DLL) file. UDSM subroutine has 31 arguments of which some should be assigned by the user and the rest will be provided by Plaxis. The structure of such a subroutine in Plaxis is divided into 6 IDTasks. In IDTask 1, state variables are initialised. IDTask 2 is the core of the USDM subroutine that deals with local integration. Elastic matrix should be assigned in IDTask 3 and 6 and its type should be set in IDTask 5. Number of state variables is defined in IDtask 4. In principle, UDSM gives information about the current stresses and state variables while Plaxis gives information about the previous ones as well as the strain and time increments. For more details, see Appendix B and Plaxis (2014).

Several compilers can be employed to make the DLL file including: (1) G95 (`http://www.g95.org`), (2) NAG Fortran compiler (`http://www.nag.co.uk/nagware/np.asp`), (3) Lahey Fortran compiler (`http://www.lahey.com/lgf10/lgfshasta.htm`) and (4) Intel Fortran compiler (`https://software.intel.com/en-us/fortran-compilers`). G95 is a free Fortran compiler that can be used to make a 32-bit DLL file with the following command: g95 usrmod.for -o usrmod.dll -shared -fcase-upper -fno-underscoring -mrtd

Plaxis can also run 64-bit calculation provided that the UDSM is compiled as a 64-bit DLL file as well. For this purpose other commercial compilers that introduced should be utilised. In this work both G95 and NAG Fortran compiler are used successfully.

3.2 Model development and implementation

3.2.1 Model parameters

Table 3.1 shows parameters in the CS-SSC model. Note that these are the same parameters as used in Plaxis SSC. K_0 is the ratio of horizontal stress to vertical stress at initial condition

Table 3.1: CS-SSC input parameters

Parameter	Description	Unit
λ^*	modified compression index	[-]
κ^*	modified swelling index	[-]
μ^*	modified creep index	[-]
ν_{ur}	Poisson's ratio for unloading-reloading	[-]
K_0^{NC}	horizontal to vertical stress ratio at NC region	[-]
OCR_τ	overconsolidation ratio at reference time	[-]
POP_τ	preoverburden stress at reference time	[kPa]
K_0	horizontal to vertical stress ratio at rest	[-]
M	model internal parameter	[-]
τ	reference time	[day]

(K_0-condition), see Equation (3.1). K_0^{NC} is the ratio of horizontal stress increment to vertical stress increment at normally consolidated stress range as expressed by Equation (3.2). This value is of high significance for settlement problems and preferably should be determined from K_0-oedometer test in NC-region. In case no information is available for K_0^{NC}, its value can be estimated using Jaky's formula (3.3). Similarly, for oedometer OC-region the parameter K_0^{OC} can be defined with Equation (3.4). Theoretically, this ratio is dependent on Poisson's ratio for unloading-reloading, see Equation (3.5).

$$K_0 = \frac{\sigma_{xx0}}{\sigma_{yy0}} \tag{3.1}$$

$$K_0^{NC} = \left(\frac{\Delta\sigma_{xx}}{\Delta\sigma_{yy}}\right)_{NC} \tag{3.2}$$

$$K_0^{NC} = 1 - \sin\phi \tag{3.3}$$

$$K_0^{OC} = \left(\frac{\Delta\sigma_{xx}}{\Delta\sigma_{yy}}\right)_{OC} \tag{3.4}$$

$$K_0^{OC} = \frac{\nu_{ur}}{1-\nu_{ur}} \tag{3.5}$$

OCR_τ is initial overconsolidation ratio corresponding to the reference time τ. The subscript τ is given to emphasise that OCR in not an intrinsic soil property but a rate dependent parameter which is linked to the reference time. OCR and POP relates the initial vertical stress to the initial vertical preconsolidation stress $\sigma_{vc}(P_c)$, see Equation (3.6) and (3.7).

$$OCR_\tau = \frac{\sigma_{vc0}}{\sigma_{v0}} = \frac{\sigma_{yyc0}}{\sigma_{yy0}} \tag{3.6}$$

$$POP_\tau = \sigma_{vc0} - \sigma_{v0} = \sigma_{yyc0} - \sigma_{yy0} \tag{3.7}$$

3.2.2 Mathematical formulation

Similar to Plaxis SSC the potential surface is a non-rotated symmetrical ellipse formulated by Equation (3.8). The potential surface can also be expressed by deviatoric stress vector, see Equation (3.9). The definition of potential function in terms of deviatoric stress $\boldsymbol{\sigma_d}$ can be advantageous, especially when including other vector variables in the constitutive model e.g. anisotropy.

$$p^{eq} = p + \frac{q^2}{p\mathrm{M}^2} \tag{3.8}$$

$$p^{eq} = p + \frac{\frac{3}{2}\left(\boldsymbol{\sigma_d^T} \cdot \boldsymbol{\sigma_d}\right)}{pM^2} \tag{3.9}$$

Where p is the mean stress or isotropic stress, q is the deviatoric stress invariant, p^{eq} is the equivalent mean stress or equivalent isotropic stress. The stress ratio η is the ratio between the deviatoric stress and the mean stress, see Equation (3.10). The range of the stress ratio is: $0 \le \eta \le M$. The lower limit implies isotropic stress state whereas the upper limit indicates critical state (CS). Critical state is when the stress path in $p-q$ plot reaches the top of ellipse where the potential surface gradient vector has no horizontal component. Therefore unlimited amount of shear strain can occur while the volumetric deformation is almost constant (failure). Equation (3.11) and (3.12) are horizontal and vertical components of the potential surface gradient vector in p-q plot. The stress ratio for NC-region and K_0-condition can be defined by Equation (3.13) and (3.14). Note that: $0 < \eta_{K_0^{NC}} \le \eta_{K_0} \le M$.

$$\eta = \frac{q}{p} \tag{3.10}$$

$$\frac{\partial p^{eq}}{\partial p} = \frac{M^2 - \eta^2}{M^2} \tag{3.11}$$

$$\frac{\partial p^{eq}}{\partial q} = \frac{2\eta}{M} \tag{3.12}$$

$$\eta_{K_0^{NC}} = \frac{3(1 - K_0^{NC})}{1 + 2K_0^{NC}} \tag{3.13}$$

$$\eta_{K_0} = \frac{3(1 - K_0)}{1 + 2K_0} \tag{3.14}$$

The strain rate is the ratio of the strain increment to the time increment, see Equation (3.15). In contrast to Plaxis SSC where the creep term ($\frac{\lambda^*-\kappa^*}{\mu^*}$) is applied to the volumetric creep strain rate (Equation (3.16)), in this work creep term is applied to the plastic multiplier Λ. This relationship is given in Equation (3.17). Where p_p^{eq} is the equivalent isotropic preconsolidation stress. At the initial condition this value (p_{p0}^{eq}) is calculated with Equation (3.18). Where $p_{p_0^{NC}}$ is initial isotropic preconsolidation stress and $q_{p_0^{NC}}$ is initial deviatoric preconsolidation stress at normally consolidated region which can be calculated by Equation (3.19) and (3.20) , respectively. Note that all the stresses are effective.

As can be seen from Equation (3.21), the equivalent overconsolidation stress OCR_τ^{eq} is of great importance for creep calculation and its initial value will determine the initial creep strain rate. Equation (3.22) states how the equivalent isotropic preconsolidation stress will evolve with the accumulated plastic multiplier. The gradient of the potential surface in 3D-Cartesian space is given by Equation (3.23).

$$\dot{\varepsilon} = \frac{d\varepsilon}{dt} \tag{3.15}$$

$$\dot{\varepsilon}_{vol}^{vp} = \frac{\mu^*}{\tau}\left(\frac{p^{eq}}{p_p^{eq}}\right)^{\frac{\lambda^*-\kappa^*}{\mu^*}} \tag{3.16}$$

$$\dot{\Lambda} = \frac{d\Lambda}{dt} = \frac{\mu^*}{\tau}\left(\frac{M^2}{M^2-\eta_{K_0^{nc}}^2}\right)\left(\frac{p^{eq}}{p_p^{eq}}\right)^{\frac{\lambda^*-\kappa^*}{\mu^*}} \tag{3.17}$$

$$p_{p0}^{eq} = p_{p_0^{NC}} + \frac{q_{p_0^{NC}}^2}{\left(p_{p_0^{NC}}\right)\mathrm{M}^2} \tag{3.18}$$

$$p_{p_0^{NC}} = \left(\frac{1+2K_0^{NC}}{3}\right)\sigma_{vc} \tag{3.19}$$

$$q_{p_0^{NC}} = \left(1-K_0^{NC}\right)\sigma_{vc} \tag{3.20}$$

$$OCR_\tau^{eq} = \frac{p_p^{eq}}{p^{eq}} \tag{3.21}$$

$$\frac{dp_p^{eq}}{d\Lambda} = \frac{p_p^{eq}}{\lambda^*-\kappa^*}\frac{\partial p^{eq}}{\partial p} \tag{3.22}$$

$$\frac{\partial p^{eq}}{\partial \boldsymbol{\sigma}} = \begin{pmatrix} \frac{2\mathrm{pM}^2 - \mathrm{p}^{\mathrm{eq}}\mathrm{M}^2 + 3\left[(\sigma_{\mathrm{xx}} - \sigma_{\mathrm{yy}}) + (\sigma_{\mathrm{xx}} - \sigma_{\mathrm{zz}})\right]}{3\mathrm{PM}^2} \\ \frac{2\mathrm{pM}^2 - \mathrm{p}^{\mathrm{eq}}\mathrm{M}^2 + 3\left[(\sigma_{\mathrm{yy}} - \sigma_{\mathrm{xx}}) + (\sigma_{\mathrm{yy}} - \sigma_{\mathrm{zz}})\right]}{3\mathrm{PM}^2} \\ \frac{2\mathrm{pM}^2 - \mathrm{p}^{\mathrm{eq}}\mathrm{M}^2 + 3\left[(\sigma_{\mathrm{zz}} - \sigma_{\mathrm{xx}}) + (\sigma_{\mathrm{zz}} - \sigma_{\mathrm{yy}})\right]}{3\mathrm{PM}^2} \\ \frac{6\sigma_{\mathrm{xy}}}{\mathrm{pM}^2} \\ \frac{6\sigma_{\mathrm{yz}}}{\mathrm{pM}^2} \\ \frac{6\sigma_{\mathrm{zx}}}{\mathrm{pM}^2} \end{pmatrix} \tag{3.23}$$

3.2.3 Numerical implementation

As discussed earlier, in finite element analysis integration of constitutive equations is taken at finite number of points within the mesh. These points are called integration points. The global iterative scheme in Plaxis will give strain increment for each integration point. Accordingly for each integration point, UDSM should provide admissible stress increment to the given strain increment. This procedure is called local integration or return mapping.

Two distinguished numerical schemes can be adopted for the local integration scheme: (1) Explicit Forward Euler integration scheme and (2) Implicit Backward Euler integration scheme (Benz, 2010). Explicit scheme uses the priori known initial stresses and state variables at the beginning of a load step for integration whereas implicit scheme uses the priori not-known stresses and state variables at the end of a load step. Explicit scheme is therefore more straight forward to implement compared to the implicit scheme that requires iterative procedure. Theoretically for the infinitesimal time increments the two schemes will give identical solutions. The level of accuracy for an explicit scheme is highly dependent on the time increment which is provided by Plaxis and solution is not always guaranteed. In practice implicit scheme is commonly used for implementation of UDSMs.

Explicit scheme

The explicit scheme was not adopted for the implementation purpose in this work. It is given here to compare the creep formulation used in Plaxis SSC and CS-SSC in a more straightforward way. Algorithm 1 shows an explicit scheme procedure that can be used for the CS-SSC model. The equivalent stresses at the beginning and at the end of the current step are denoted by subscript n and $n+1$, respectively with the initial condition $n = 0$. Algorithm 2 shows an explicit scheme procedure that can be used for Plaxis SSC. Note that Plaxis adopts Mohr-Coulomb failure criteria that is not included in this algorithm.

Algorithm 1 Explicit scheme for CS-SSC

$$\Delta\Lambda = \frac{\mu^*}{\tau}\left(\frac{M^2}{M^2-\eta^2_{k_0^{NC}}}\right)\left(\frac{p^{eq}}{p_p^{eq}}\right)_n^{\frac{\lambda^*-\kappa^*}{\mu^*}}\Delta t \tag{3.24}$$

$$\Delta p_p^{eq} = \frac{p_p^{eq}}{\lambda^*-\kappa^*}\left(\frac{\partial p^{eq}}{\partial p}\right)_n \Delta\Lambda \tag{3.25}$$

$$\Delta\boldsymbol{\varepsilon}^{vp} = \left(\frac{\partial p^{eq}}{\partial \boldsymbol{\sigma}}\right)_n \Delta\Lambda \tag{3.26}$$

$$\Delta\boldsymbol{\varepsilon}^{e} = \Delta\boldsymbol{\varepsilon} - \Delta\boldsymbol{\varepsilon}^{vp} \tag{3.27}$$

$$\Delta\boldsymbol{\sigma} = \boldsymbol{D}\cdot\Delta\boldsymbol{\varepsilon}^{e} \tag{3.28}$$

$$p_p^{eq}{}_{n+1} = p_p^{eq}{}_{n} + \Delta p_p^{eq} \tag{3.29}$$

$$\boldsymbol{\sigma}_{n+1} = \boldsymbol{\sigma}_{n} + \Delta\boldsymbol{\sigma} \tag{3.30}$$

Implicit scheme

The implicit scheme is adopted in this work for implementation of the CS-SSC model and the CS-SSCG model. The state variables are vector or scalar quantities that describes the soil response in each integration point to external actions. For instance, stress, equivalent preconsolidation pressure, plastic multiplier and void ratio can be state variables while strain and time can be external actions. In numerical implementation it is advantageous to introduce the state variables that are not dependent. Equation (3.45) gives the state variables used in CS-SSC. As can bee seen from the equation, the stress components, the equivalent preconsolidation pressure and the plastic multiplier are the state variables. Note that in this work the strain increment and the time increment are the external actions. Algorithm 3 illustrates the implicit scheme used for implementation of the CS-SSC model. The state variables at the beginning and at the end of the current step are denoted by subscript n and $n+1$, respec-

Algorithm 2 Explicit scheme for Plaxis SSC

$$\Delta\varepsilon^{vp}_{vol} = \frac{\mu^*}{\tau}\left(\frac{p^{eq}}{p^{eq}_{p}}\right)_n^{\frac{\lambda^*-\kappa^*}{\mu^*}} \times \Delta t \tag{3.31}$$

$$\Delta p^{eq}_{p} = \frac{{p^{eq}_{p}}_{n}}{\lambda^*-\kappa^*}\Delta\varepsilon^{vp}_{vol} \tag{3.32}$$

$$\Delta\Lambda = \frac{\Delta\varepsilon^{vp}_{vol}}{\left(\frac{\partial p^{eq}}{\partial p}\right)_n} \tag{3.33}$$

$$\Delta\boldsymbol{\varepsilon}^{vp} = \Delta\Lambda\left(\frac{\partial p^{eq}}{\partial\boldsymbol{\sigma}}\right)_n \tag{3.34}$$

$$\Delta\boldsymbol{\varepsilon}^{e} = \Delta\boldsymbol{\varepsilon} - \Delta\boldsymbol{\varepsilon}^{vp} \tag{3.35}$$

$$\Delta\boldsymbol{\sigma} = \boldsymbol{D}\cdot\Delta\boldsymbol{\varepsilon}^{e} \tag{3.36}$$

$${p^{eq}_{p}}_{n+1} = {p^{eq}_{p}}_{n} + \Delta p^{eq}_{p} \tag{3.37}$$

$$\boldsymbol{\sigma}_{n+1} = \boldsymbol{\sigma}_{n} + \Delta\boldsymbol{\sigma} \tag{3.38}$$

tively. Superscript i and $i+1$ indicates the current and the next iteration. Corresponding to the state variables the residuals at the current iteration i are defined through Equation (3.47) to (3.49). Note that $\boldsymbol{r_1}$ is the vector of stress residual that contains 6 stress components while r_2 and r_3 are scalar residuals that are defined for equivalent mean preconsolidation pressure and plastic multiplier, respectively. The Jacobian matrix $\boldsymbol{J}$ is the partial derivative of the residuals with respect to the variables, see Equation (3.39). In a closed form Jacobian matrix can be expressed by Equation (3.40). Equation (3.41) to (3.44) state some of the partial derivatives in the Jacobian matrix. MATLAB (`www.mathworks.com/products/matlab/`) can be used to facilitate the calculation of other partial derivatives in the Jacobian matrix.

$$\boldsymbol{J} = \left(\begin{array}{cccccc|c|c}
\partial r_1/\partial\sigma_{xx} & \partial r_1/\partial\sigma_{yy} & \partial r_1/\partial\sigma_{zz} & \partial r_1/\partial\sigma_{xy} & \partial r_1/\partial\sigma_{yz} & \partial r_1/\partial\sigma_{zx} & \partial r1/\partial p_p^{eq} & \partial r1/\partial\Lambda \\
\partial r_2/\partial\sigma_{xx} & \partial r_2/\partial\sigma_{yy} & \cdots & \cdots & \cdots & \partial r_2/\partial\sigma_{zx} & \partial r_2/\partial p_p^{eq} & \partial r_2/\partial\Lambda \\
\partial r_3/\partial\sigma_{xx} & \vdots & \ddots & & & \vdots & \vdots & \vdots \\
\partial r_4/\partial\sigma_{xx} & \vdots & & \ddots & & \vdots & \vdots & \vdots \\
\partial r_5/\partial\sigma_{xx} & \vdots & & & \ddots & \vdots & \vdots & \vdots \\
\partial r_6/\partial\sigma_{xx} & \partial r_6/\partial\sigma_{yy} & \cdots & \cdots & \cdots & \partial r_6/\partial\sigma_{zx} & \partial r_6/\partial p_p^{eq} & \partial r_6/\partial\Lambda \\
\hline
\partial r_7/\partial\sigma_{xx} & \partial r_7/\partial\sigma_{yy} & \cdots & \cdots & \cdots & \partial r_7/\partial\sigma_{zx} & \partial r_7/\partial p_p^{eq} & \partial r_7/\partial\Lambda \\
\hline
\partial r_8/\partial\sigma_{xx} & \partial r_8/\partial\sigma_{yy} & \cdots & \cdots & \cdots & \partial r_8/\partial\sigma_{zx} & \partial r_8/\partial p_p^{eq} & \partial r_8/\partial\Lambda
\end{array}\right) \tag{3.39}$$

$$\boldsymbol{J} = \begin{pmatrix}
\partial\boldsymbol{r_1}/\partial\boldsymbol{\sigma} & \partial\boldsymbol{r_1}/\partial p_p^{eq} & \partial\boldsymbol{r_1}/\partial\Lambda \\
\left(\partial r_7/\partial\boldsymbol{\sigma}\right)^T & \partial r_7/\partial p_p^{eq} & \partial r_7/\partial\Lambda \\
\left(\partial r_8/\partial\boldsymbol{\sigma}\right)^T & \partial r_8/\partial p_p^{eq} & \partial r_8/\partial\Lambda
\end{pmatrix} \tag{3.40}$$

$$\partial\boldsymbol{r_1}/\partial p_p^{eq} = \boldsymbol{0} \tag{3.41}$$

$$\partial\boldsymbol{r_1}/\partial\Lambda = \boldsymbol{D}\cdot\frac{\partial p^{eq}}{\partial\boldsymbol{\sigma}} \tag{3.42}$$

$$\partial r_7/\partial\Lambda = -\frac{dp_p^{eq}}{d\Lambda} \tag{3.43}$$

$$\partial r_8/\partial\Lambda = 1 \tag{3.44}$$

Algorithm 3 Implicit scheme for CS-SSC

$$\boldsymbol{V}_{n+1}^{T} = \left(\ \sigma_{\mathrm{xx}}, \sigma_{\mathrm{yy}}, \sigma_{\mathrm{zz}}, \sigma_{\mathrm{xy}}, \sigma_{\mathrm{yz}}, \sigma_{\mathrm{zx}}, \mathrm{p}_{\mathrm{p}}^{\mathrm{eq}}, \Lambda\ \right)_{n+1} \tag{3.45}$$

The state variables above can be expressed in a closed form by replacing the stress components with the stress vector:

$$\boldsymbol{V}_{n+1} = \begin{pmatrix} \boldsymbol{\sigma} \\ \mathrm{p}_{\mathrm{p}}^{\mathrm{eq}} \\ \Lambda \end{pmatrix}_{n+1} \tag{3.46}$$

The following residuals at the current iteration i corresponding to the state variables are defined:

$$\boldsymbol{r_1}_{n+1} = \boldsymbol{\sigma}_{n+1} - \left[\boldsymbol{\sigma}_n + \boldsymbol{D}_{n+1} \cdot (\boldsymbol{\varepsilon}_{n+1} - \boldsymbol{\varepsilon}_n) - \boldsymbol{D}_{n+1} \cdot \frac{\partial p^{eq}}{\partial \boldsymbol{\sigma}} (\Lambda_{n+1} - \Lambda_n)\right] \tag{3.47}$$

$$r_{7\,n+1} = {p_p^{eq}}_{n+1} - \left[{p_p^{eq}}_n + \left(\frac{dp_p^{eq}}{d\Lambda}\right)_{n+1} (\Lambda_{n+1} - \Lambda_n)\right] \tag{3.48}$$

$$r_{8\,n+1} = \Lambda_{n+1} - \left[\Lambda_n + \dot{\Lambda}_{n+1} (t_{n+1} - t_n)\right] \tag{3.49}$$

The Jacobian matrix $\boldsymbol{J}$ is the partial derivative of the residuals with respect to the variables:

$$\boldsymbol{J}_{n+1} = (\partial \boldsymbol{r} / \partial \boldsymbol{V})_{n+1} \tag{3.50}$$

The following non-linear system of partial differential equations should be solved:

$$\boldsymbol{J}_{n+1} \cdot d\boldsymbol{V}_{n+1} = -\boldsymbol{r}_{n+1} \tag{3.51}$$

For implementation purpose the iterative Newton-Raphson method is adopted to solve the incremental format of the above equation:

$$\boldsymbol{J}_{n+1}^{i} \cdot \Delta \boldsymbol{V}_{n+1}^{i} = -\boldsymbol{r}_{n+1}^{i} \tag{3.52}$$

By multiplying the above equation with inverse of the Jacobian matrix $\boldsymbol{J}^{-1}$:

$$\Delta \boldsymbol{V}_{n+1}^{i} = -\left(\boldsymbol{J}_{n+1}^{-1} \cdot \boldsymbol{r}_{n+1}\right)^{i} \tag{3.53}$$

The state variables at the current iteration i will be updated for the next iteration $i+1$:

$$\boldsymbol{V}_{n+1}^{i+1} = \boldsymbol{V}_{n+1}^{i} + \Delta \boldsymbol{V}_{n+1}^{i} \tag{3.54}$$

The iterative scheme will continue until the desired tolerance is reached at the current iteration:

$$\left(\boldsymbol{r}_{n+1}^{T} \cdot \boldsymbol{r}_{n+1}\right)^{i} < TOl^{2} \tag{3.55}$$

3.2.4 Numerical aspects

Some of the important numerical aspects when implementing a UDSM in Plaxis are summarised:

- In soil mechanics it is a tradition to use the positive sign convection for compression and negative for extension. In Plaxis implementation, however, the sign convection is opposite.
- Model performance should be tested first at the element level and with different type of tests e.g. triaxial or oedometer test and with different initial conditions e.g. isotropic or anisotropic initial condition. This should be carried out to ensure that the model performance is as expected and/or possible bugs can be diagnosed. Note that sometimes a small change in the computer code may improve the performance of the model significantly. The second step is to test the model in a boundary value problem.
- At the beginning of the each phase Plaxis will call IDTask 1 for initialising the state variables in a boundary value problem. Therefore the state variables in Fortran code must be programmed such that their initial value assigned only once.
- Note the numerical difference between the state variables and the model parameters. Plaxis stores state variables for each integration points whereas the model parameters are scalars that are stored in a vector named ‘props’.
- In the implicit scheme another alternative approach to solve the system of equations is to use the guess elimination method.
- If the Jacobian matrix is close to the singular matrix (ill-conditioned), the iteration procedure might not converge. Therefore, for the implementation purpose it is advantageous to control the condition of Jacobian matrix. If iteration does not converge until maximum number of iterations, substeppping (recursive procedure) should be carried out - the strain increment and/or time increment will be divided into smaller steps. In a boundary value problem in Plaxis, ‘NaN found error’ is usually caused by this problem. This issue can also be resolved by decreasing the tolerance error and/or decreasing the maximum load fraction per step in ‘control parameters’ tab. This error could also be due to bad input parameters.

3.3 Model verification at element level

From Boston Blue Clay (BBC) layer under the MIT-MDPW embankment two soil elements BBC1 and BBC2 were studied (more details about the MIT-MDPW embankment and selection of parameters will be given in Chapter 4). BBC1 and BBC2 elements are from the representative depths of 10 m and 28 m under the embankment, respectively. The initial stress condition can be seen in Table 3.2. The clay parameters are given in Table 3.3. Incremental loading (IL) oedometer test and triaxial undrained K_0-consolidated test are simulated with both Plaxis SSC model and the implemented CS-SSC model. Results from CS-SSC are verified against Plaxis SSC.

Table 3.2: Initial stress for the two soil elements BBC1 and BBC2

Soil element	σ_{xx}	σ_{yy}	σ_{zz}
BBC1	-83.66	-94	-83.66
BBC2	-134.4	-240	-134.4

Table 3.3: BBC1 and BBC2 clay parameters

Centre [m]	Layer	γ $[kN/m^3]$	POP_τ OCR_τ	K_0	e_0	λ^*	κ^*	μ^*	k_{x0} [m/day]	k_{y0} [m/day]
-10.5	BBC1	18.5	120	0.89	0.970	0.079	0.020	0.0023	1.51E-04	8.21E-05
-31	BBC2	17.7	1.5	0.56	1.180	0.171	0.043	0.0049	8.73E-05	5.82E-05

$c = 1\ kPa, \phi = 33.4°, \nu_{ur} = 0.1, K_0^{NC} = 0.45$

3.3.1 Simulation of oedometer test

From representative depths of 10 m and 28 m with initial vertical effective stress of 94 kPa and 240 kPa, two oedometer tests are simulated. General soil test facility in Plaxis is used for simulation. No strain increment is allowed for the radial direction x and z while stress increment is applied in the vertical direction y. This will simulate the oedometer test condition. The parameters for soil element at the shallower depth 10 m are taken from BBC1 and for the deeper depth 28 m from BBC2 layer. In each simulation, the sample is loaded from the initial stress condition. From phase 1 onwards the soil element is consolidated with 24-h conventional load increments during 4 days. The summary of the load application can be

Table 3.4: IL oedometer test simulation as defined in Plaxis General Soil Test

IL Oedometer	$\Delta\varepsilon_{xx}$	$\Delta\sigma_{yy}$ [kPa]	$\Delta\varepsilon_{zz}$	Duration [Day]
phase 1	0	-50	0	0.01
phase 2	0	0	0	0.99
phase 3	0	-100	0	0.01
phase 4	0	0	0	0.99
phase 5	0	-200	0	0.01
phase 6	0	0	0	0.99
phase 7	0	-400	0	0.01
phase 8	0	0	0	0.99

seen in Table 3.4. Figure 3.1 shows results from the simulations. The curves are obtained by calculation of the difference between the results from CS-SSCG and Plaxis SSC in percentage. The difference d and the normalised difference d_N are defined by Equation (3.56) and (3.57), respectively.

$$d = (CS - SSCG) - (PlaxisSSC) \tag{3.56}$$

$$d_N = \frac{(CS - SSCG) - (PlaxisSSC)}{PlaxisSSC} \tag{3.57}$$

Figure 3.1a and 3.1b shows the difference in vertical strain versus time in IL oedometer test for BBC1 and BBC2, respectively. As can be seen from the figure the difference between the result from CS-SSC and Plaxis SSC is negligible. The maximum difference occurs at the load application with 0.15 % and 0.3 % for BBC1 and BBC2. Figure 3.1c and 3.1d shows the difference in vertical strain versus vertical stress predicted by the two models for BBC1 and BBC2. Note that the difference is more pronounced at the instant application of the load increments. Figure 3.1e and 3.1f illustrate the normalised difference in predicted deviatoric stress versus mean stress for BBC1 and BBC2 which is less than 0.5 %.

To conclude: In oedometer test the CS-SSC model predicts similar results as Plaxis SSC. Assuming 100 cm vertical displacement the difference as high as 0.1 % will give the deviation as low as 1 mm between the results predicted by the two models. The difference is more pronounced at the points when load increment is applied. Even in these points the difference in vertical strain is less than 0.4 %. The purpose of this type of presentation was to magnify the deviation of the results simulated by the two models, otherwise one can say that CS-SSC and Plaxis SSC are identical under oedometer condition. This verifies the performance of the CS-SSC model at element level. For standard representation of results see Chapter 4.

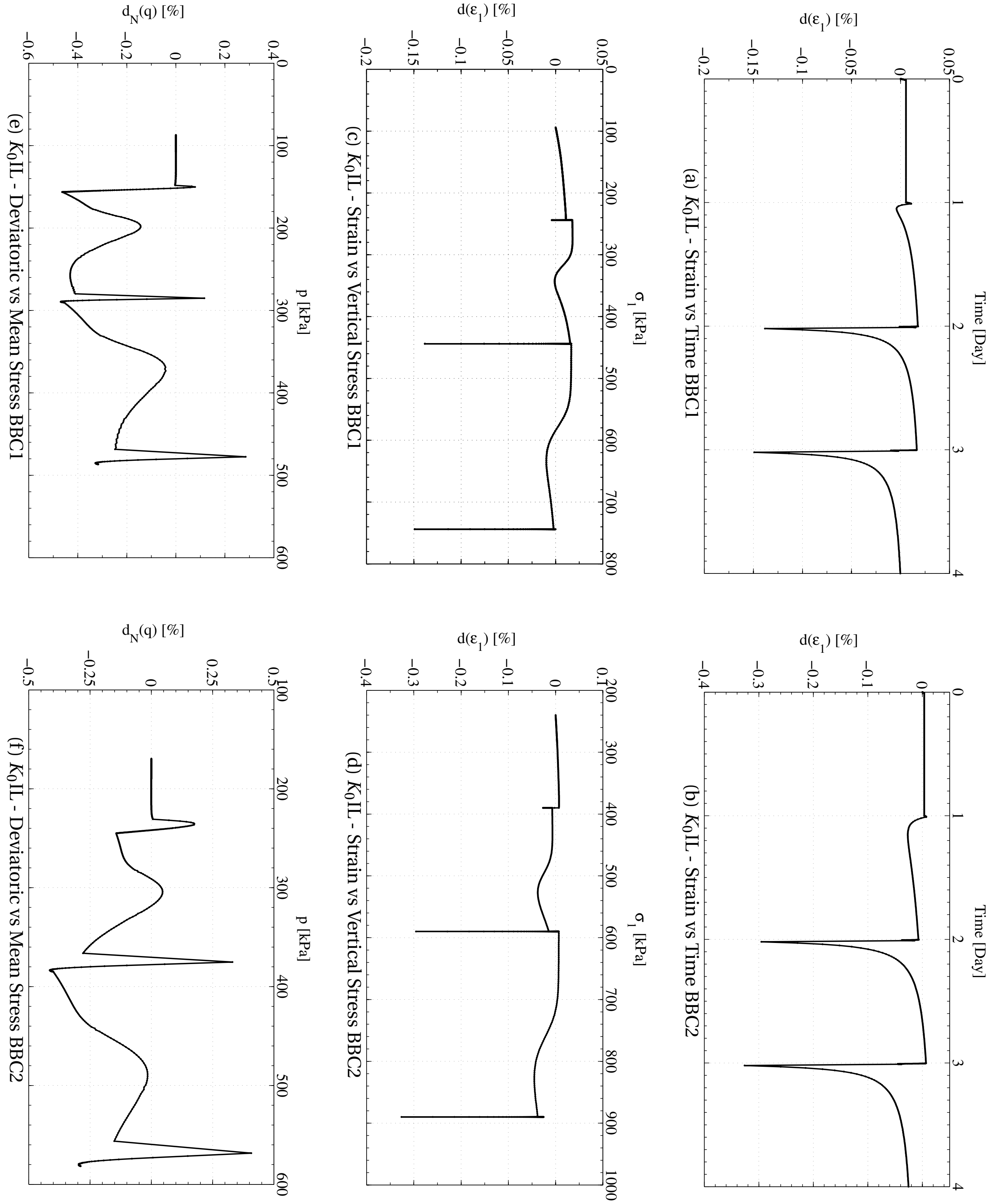

(a) K_0IL - Strain vs Time BBC1

(b) K_0IL - Strain vs Time BBC2

(c) K_0IL - Strain vs Vertical Stress BBC1

(d) K_0IL - Strain vs Vertical Stress BBC2

(e) K_0IL - Deviatoric vs Mean Stress BBC1

(f) K_0IL - Deviatoric vs Mean Stress BBC2

Figure 3.1: CS-SSC & Plaxis SSC (normalised) difference [%] in IL oedometer test

3.3.2 Simulation of triaxial test

Two undrained triaxial compression tests are simulated. First samples are consolidated to K_0-condition and then sheared to failure. The triaxial soil test facility in Plaxis is used for simulation.

Figure 3.2 shows the results from the simulations. The curves are obtained by calculation of normalised stress difference between the prediction from CS-SSC and Plaxis SSC model in percentage. Figure 3.2a and Figure 3.2b shows the normalised difference in deviatoric stress versus major (axial) principal strain for BBC1 and BBC2, respectively. As can be seen from figure the difference is negligible before 0.7 % and 0.85 % strains which represent failure for BBC1 and BBC2 in Plaxis SSC. Large deviation between the prediction of the models after failure is due to different failure criteria. Thus, for the validation purpose our interest should be limited to the stress state before failure. The CS-SSC model allows for reaching critical state. This implies higher deviatoric stress in failure as can bee seen in Figures 3.2a and 3.2b. For stress states before failure the difference between the predictions are negligible, this is less than 2.0 %. Figures 3.2c and 3.2d shows the difference in pore pressure response for BBC1 and BBC2, respectively. Similarly for strains before failure the two models reproduce almost the same results.

To conclude: For strains before Plaxis SSC's failure the performance of the CS-SSC model and the Plaxis SSC model are identical in undrained triaxial compression tests. This verifies the performance of the SSC model at element level.

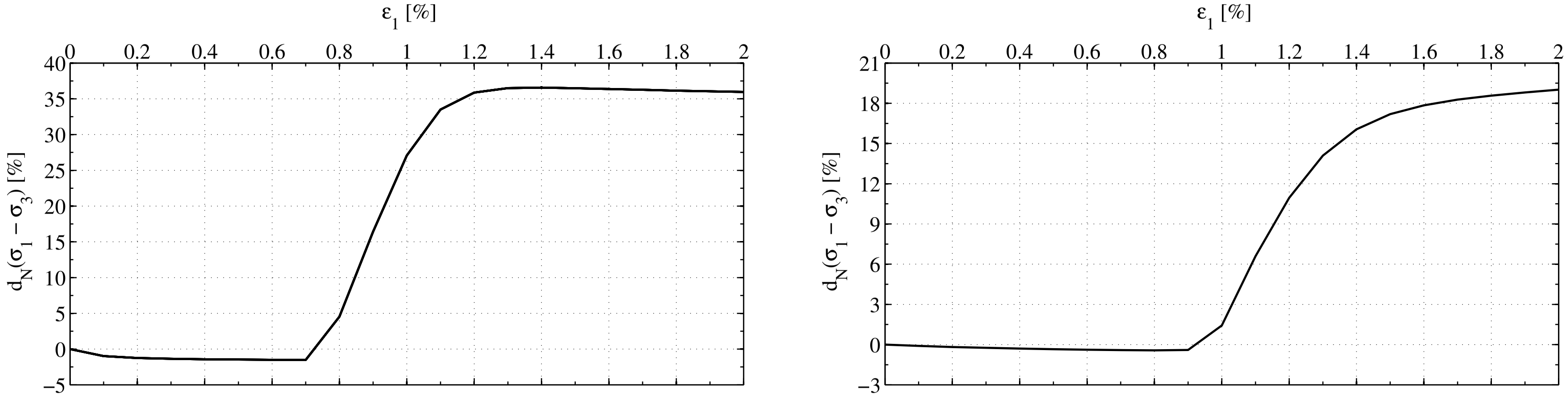

(a) Normalised deviatoric stress-BBC1

(b) Normalised deviatoric stress-BBC2

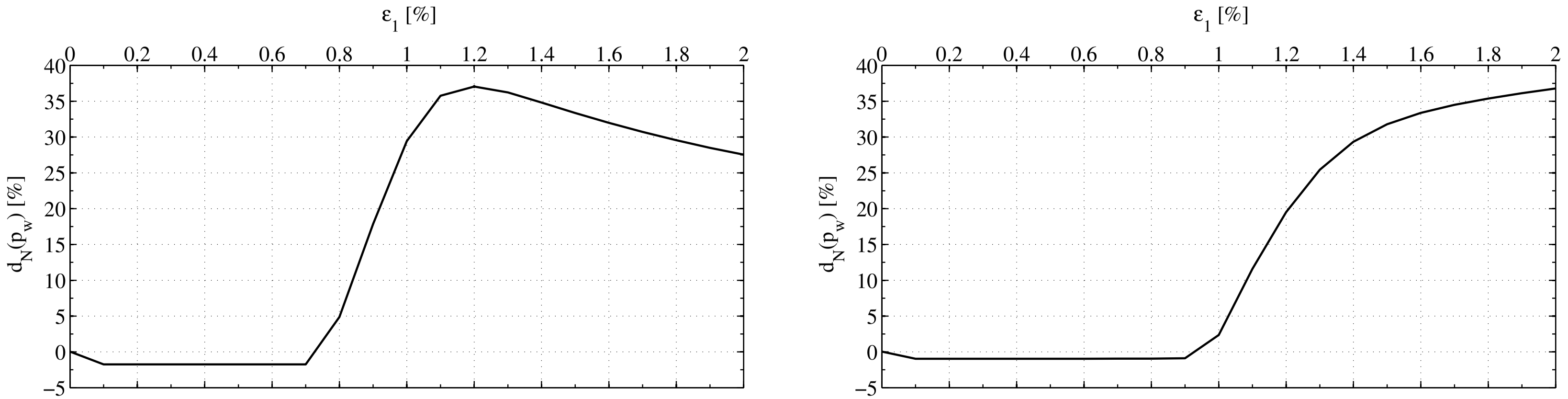

(c) Normalised pore pressure -BBC1

(d) Normalised pore pressure -BBC2

Figure 3.2: CS-SSC & Plaxis SSC normalised difference [%] in UK_0TC test

Chapter 4

Implementation and Verification of a Critical State Soft Soil Creep Model with Shear Stiffness (CS-SSCG)

In this chapter a critical state soft soil creep model with shear stiffness (CS-SSCG) will be implemented and validated. The model is an extension to the CS-SSC model in which constant Poisson's ratio is replaced with mobilised shear stiffness. Lode angle is also adapted to reflect the soil strength anisotropy. To study the influence of this elastic modification (adopting shear stiffness) other features are kept unchanged. Therefore, CS-SSCG and Plaxis SSC are very similar from implementation point of view. The purpose of this study is to improve the horizontal displacements predicted by Plaxis SSC and CS-SSC. The CS-SSCG model will be verified at soil element level. Finally, the model will be validated in a boundary value problem (MIT-MDPW embankment).

4.1 Model development and implementation

4.1.1 Model parameters

Table 4.1 shows the model parameters. The CS-SSCG model requires the same input parameters as Plaxis SSC, except that the Poisson's ratio for unloading-reloading ν_{ur} is replaced by the shear stiffness parameters (y_{ref}, G_{ref}, G_{inc} and η). Figure 4.1 shows a screenshot from the model parameters window in Plaxis.

Table 4.1: CS-SSCG input parameters

Parameter	Description	Unit
λ^*	modified compression index	[-]
κ^*	modified swelling index	[-]
μ^*	modified creep index	[-]
K_0^{NC}	horizontal to vertical stress ratio at NC region	[-]
OCR_τ	overconsolidation ratio at reference time	[-]
POP_τ	preoverburden pressure at reference time	[kPa]
K_0	horizontal to vertical stress ratio at rest	[-]
M_c	model internal parameter	[-]
τ	reference time	[day]
y_{ref}	reference depth	[m]
G_{ref}	shear stiffness at the reference depth	[kPa]
G_{inc}	shear stiffness increment	[kPa/m]

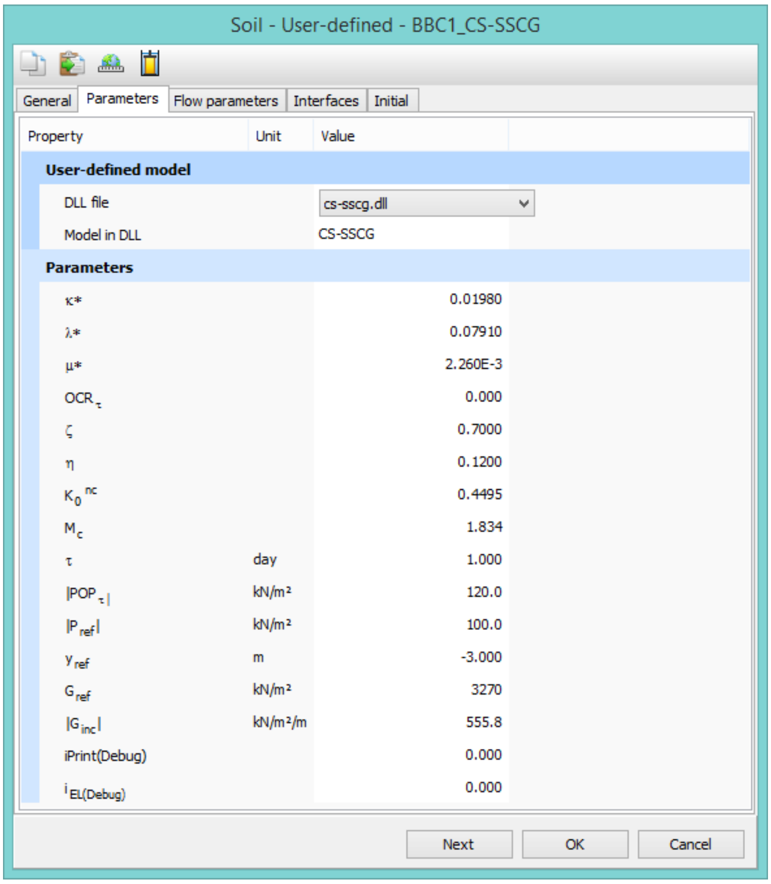

Property	Unit	Value
User-defined model		
DLL file		cs-sscg.dll
Model in DLL		CS-SSCG
Parameters		
κ*		0.01980
λ*		0.07910
μ*		2.260E-3
OCR_τ		0.000
ς		0.7000
η		0.1200
K_0^{nc}		0.4495
M_c		1.834
τ	day	1.000
$\lvert POP_\tau \rvert$	kN/m²	120.0
$\lvert P_{ref} \rvert$	kN/m²	100.0
y_{ref}	m	-3.000
G_{ref}	kN/m²	3270
$\lvert G_{inc} \rvert$	kN/m²/m	555.8
iPrint(Debug)		0.000
$i_{EL(Debug)}$		0.000

Figure 4.1: The CS-SSCG model input parameters window in Plaxis

4.1.2 Mathematical formulation

The CS-SSCG model is developed within the framework of elastoplasticity. The model uses the similar governing equations given in Chapter 3 except for the following differences:

1. Shear stiffness: Poisson's ratio is replaced with shear stiffness in the elastic stiffness matrix.
2. Lode angle dependency: The slope of the critical state line (CSL), M, is a function of the Lode angle.

Degradation of initial shear stiffness

The maximum strain at which soils exhibit almost fully recoverable behaviour is found to be very small. With increasing strain (mobilisation), soil stiffness decays non-linearly. The initial shear stiffness degradation versus logarithmic scale strain exhibits a characteristic S-shape curve, see Figure 4.2. This behaviour is believed to be a fundamental property of all types of geotechnical materials including clays, silts, sands, gravels and rocks under static and dynamic loading and for drained and undrained loading conditions (Benz, 2007). In this work the degradation of initial shear stiffness is formulated in terms of mobilisation degree.

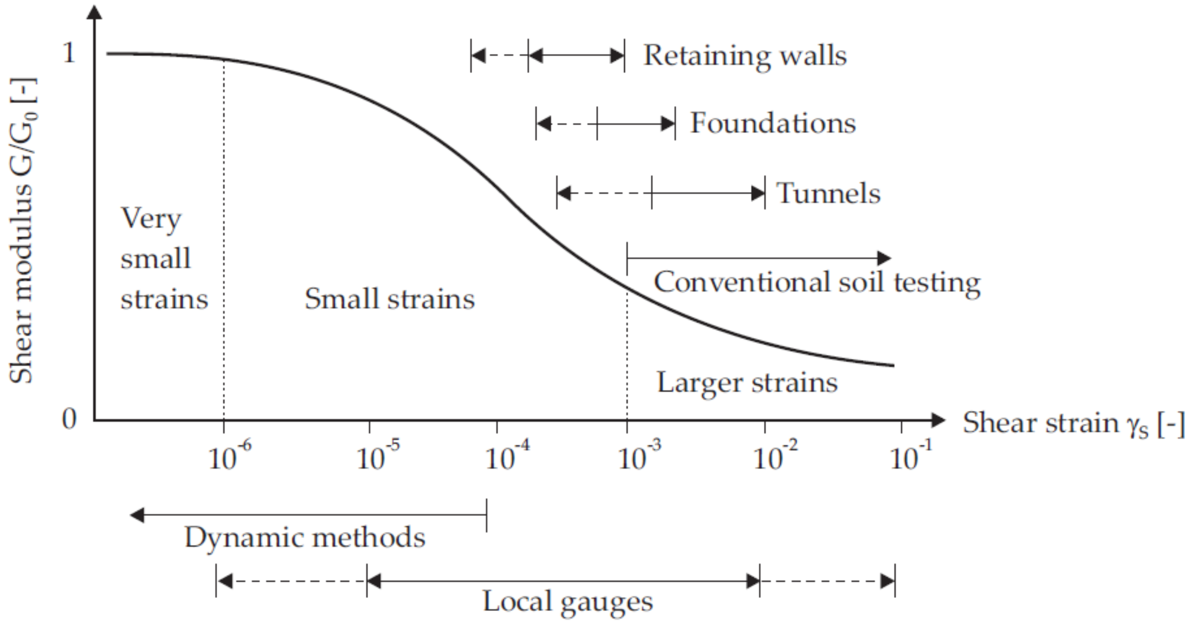

Figure 4.2: Characteristic shear stiffness of soil with typical strain ranges for laboratory tests and structures; after Atkinson and Sällfors (1991) and Mair (1993), from Benz (2007)

For each soil cluster in Plaxis it is possible to specify an initial shear stiffness that varies linearly with depth, see Equation (4.1) and Figure 4.3. For depths above the reference depth y_{ref} the initial shear stiffness is equal to G_{ref} and for y-coordinates below the reference depth the initial shear stiffness varies linearly with depth. Parameter G_{inc} is the increment of initial shear stiffness per unit of depth.

The degree of mobilisation f is defined with Equation (4.2). Where M_θ is the slope of the critical state line which is dependent on lode angle θ. The Macaulay brackets is equivalent to the Equation (4.3). Note that the mobilisation degree (f) is zero for stress ratios (η) equal or less than the stress ratio at rest (η_{K0}). The mobilised shear stiffness G_M is defined by Equation (4.4). Where ζ is the degradation factor that controls the decay of the initial shear stiffness with increasing mobilisation, see Figure 4.4. This parameter can be obtained by curve fitting to the laboratory tests. Numerically, it can be in the range: $0 < \zeta < 1$. Another alternative for using this model is to set $\zeta = 0$ and use G_{50} instead of G_0. For $\zeta = 0$ nonlinear elasticity (hypoelasticity) will be deactivated. It means that degradation of shear stiffness will be switched off.

$$G_0 = G_{ref} + max\left[\left(y_{ref} - y\right) G_{inc},\ 0\right] \tag{4.1}$$

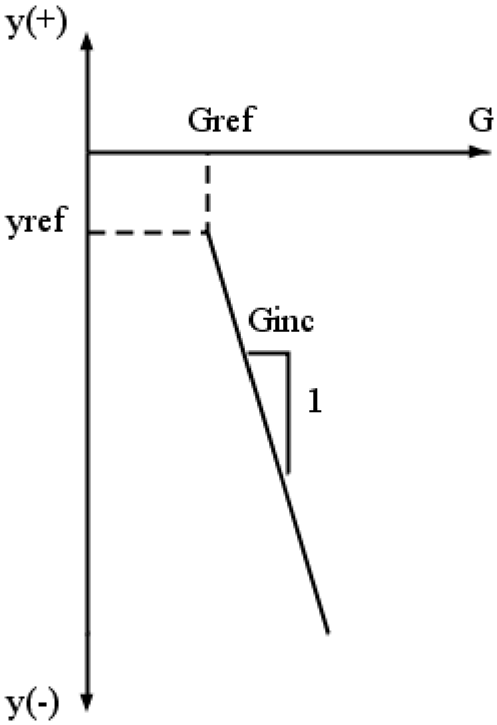

Figure 4.3: Increasing initial shear stiffness with depth

$$f = \frac{\langle \eta - \eta_{K_0} \rangle}{M_\theta - \eta_{K_0}} \tag{4.2}$$

$$\langle \eta - \eta_{K_0} \rangle = \begin{cases} \eta - \eta_{K_0} & : \eta > \eta_{K_0} \\ 0 & : \eta \leq \eta_{K_0} \end{cases} \tag{4.3}$$

$$G_M = G_0 \left(1 - \zeta f\right)^2 \tag{4.4}$$

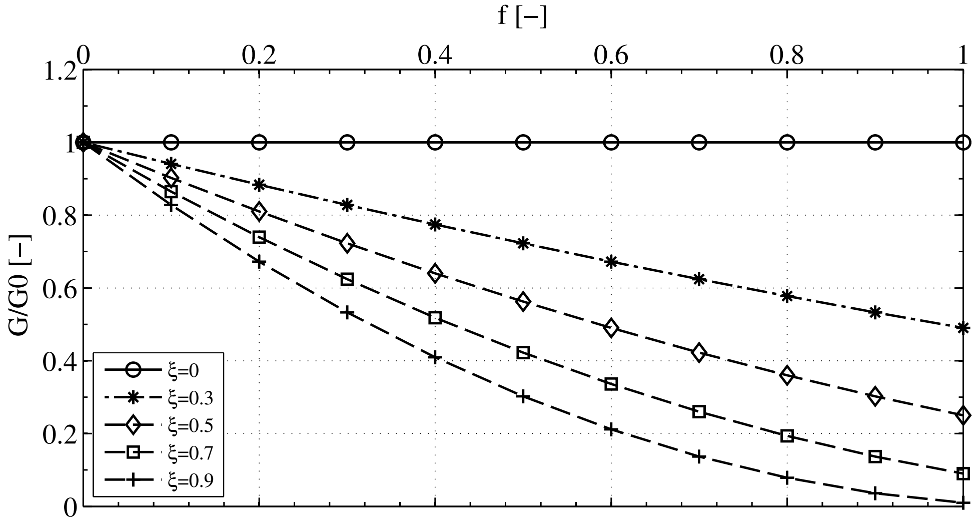

Figure 4.4: Degradation of initial shear stiffness with degree of mobilisation

The elastic matrix is denoted by $\boldsymbol{D}_G$ to distinguish it from $\boldsymbol{D}$ matrix used in Plaxis SSC and CS-SSC, see Equation (4.5).

$$\boldsymbol{D}_G = \left(\begin{array}{cccccc} F_1 & F_2 & F_2 & & & \\ & F_1 & F_2 & & \mathbf{0} & \\ & & F_1 & & & \\ & & & G_M & 0 & 0 \\ & SYM & & & G_M & 0 \\ & & & & & G_M \end{array} \right) \tag{4.5}$$

Lode angle dependency

It has been experimentally observed that both the critical state (CS) and yield surface in soils are Lode angle dependent (Lade and Duncan, 1973). This will take into account soil strength anisotropy e.g. in a triaxial compression test $M = M_C$ whereas in an extension test $M = M_E$. Several Lode angle shape functions for particulate media have been proposed (Coombs et al., 2009). In CS-SSCG formulation, Mohr Coulomb shape function (4.6) is used. Where ϕ is the friction angle that is given by Equation (4.7) and θ is the Lode angle which is determined with Equation (4.8). Note that for triaxial compression and extension M will be simplified to the well-known Equation (4.9) and (4.10), respectively. The lode angle lies within the range: $-\frac{\pi}{6} \leq \theta \leq +\frac{\pi}{6}$, where $\theta = -\frac{\pi}{6}$ represents 'pure' compression and $\theta = +\frac{\pi}{6}$ 'pure' extension. The ratio M_C/M_E is given by Equation (4.11). Theoretically the lower limit of this ratio is 1.0 for an ideal soil with friction angle $\phi = 0°$, and the upper limit is 2.0 for an ideal soil with $\phi = 90°$.

$$M_\theta = \frac{3sin\phi}{\sqrt{3}\cos\theta + \sin\theta\sin\phi} \tag{4.6}$$

$$\phi = \sin^{-1}\left(\frac{3M_c}{6+M_c}\right) \tag{4.7}$$

$$\theta = -\frac{1}{3}\sin^{-1}\left(\frac{27}{2}\frac{J_3}{q^3}\right) \tag{4.8}$$

$$M_C = \frac{6\sin\phi}{3-\sin\phi} \tag{4.9}$$

$$M_E = \frac{6\sin\phi}{3+\sin\phi} \tag{4.10}$$

$$1 \leq \frac{M_C}{M_E} = \frac{3+\sin\phi}{3-\sin\phi} \leq 2 \tag{4.11}$$

Model calibration

The slope of the CS-line for compression M_c is an internal model parameter. This parameter is derived based on the IL oedometer test in NC-region where the ratio of volumetric and deviatoric viscoplastic strain increments can be estimated by Equation (4.12). From the flow rule, $d\varepsilon_{vol}^{vp}$ and $d\varepsilon_q^{vp}$ can be calculated using Equation (4.13) and (4.14). Equation (4.15) shows the expression that is deduced for M_c.

$$\frac{d\varepsilon_{vol}^{vp}}{d\varepsilon_q^{vp}} \approx \frac{d\varepsilon_1^{vp}}{\frac{2}{3}d\varepsilon_1^{vp}} = \frac{3}{2} \tag{4.12}$$

$$d\varepsilon_{vol}^{vp} = d\Lambda\frac{\partial p^{eq}}{\partial p} \tag{4.13}$$

$$d\varepsilon_q^{vp} = d\Lambda \frac{\partial p^{eq}}{\partial q} \tag{4.14}$$

$$M_c \approx \sqrt{\eta_{K_0^{NC}}^2 + 3\,\eta_{K_0^{NC}}} \tag{4.15}$$

4.1.3 Numerical implementation

For implementation of the CS-SSCG model using implicit scheme, similar procedure with same residuals and variables are used as in the CS-SSC model, see Algorithm 4. The differences are: (1) the initial shear stiffness will be assigned by Equation (4.1). For this purpose one more state variable for initial shear stiffness G_0 is included. However this state variable does not enter to variables defined by Equation (4.16) since it is a constant; (2) the elastic matrix $\boldsymbol{D}_G$ is both mean stress and deviatoric stress dependent that will enter to $\boldsymbol{r}_1$. Note that the partial derivatives of this residual in Jacobian matrix $\boldsymbol{J}_G$ are therefore different than the ones for the CS-SSC model; (3) the slope of critical state line will be updated in each iteration. Appendix B contains Fortran pseudo code of the CS-SSCG model subroutine.

4.2 MIT-MDPW embankment

In 1967, 12.2 m high MIT-MDPW embankment, see (Karlsrud, 1969) and (Whittle, 1974), was constructed and heavily instrumented with settlement rods (SR), piezometers (P), and inclinometers (I) to measure the vertical displacement, excess pore pressure, and horizontal displacement of the underlying 40 m thick deposit of Boston Blue Clay (BBC), see Figure 4.5. The field measurements were carried out during staged loading until construction day 620 (CD 620) and four years of subsequent consolidation (CD 2053).

In this study finite element analysis of the embankment was undertaken using the following models: (1) built-in soft soil creep model in Plaxis (Plaxis SSC) and the two implemented models: (2) critical state soft soil creep model (CS-SSC), and (3) critical state soft soil creep model with shear stiffness (CS-SSCG). Note that Plaxis SSC and the two implemented models have been developed primarily for application to settlement problems e.g. foundations and embankments and not for unloading cases that normally are encountered e.g. in excavation and tunnelling or cyclic loading. These models hardly supersedes the well-known linear elastic-perfectly plastic Mohr-Coulomb model (MC) for unloading problems (PLAXIS, 2012). Comparisons of in-situ and predicted measurements by the models used in this study will be presented in this chapter.

Algorithm 4 Implicit scheme for CS-SSCG

The following variables are defined:

$$\boldsymbol{V}_{n+1} = \begin{pmatrix} \boldsymbol{\sigma} \\ \mathrm{p}_{\mathrm{p}}^{\mathrm{eq}} \\ \Lambda \end{pmatrix}_{n+1} \tag{4.16}$$

The following residuals at the current iteration i corresponding to the state variables are:

$$\boldsymbol{r_1}_{n+1} = \boldsymbol{\sigma}_{n+1} - \left[\boldsymbol{\sigma}_n + \boldsymbol{D}_{G_{n+1}} \cdot (\boldsymbol{\varepsilon}_{n+1} - \boldsymbol{\varepsilon}_n) - \boldsymbol{D}_{G_{n+1}} \cdot \frac{\partial p^{eq}}{\partial \boldsymbol{\sigma}} (\Lambda_{n+1} - \Lambda_n)\right] \tag{4.17}$$

$$r_{7\,n+1} = p_p^{eq}{}_{n+1} - \left[p_p^{eq}{}_{n} + \left(\frac{dp_p^{eq}}{d\Lambda}\right)_{n+1} (\Lambda_{n+1} - \Lambda_n)\right] \tag{4.18}$$

$$r_{8\,n+1} = \Lambda_{n+1} - \left[\Lambda_n + \dot{\Lambda}_{n+1} (t_{n+1} - t_n)\right] \tag{4.19}$$

The iterative Newton-Raphson method is adopted to solve the system of equations below:

$$\boldsymbol{J}^i_{G_{n+1}} \cdot \Delta \boldsymbol{V}^i_{n+1} = -\boldsymbol{r}^i_{n+1} \tag{4.20}$$

$$\Delta \boldsymbol{V}^i_{n+1} = -\left(\boldsymbol{J}^{-1}_{G_{n+1}} \cdot \boldsymbol{r}_{n+1}\right)^i \tag{4.21}$$

The variables at the current iteration i will be updated for the next iteration $i+1$:

$$\boldsymbol{V}^{i+1}_{n+1} = \boldsymbol{V}^i_{n+1} + \Delta \boldsymbol{V}^i_{n+1} \tag{4.22}$$

The lode angle will be updated in each iteration:

$$\theta^i_{n+1} = -\frac{1}{3} \sin^{-1} \left(\frac{27}{2} \frac{J_3}{q^3}\right)^i_{n+1} \tag{4.23}$$

$$M^{i+1}_{\theta_{n+1}} = \frac{3 sin\phi}{\sqrt{3} \cos\theta^i_{n+1} + \sin\theta^i_{n+1} \sin\phi} \tag{4.24}$$

The iterative scheme will continue until the desired tolerance is reached at the current iteration:

$$\left(\boldsymbol{r}^T_{n+1} \cdot \boldsymbol{r}_{n+1}\right)^i < TOl^2 \tag{4.25}$$

4.2.1 Background

Several researchers have studied numerical analysis of MIT-MDPW embankment. Neher et al. (2001) and Fatahi et al. (2012) use Plaxis SSC for their simulation. They are able to show a good agreement for vertical settlement under the centre of the embankment based on 12-layer model with parameters adopted from Ladd et al. (1994). However, they overestimate the settlements under the toe of the embankment and also at the deep layers. The main reason is that they do not reflect on importance of selection of OCR in settlement problems. When using Plaxis SSC the overconsolidation ratio should be determined from high quality samples obtained from 24-hr IL test. In addition, when reducing a real problem into a numerical idealization that can be readily analysed, it is vital that soil parameters are interpreted with special emphasis on the numerical model, its underlying assumptions and nature of the problem such as the expected stress interval during the life time. Grimstad et al. (2013) addressed this issue and examined the simplified model of the embankment with two layer of clay with focus on the 'proper' selection of OCR. They are successful to improve the vertical settlements significantly but the horizontal displacements are still overestimated. In this work the focus is on improving the horizontal displacements using the CS-SSCG model.

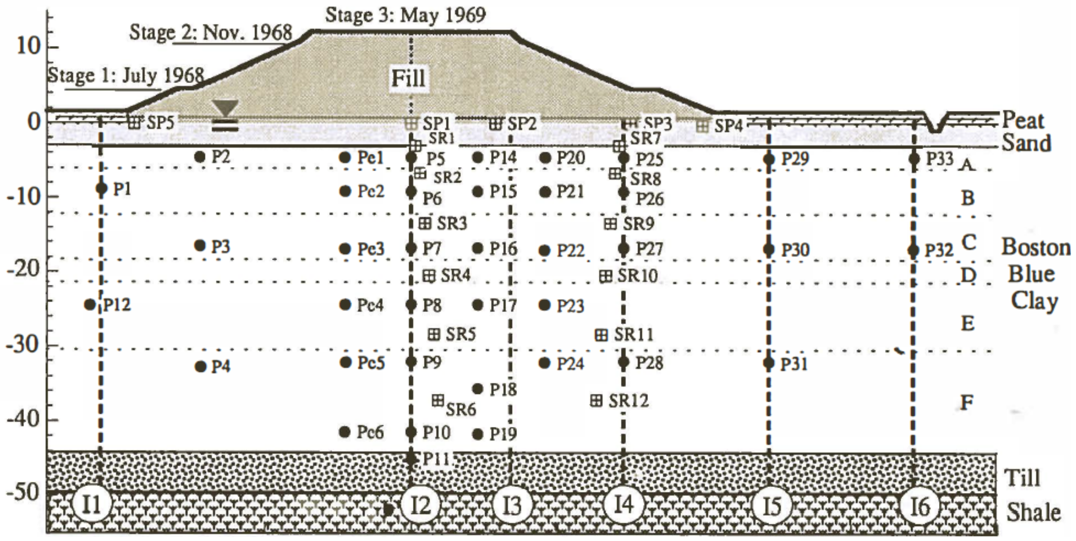
Stage 3: May 1969
Stage 2: Nov. 1968
Stage 1: July 1968
Fill
10
0
-10
-20
-30
-40
-50
SP5
SP1
SR1
SP2
SP3
SR7
SP4
Peat
Sand
P2
Pc1
P5
P14
P20
P25
P29
P33
A
P1
Pc2
SR2
P6
P15
P21
SR8
P26
B
SR3
SR9
P3
Pc3
P7
P16
P22
P27
P30
P32
C
Boston
Blue
Clay
SR4
SR10
D
P12
Pc4
P8
P17
P23
E
SR5
SR11
P4
Pc5
P9
P24
P28
P31
P18
SR6
SR12
F
Pc6
P10
P19
P11
Till
Shale
I1
I2
I3
I4
I5
I6

Figure 4.5: MIT-MDPW embankment with instrumentation (Ladd et al., 1994)

4.2.2 Selection of parameters

MIT-MDPW embankment is used as a basis to validate the implemented models and to illustrate the effect of using shear stiffness on calculation of creep settlements. Selection of parameters in this work was primarily based on laboratory tests given by (Whittle, 1974) and (Ladd et al., 1994), see Table 4.2. For purpose of simplifying the illustration a profile with only two clay layers (BBC1 and BBC2) is used in this work. Selection of clay parameters for the two-layer model is based on the average 12-layer parameters with focus on selecting a proper OCR for creep rate models, see Table 4.3. Figure 4.6 illustrates definition of overconsolidation ratio (OCR) and preoverburden pressure (POP) in Plaxis. In the embankment simulation $POP = 120$ kPa is used for BBC1 layer instead of using OCR since POP fits better to the results obtained from the oedometer test, see Figure 4.7. Note that the test data only from oedometer with 1 day load step should be considered. Table 4.4 presents Mohr-Coulomb parameters used for peat and till. Table 4.5 shows hardening soil parameters used for sand. Permeability of clay layer is expressed by $log(k) = log(k_0) + 1.0\Delta e$. Where Δe is the change in void ratio (negative for compression) and k_0 is the initial permeability.

Table 4.6 shows shear stiffness parameters used for the CS-SSCG model. Initial shear stiffness G_0 is determined from the direct simple shear tests (DSS) (Whittle, 1974). Table 4.7 shows back-calculated shear stiffness parameters from the Plaxis SSC model. Note that for BBC2 mid-layer the initial shear stiffness from the DSS test is approximately 4 times higher than the one which is implicitly being used in Plaxis SSC, see Figure 4.8.

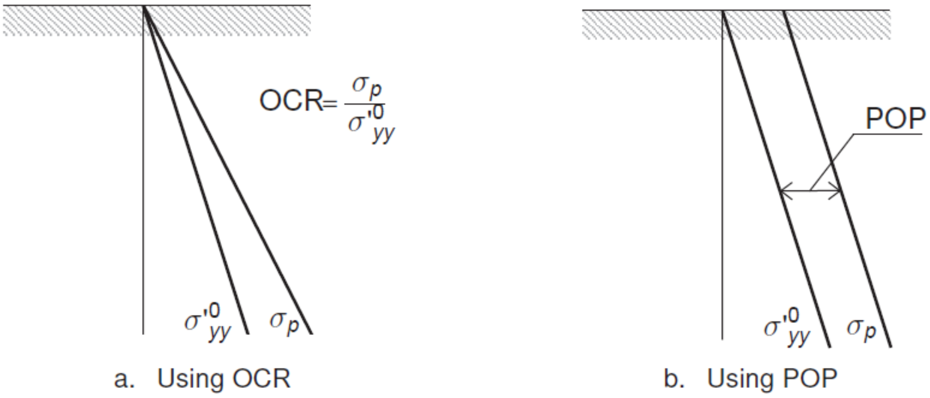

a. Using OCR b. Using POP

Figure 4.6: OCR and POP as defined in Plaxis (Plaxis2DManual, 2012)

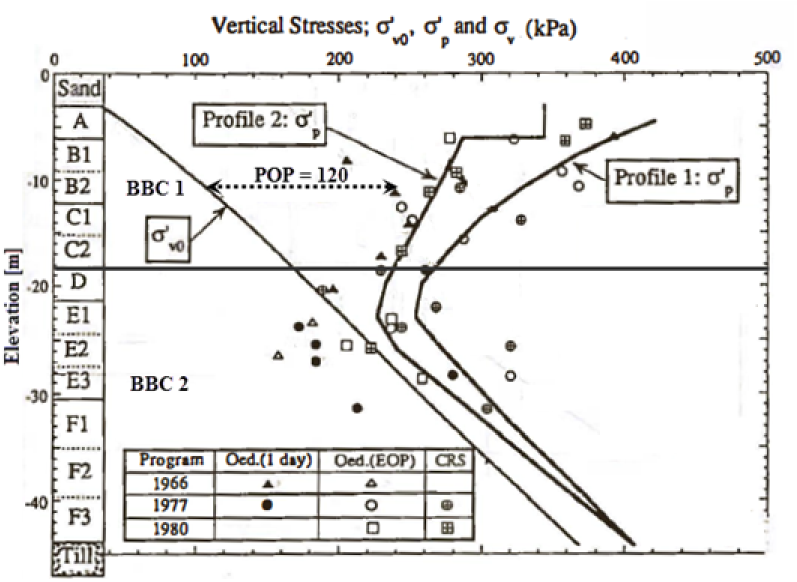

Figure 4.7: Selection of POP for BBC1 layer based on test data after (Ladd et al., 1994)

Table 4.2: Clay parameters for 12-layer model

Centre EL. [m]	Layer	γ $[kN/m^3]$	OCR_τ	K_0	e_0	λ^*	κ^*	μ^*	k_{x0} [m/day]	k_{y0} [m/day]
-4.6	A	19.0	8.34	1.35	0.62	0.052	0.013	0.0015	2.73E-04	1.37E-04
-7.6	B1	19.0	4.60	1.08	0.88	0.065	0.016	0.0019	1.80E-04	8.99E-05
-10.7	B2	19.0	3.07	0.85	0.88	0.065	0.016	0.0019	1.80E-04	8.99E-05
-13.7	C1	17.7	2.25	0.80	1.17	0.087	0.022	0.0025	8.16E-05	5.44E-05
-16.8	C2	17.7	1.77	0.65	1.17	0.087	0.022	0.0025	8.16E-05	5.44E-05
-19.8	D	17.7	1.44	0.60	1.17	0.130	0.033	0.0037	9.20E-05	6.13E-05
-22.9	E1	17.7	1.25	0.57	1.26	0.196	0.049	0.0056	1.01E-04	6.74E-05
-25.9	E2	17.7	1.21	0.57	1.26	0.196	0.049	0.0056	1.01E-04	6.74E-05
-29	E3	17.7	1.18	0.56	1.26	0.196	0.049	0.0056	1.01E-04	6.74E-05
-32.8	F1	17.7	1.16	0.56	1.12	0.152	0.038	0.0043	7.65E-05	5.10E-05
-37.3	F2	17.7	1.14	0.56	1.12	0.152	0.038	0.0043	7.65E-05	5.10E-05
-42	F3	17.7	1.11	0.55	1.12	0.152	0.038	0.0043	7.65E-05	5.10E-05

$c = 1\ kPa, \phi = 33.4°, \nu_{ur} = 0.1, K_0^{NC} = 0.45$

Table 4.3: Clay parameters used in this study for two-layer model

Centre EL. [m]	Layer	γ $[kN/m^3]$	POP_τ OCR_τ	K_0	e_0	λ^*	κ^*	μ^*	k_{x0} [m/day]	k_{y0} [m/day]
-10.5	BBC1	18.5	120	0.89	0.970	0.079	0.020	0.0023	1.51E-04	8.21E-05
-31	BBC2	17.7	1.5	0.56	1.180	0.171	0.043	0.0049	8.73E-05	5.82E-05

$c = 1\ kPa, \phi = 33.4°, \nu_{ur} = 0.1, K_0^{NC} = 0.45$

Table 4.4: Mohr-Coulomb (MC) parameters used for peat and till

Centre EL. [m]	Layer	γ $[kN/m^3]$	K_0	e_0	E' [MPa]	ν'	c [kPa]	ϕ [°]	ψ [°]	k_{x0} [m/day]	k_{y0} [m/day]
0.75	Peat	11.8	0.58	0.5	0.208	0.3	5	25	0	1	1
-47	TILL	20.4	0.50	0.5	100	0.3	0	43	13	7	7

Table 4.5: Hardening soil (HS) parameters used for sand

Centre EL. [m]	Layer	γ $[kN/m^3]$	K_0	e_0	E_{50}^{ref} [MPa]	E_{oed}^{ref} [MPa]	E_{ur}^{ref} [MPa]	c [kPa]	ϕ [°]	ψ [°]	$k_{x0} = k_{y0}$ [m/day]
-1.5	Sand	18.8	0.40	0.5	40	40	120	1	37	7	7

Table 4.6: Shear stiffness parameters used for CS-SSCG

Layer	Position	Elevation [m]	σ_{v0} [kPa]	POP_τ OCR_τ	G_0/σ_{v0}	G_0 [kPa]	G_{inc} [kPa/m]
BBC1	Top	-3	33.71	120	97	3269.9	555.8
	Middle	-10	94			7160.5	
	Bottom	-18.6	166.3		71.8	11940.3	
BBC2	Top	-18.6	166.3	1.5	71.8	11940.3	552.9
	Middle	-28	240			17137.2	
	Bottom	-44.2	363.42		71.8	26093.6	

$\xi = 0.7$, $M_c = 1.834$

Table 4.7: Back-calculated shear stiffness from Plaxis SSC

Layer	Position	El. [m]	σ_{v0} [kPa]	K_0	κ^*	p [kPa]	K [kPa]	G_0 [kPa]	G_{inc} [kPa/m]
BBC1	Top	-3	33.71	0.89	0.0198	31.2	1577.7	1721.1	433.9
	Middle	-10	94			87.1	4399.3	4799.3	
	Bottom	-18.6	166.3			154.1	7783.1	8490.6	
BBC2	Top	-18.6	166.3	0.56	0.0428	117.5	2745.8	2995.4	138.7
	Middle	-28	240			169.6	3962.6	4322.9	
	Bottom	-44.2	363.42			256.8	6000.4	6545.9	

$\nu_{ur} = 0.1$

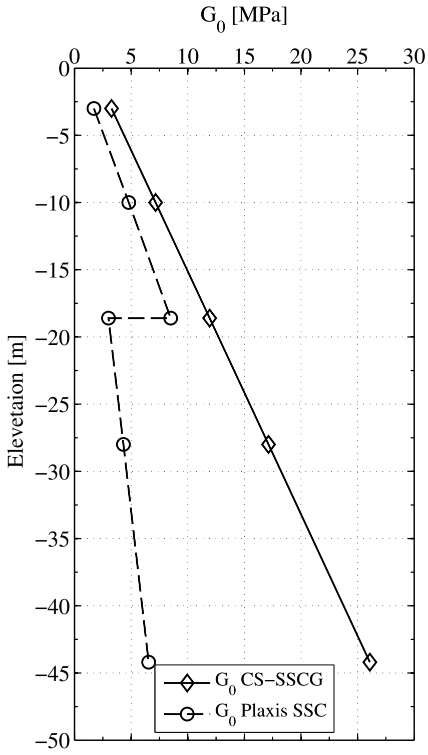

Figure 4.8: G_0 used in CS-SSCG and G_0 back-calculated from Plaxis SSC

4.3 Model verification and validation at element level

Two soil elements are studied from the representative depths of 10 m and 28 m from BBC1 and BBC2 layer. BBC1 element is nearly normally consolidated ($OCR = 1.5$) and BBC2 is slightly overconsolidated ($OCR = 2.3$). In each simulation, the sample is loaded from the initial stress condition given in Table 4.8. The parameters at the shallower depth 10 m are taken from BBC1 layer and for the deeper depth 28 m from BBC2 layer, see Table 4.3. IL oedometer tests and undrained triaxial K_0-consolidated tests are simulated with the models used in this study: (1) Plaxis SSC, (2) CS-SSC and (3) CS-SSCG with varying degradation factor ξ. Figure 4.9 shows degradation of initial shear stiffness versus stress ratio for the two elements. For $\xi = 0$, degradation of initial shear stiffness is deactivated. Here for the CS-SSCG model back-calculated shear stiffness parameters from Plaxis SSC model is used for the purpose of model performance comparison.

Table 4.8: Initial stress for the two soil elements BBC1 and BBC2

Soil element	σ_{xx} [kPa]	σ_{yy} [kPa]	σ_{zz} [kPa]	$\lvert\sigma_{vc}\rvert$ [kPa]	OCR [-]
BBC1	-83.66	-94	-83.66	214	2.28
BBC2	-134.4	-240	-134.4	360	1.50

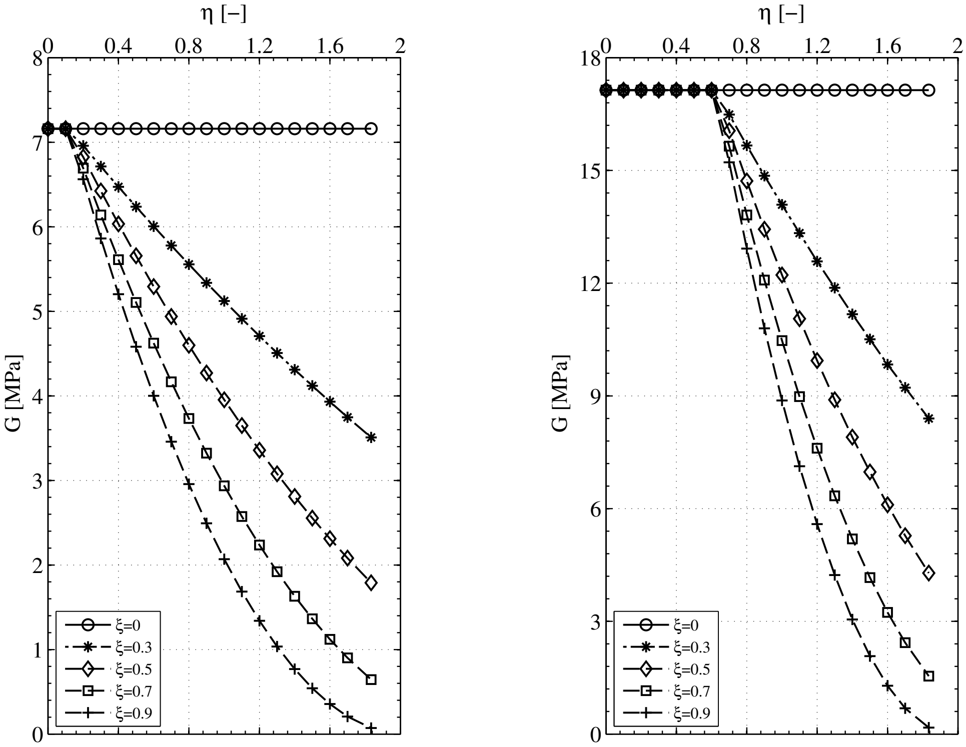

(a) BBC1 ($\eta_{K_0} = 0.12$)　(b) BBC2 ($\eta_{K_0} = 0.62$)

Figure 4.9: Degradation of initial shear stiffness

4.3.1 Simulation of oedometer tests

From representative depths of 10 m and 28 m, two oedometer tests are simulated using the General Soil Test facility in Plaxis. The boundary conditions are assigned such that no strain increment is allowed for the radial direction x and z while the stress increment is being applied in the vertical direction y. This will simulate the oedometer test condition. The parameters at the shallower depth 10 m are taken from BBC1 layer and for the deeper depth 28 m from BBC2. In each simulation, the sample is loaded from the initial in-situ stress state. From phase 1 onwards the soil element is consolidated with 24-h load increments during 4 days. The summary of the load application can be seen in Table 4.9.

Figure 4.10 shows the results from the simulations. In general all the models reproduce similar results for the strain curves. However, CS-SSCG simulate stress path that is different than Plaxis SSC and CS-SSC. Figure 4.10a and 4.10b show vertical strain versus time for BBC1 and BBC2, respectively. As can be seen from the figures all the models give similar results. Figure 4.10c and 4.10d show vertical strain versus vertical stress in IL oedometer test for BBC1 and BBC2. The difference between the prediction of CS-SSCG and other models is more pro-

Table 4.9: Incremental oedometer test simulation defined in Plaxis General Soil Test

IL Oedometer	$\Delta\varepsilon_{xx}$	$\Delta\sigma_{yy}$ [kPa]	$\Delta\varepsilon_{zz}$	Duration [Day]
phase 1	0	-50	0	0.01
phase 2	0	0	0	0.99
phase 3	0	-100	0	0.01
phase 4	0	0	0	0.99
phase 5	0	-200	0	0.01
phase 6	0	0	0	0.99
phase 7	0	-400	0	0.01
phase 8	0	0	0	0.99

nounced at the beginning of the curves where elasticity dominates. Figure 4.10e and 4.10f illustrate deviatoric stress versus mean stress for BBC1 and BBC2. The stress path pattern for CS-SSCG is not similar to Plaxis SSC and CS-SSC. This is due to the fact that shear stiffness in Poisson's ratio based models is mean stress dependent and it increases with isotropic stress whereas in the CS-SSCG model initial shear stiffness is constant for $\xi = 0$ and it will be degraded for $\xi \neq 0$. It should be also noted that selection of parameters in practice should be based on expected stress interval. The simulation of the embankment can be extended to CD 36500 to find out the relevant stress interval for possible embankment lifetime of 100 years. The field measurements are only available until CD 2053 though. For BBC1 element with initial vertical stress 94 kPa expected vertical effective stresses at CD 2053 and 36500 are 194 and 237 kPa, respectively and for BBC2 with initial vertical stress 240 kPa the expected stresses are 273 and 362 kPa.

4.3.2 Simulation of triaxial tests

Two undrained triaxial compression (UK$_0$TC) and extension (UK$_0$TE) tests are simulated for an element at EL -10 m from BBC1 (Figure 4.11) and at EL -28 m from BBC2 layer (Figure 4.12). First samples are consolidated to the initial K_0-condition and then they sheared to failure. The major principal strain in triaxial compression and extension test is equal to axial and radial strain, respectively. Note that the implemented CS models allow for reaching the stress path to the top of ellipse. Therefore, the model verification is of significance before Plaxis SSC failure. This is discussed earlier in Section 3.3.2.

Figure 4.11 shows results from simulation of triaxial tests for BBC1 soil element. In general,

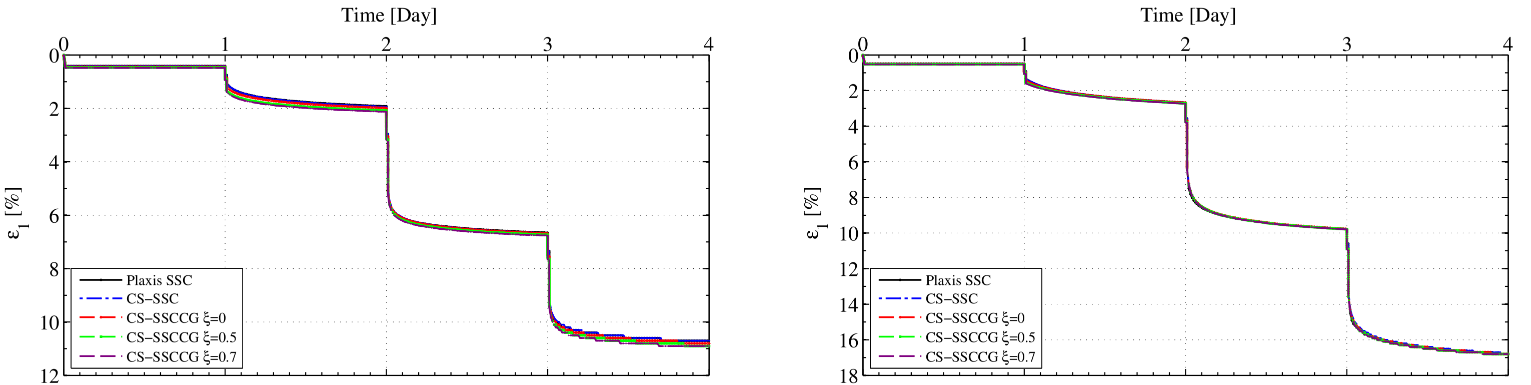

(a) K_0IL - Strain vs Time BBC1

(b) K_0IL - Strain vs Time BBC2

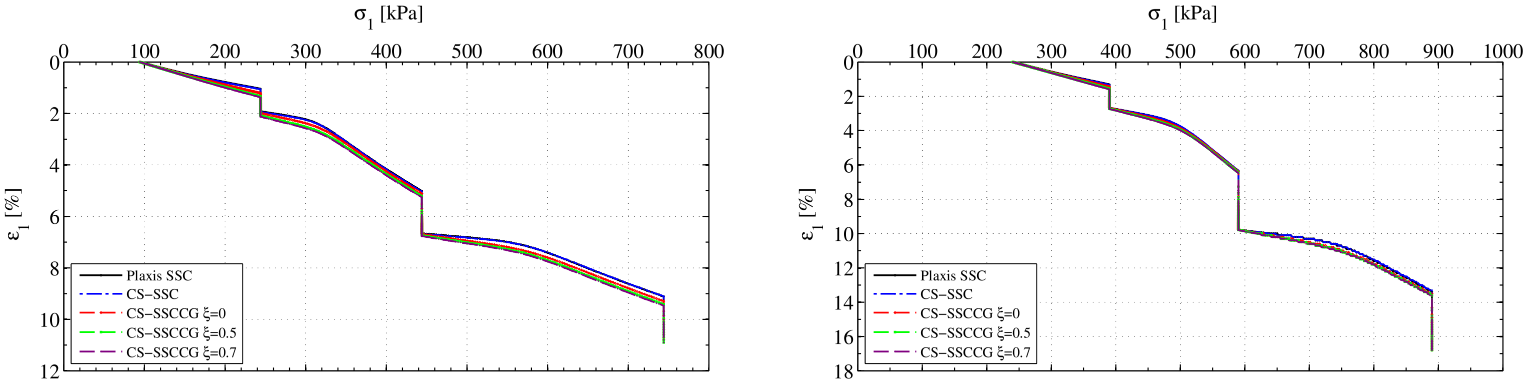

(c) K_0IL - Strain vs Vertical Stress BBC1

(d) K_0IL - Strain vs Vertical Stress BBC2

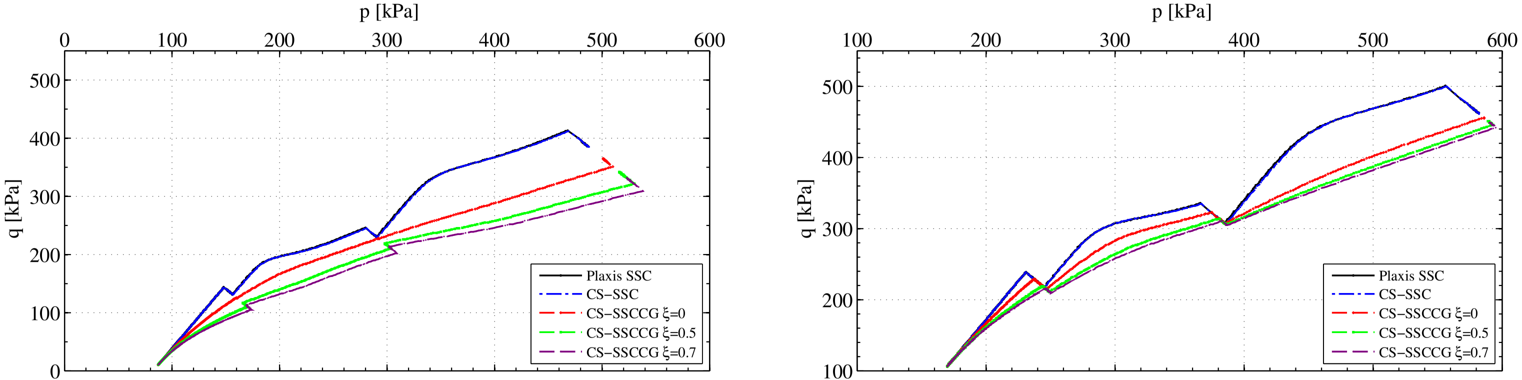

(e) K_0IL - Deviatoric vs Mean Stress BBC1

(f) K_0IL - Deviatoric vs Mean Stress BBC2

Figure 4.10: Oedometer simulation for soil elements from BBC1 (EL -10 m) and BBC2 (EL -28 m)

Plaxis SSC, CS-SSC and CS-SSCG ($\xi = 0$) reproduce similar results before Plaxis SSC failure that is around 0.8 % strain. This verifies the performance of the CS-SSCG model. Figure 4.11a shows deviatoric stress versus major principal strain in compression test. Models with degradation predict equal ultimate deviatoric stress but with different shapes. The parameter η controls the shape of the obtained curves; the more degradation factor, the more curvature. Figure 4.11b shows deviatoric stress versus major principal strain in extension test. Note that CS-SSC does not distinguish between compression and extension and the result for triaxial extension is exactly the same as for compression test. The CS-SSCG model is lode angle dependent and the soil strength is equal to M_E in extension. Therefore CS-SSCG predicts close deviatoric stress as simulated by Plaxis SSC. Figure 4.11c shows pore pressure versus major principal strain in compression test. The implemented critical state models allow for generating higher excess pore pressure as expected. BBC1 element is slightly overconsolidated. This is reflected in pore pressure response predicted by critical state models, i.e pore pressure decrease after reaching a peak value. Figure 4.11d shows pore pressure versus major principal strain in extension test. CS-SSC does not distinguish between compression and extension whereas the lode angle dependent CS-SSCG model predicts close pore pressure response to Plaxis.

Figure 4.12 shows results from simulation of triaxial tests for BBC2 soil element. In general, Plaxis SSC, CS-SSC and CS-SSCG ($\xi = 0$) reproduce similar results until Plaxis SSC reaches to failure, that is around 1.0 % strain. This verifies the performance of the CS-SSCG model. The explanation made earlier for BBC1 element is also valid for BBC2. Figure 4.12a and Figure 4.12b show deviatoric stress versus major principal strain in compression and extension tests respectively. Figure 4.12c shows pore pressure versus major principal strain in compression test. BBC2 element is nearly normally consolidated ($OCR = 1.5$). This is reflected in pore pressure response predicted by critical state models, i.e gradually reaching critical state with no peak. Figure 4.12d shows pore pressure versus major principal strain in extension test.

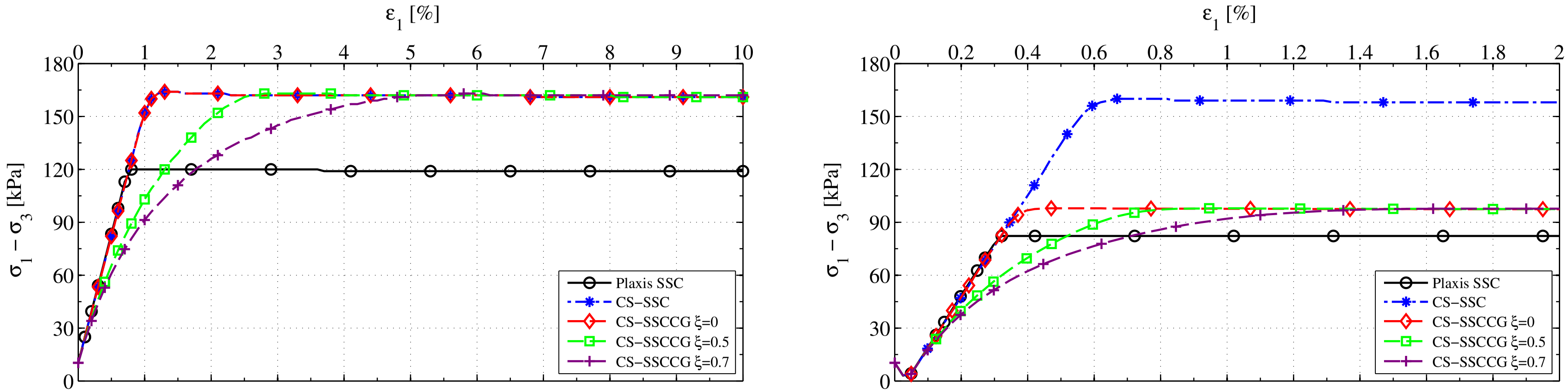

(a) UK_0TC - Deviatoric stress vs Strain

(b) UK_0TE - Deviatoric stress vs Strain

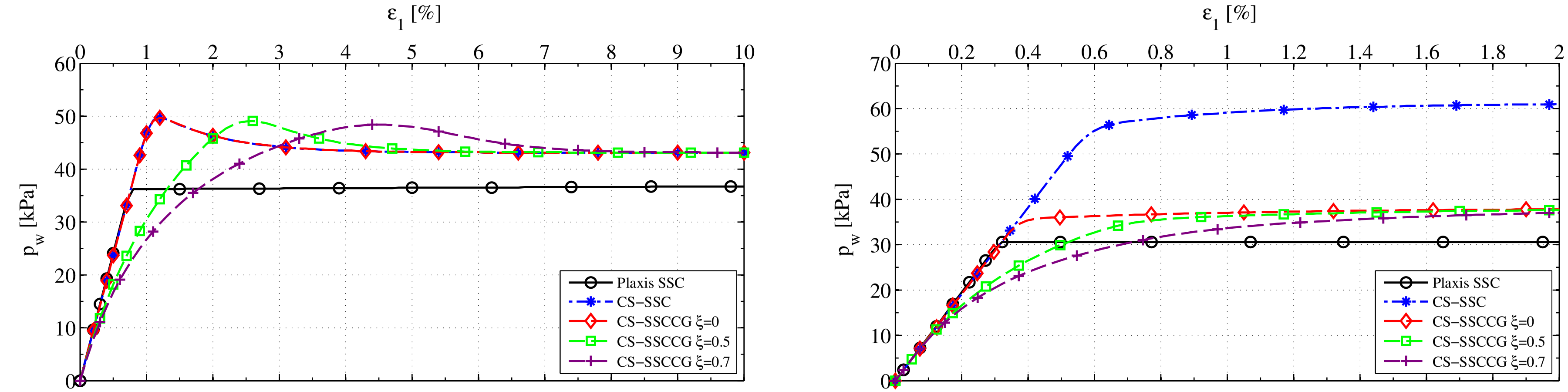

(c) UK_0TC - Pore Pressure vs Strain

(d) UK_0TE - Pore Pressure vs Strain

Figure 4.11: Triaxial Undrained Compression and Extension tests for a soil element from BBC1 Layer at EL -10 m

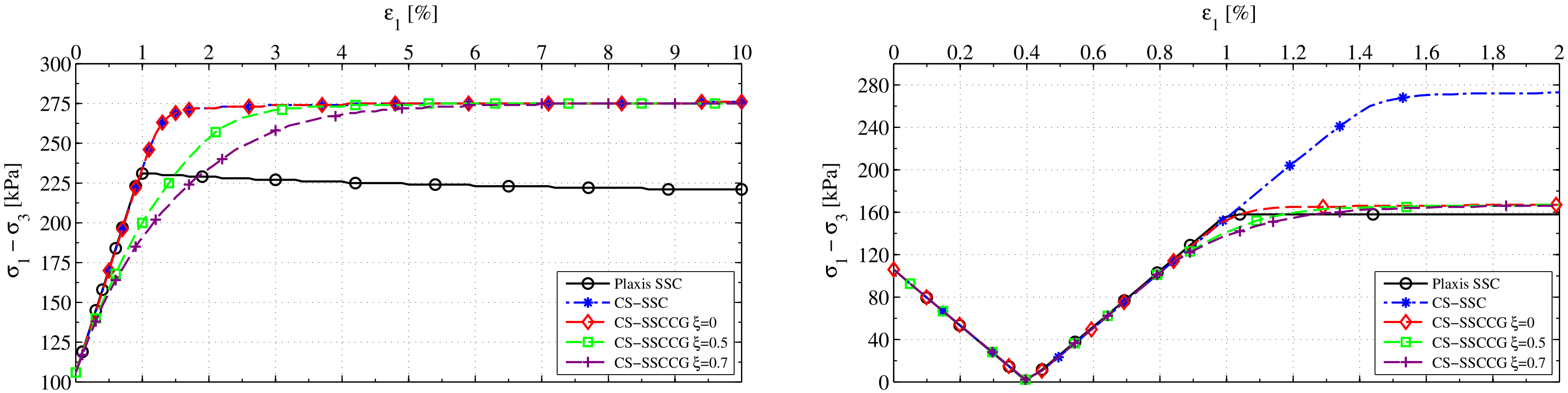

(a) UK$_0$TC - Deviatoric stress vs Strain

(b) UK$_0$TE - Deviatoric stress vs Strain

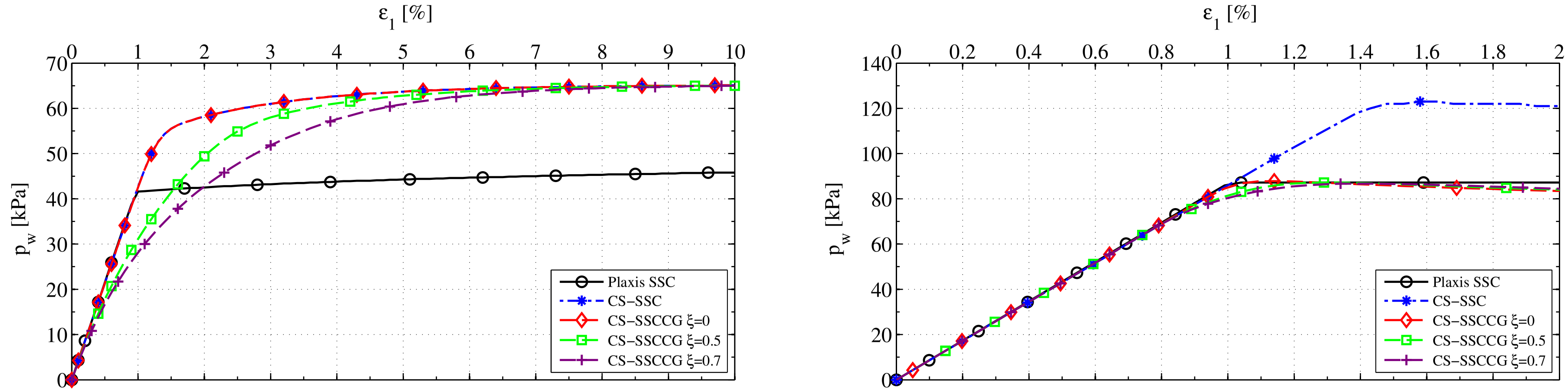

(c) UK$_0$TC - Pore Pressure vs Strain

(d) UK$_0$TE - Pore Pressure vs Strain

Figure 4.12: Triaxial Undrained Compression and Extension tests for a soil element from BBC2 Layer at EL -28 m

4.4 Model validation and verification at boundary value problem MIT-MDPW embankment

The geometry of the embankment was carefully taken from Whittle (1974). Figure 4.13 illustrates the layers and the geometry used in this work for the two layer model. Due to the profile symmetry only half of the embankment and its underlying layers were modelled in Plaxis. The centre line (C.L) of the embankment and the ground water level (GWL) are also shown in the figure. The model mesh was generated using 15-node triangular element with very fine mesh. The generated mesh is refined in areas under the embankment to improve the accuracy of the finite element calculation. Top layer is peat which was replaced by fill material under the embankment at the beginning of the construction and the bottom layer is till.

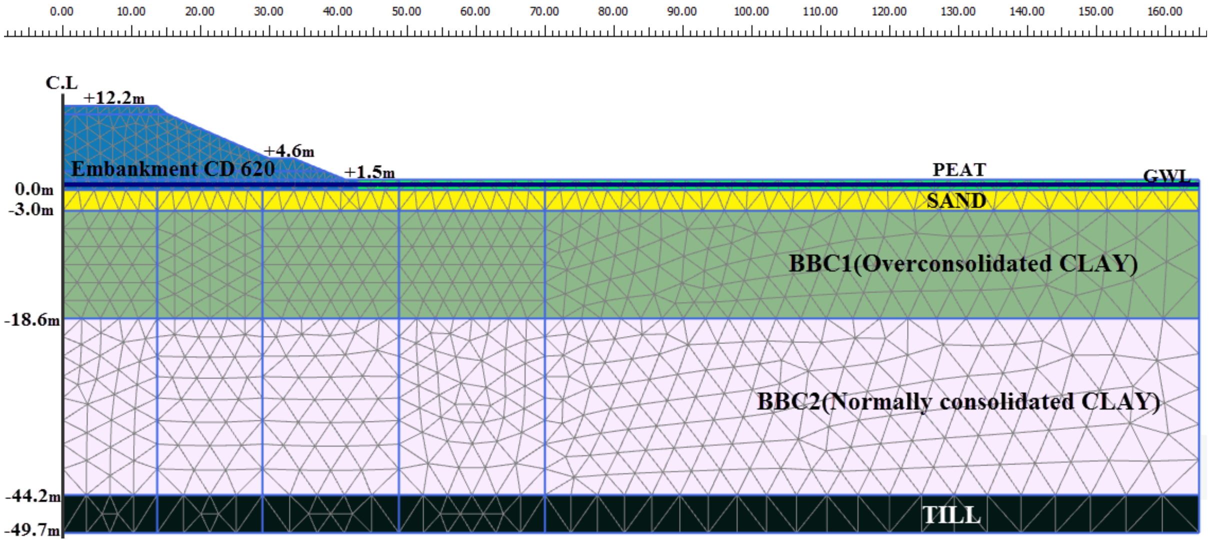
0.00
10.00
20.00
30.00
40.00
50.00
60.00
70.00
80.00
90.00
100.00
110.00
120.00
130.00
140.00
150.00
160.00
C.L
+12.2m
+4.6m
+1.5m
Embankment CD 620
PEAT
GWL
0.0m
-3.0m
SAND
BBC1(Overconsolidated CLAY)
-18.6m
BBC2(Normally consolidated CLAY)
-44.2m
-49.7m
TILL

Figure 4.13: Plaxis finite element model of two-layer embankment studied in this work

Figure 4.14 shows the construction sequence of the embankment. The corresponding construction sequence that is defined in Plaxis simulation is given in Table 4.10. The first day of embankment construction (CD 1) was on 01/09/1967. CD 0 implies initial condition with only the horizontal layers. The K_0-procedure is used to generate initial stresses in Plaxis. Construction of the embankment is comprised of 3 main stages during which the elevation of the embankment reaches from EL. +1.5 m to 12.2 m within 620 days. Construction of the embankment and its later performance simulated using consolidation calculation in Plaxis. Figure 4.15 to Figure 4.17 present some results from the simulation as well as the field measurements.

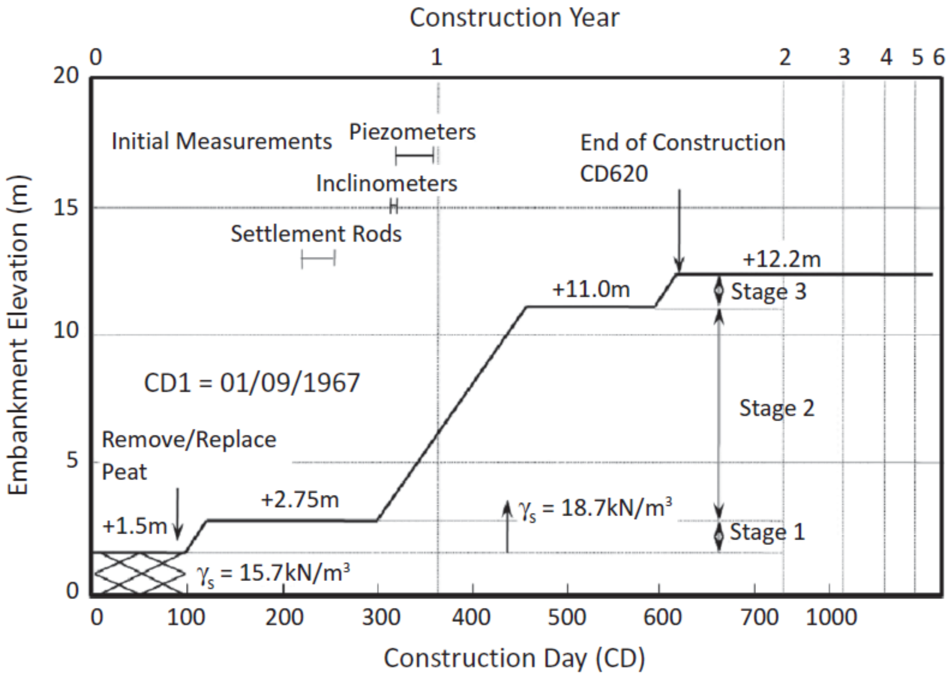

Figure 4.14: Construction sequence of MIT-MDPW embankment; after Whittle (1974), from Fatahi et al. (2012)

Table 4.10: Construction sequence of the embankment as defined in Plaxis

Identification	Calculation	Interval [Day]	CD [Day]	Remark
Initial phase	K_0 procedure	0	0	Initial condition
<Phase 1>	Consolidation	92	92	EL. +1.5 m
<Phase 2>	Consolidation	31	123	EL. +2.75 m
<Phase 3>	Consolidation	175	298	
<Phase 4>	Consolidation	163	461	EL. +11 m
<Phase 5>	Consolidation	137	598	
<Phase 6>	Consolidation	22	620	End of construction (EL. +12.2 m)
<Phase 7>	Consolidation	1324	1944	
<Phase 8>	Consolidation	109	2053	Last measurement of field data

4.4.1 Vertical displacements

Figure 4.15 shows the results from simulation of the embankment and the field data profile for vertical displacements. In general all the models used in this study show a good agreement with the field measurements. As expected the implemented CS-SSC model predicts almost the same results as built-in Plaxis SSC. This verifies the performance of CS-SSC in a boundary value problem. Figure 4.15a and 4.15b show the settlements under the embankment centre and the toe respectively. As can be seen from figure the CS-SSCG model predicts a little less settlement under the toe. Nevertheless, CS-SSCG could capture the vertical displacement better at the deeper levels both under the centreline and the toe of the embankment (Figure 4.15c and 4.15d). The first part of the curves predicted by Plaxis SSC and CS-SSCG have higher slope than the field measurements for deeper layers. This indicates that the stiffness of the clay is underestimated in the beginning of the creep settlement. The better prediction of vertical settlement by CS-SSCG was achieved by adopting higher initial shear stiffness. At the deeper levels the initial shear stiffness used in CS-SSCG is approximately four times as high as the one that is implicitly used in Plaxis SSC and CS-SSC.

4.4.2 Horizontal displacements

Figure 4.16 illustrates the results from simulations and the field data profile for horizontal displacements under the embankment at I3, I4 and I5 at day 620 (Figure 4.16a, 4.16b and 4.16c) and day 2053 (Figure 4.16d, 4.16e and 4.16f). The inclinometers I3, I4, I5 and the embankment toe are located 13.7, 29, 48.8 and 42.7 m from the embankment centreline, respectively. As can be seen from figure the implemented CS-SSC model predicts almost the same results compared to Plaxis SSC. This verifies the performance of CS-SSC in a boundary value problem. Note that the small deviation between predictions of the two models at the top layer is due to the different failure criteria for these models. During construction of the embankment some elements at the top layer will undergo to the extension failure. The CS-SSC model uses isotropic strength whereas Plaxis SSC has lower strength for extension. Nonetheless, both Plaxis SSC and CS-SSC predict significantly higher horizontal displacements than the field measurements. It may indicate that these models are not capable of simulating lateral deformation well enough. In contrast, implemented CS-SSCG shows a fairly good agreement with the field data. Better prediction of horizontal displacements is particularly achieved in the beginning of the creep settlement (until CD 620) when elasticity dominates and the importance of using proper shear stiffness is therefore of more significance. At far from the field (I5), both Plaxis SSC and CS-SSC completely fail to reproduce the field measurements whereas CS-SSCG succeeded to show a good agreement with the field data.

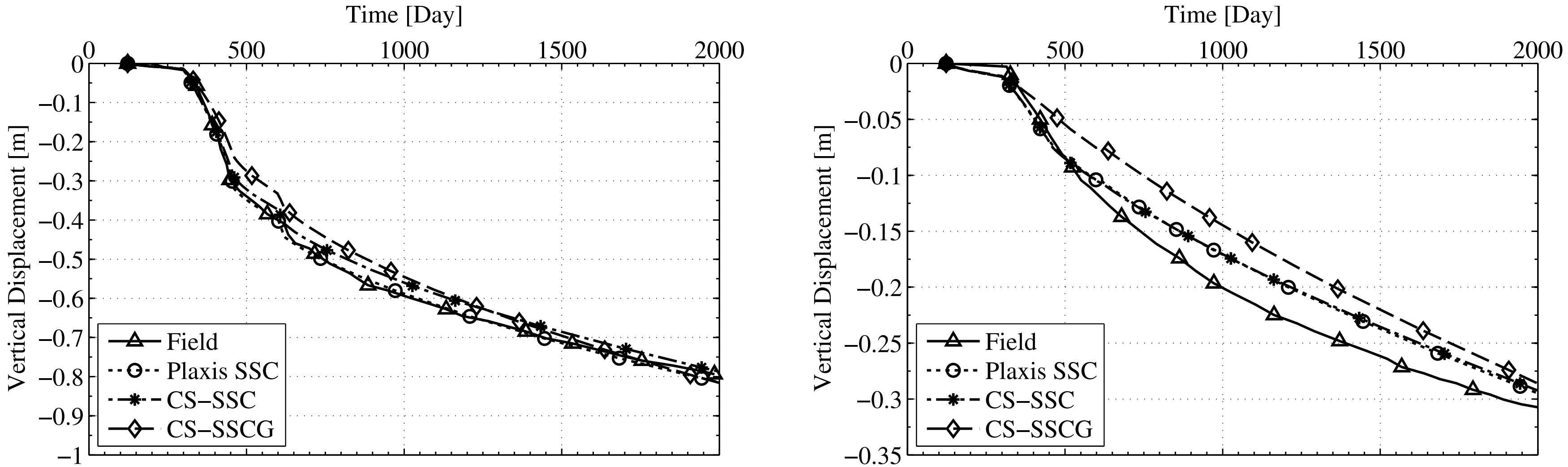

(a) SP1

(b) SP3

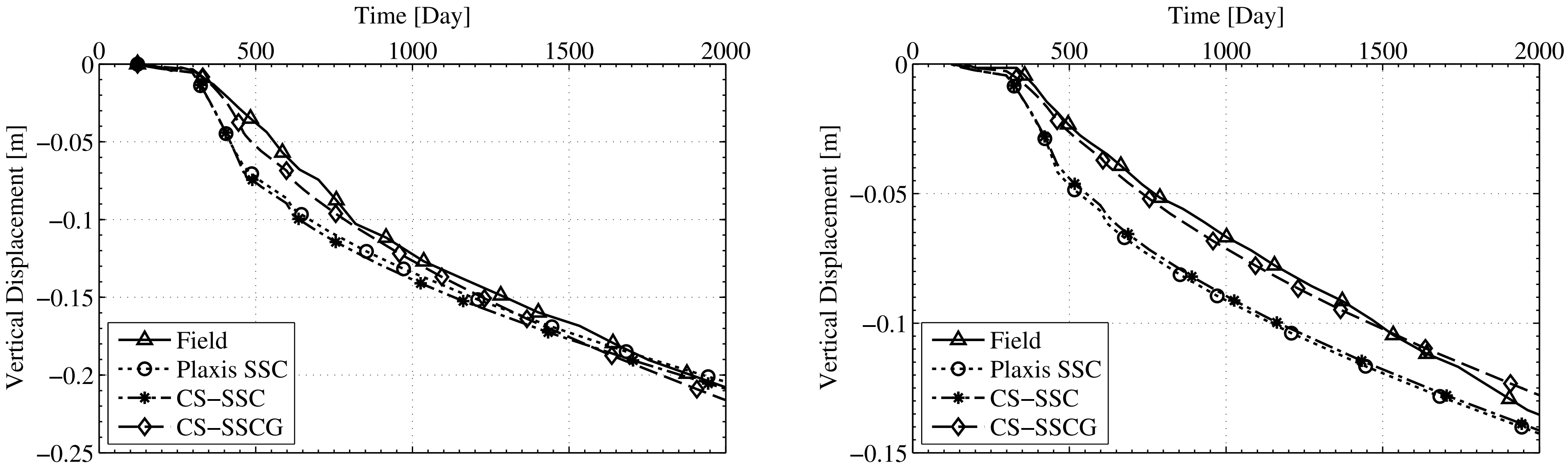

(c) SR5

(d) SR11

Figure 4.15: Calculated and measured vertical displacements

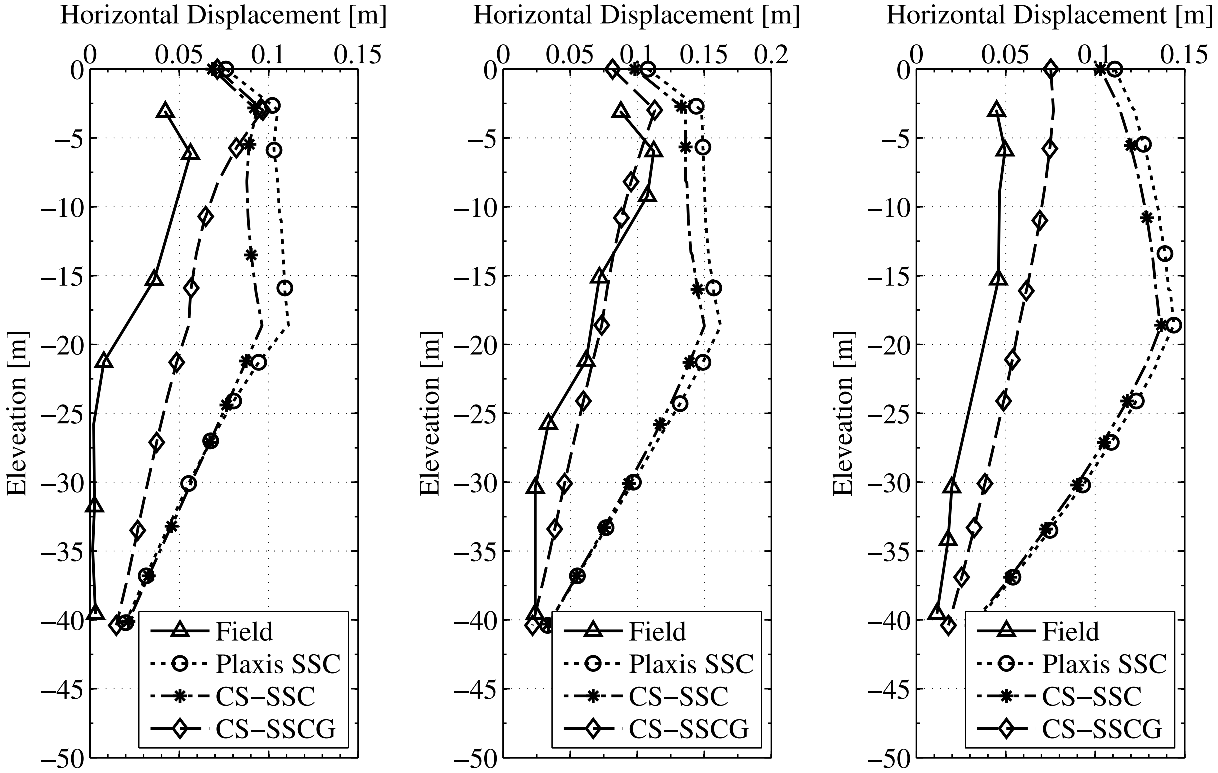

(a) I3-CD620 (b) I4-CD620 (c) I5-CD620

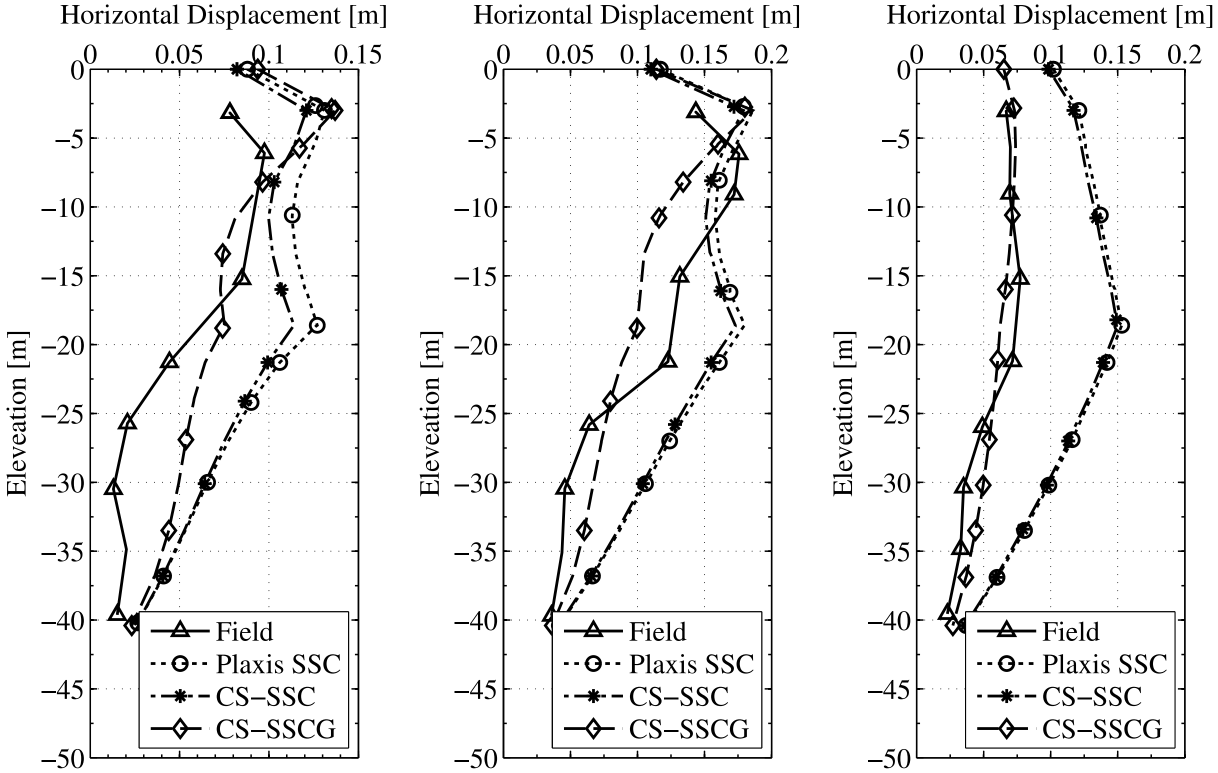

(d) I3-CD2053 (e) I4-CD2053 (f) I5-CD2053

Figure 4.16: Calculated and measured horizontal displacements at day 620 and 2053

4.4.3 Pore pressure

Figure 4.17 shows excess pore pressure distribution simulated by the models used in this study and the field measurements at P5-P11, P20-P24 and P25-P28 at day 620 (Figure 4.17a, 4.17b and 4.17c) and day 2053 (Figure 4.17d, 4.17e and 4.17f). Piezometer P5-P11 is located under the centre of the embankment and P20-P24 and P25-P28 are located 18.3 and 29 m from the embankment centreline respectively. In general all the models used in this study show a fairly good agreement with the field measurements. As can be seen from the figure the CS-SSC model predicts almost the similar profile as Plaxis SSC. This verifies the performance of CS-SSC in a boundary value problem. In general CS-SSCG predicts slightly higher pore pressure response compared to other models due to its higher shear stiffness. As expected the maximum excess pore pressure occurs approximately in the middle of clay layer (EL -25 m). At the elevations close to clay mid-layer both CS-SSC and CS-SSCG simulate slightly less maximum pore pressure than field while CS-SSCG simulates slightly higher pore pressure that fits better to the field measurements. However, all the models simulate slightly less excess pore pressure than the field measurements at the deeper levels and more at the shallower depths. This could be resolved by a more refined model at the drainage boundaries.

4.4.4 Mobilised shear stiffness

Figure 4.18 illustrates mobilised shear stiffness G_M in the clay layer at day 620 (Figure 4.18b) and day 2053 (Figure 4.18c). It can be seen that from the embankment centreline to slightly after the toe the degradation of initial shear stiffness is more important and it occurs more significantly in BBC1 layer where mobilisation is higher. In contrast, initial shear stiffness for elements far from the embankment are not degraded as expected. It means that far field elements almost do not contribute to the horizontal displacements. Therefore, in contrast to Plaxis CS-SSC and CS-SSC simulation of horizontal displacement with the CS-SSCGM model is not sensitive to the extension of the boundary for the finite element calculations.

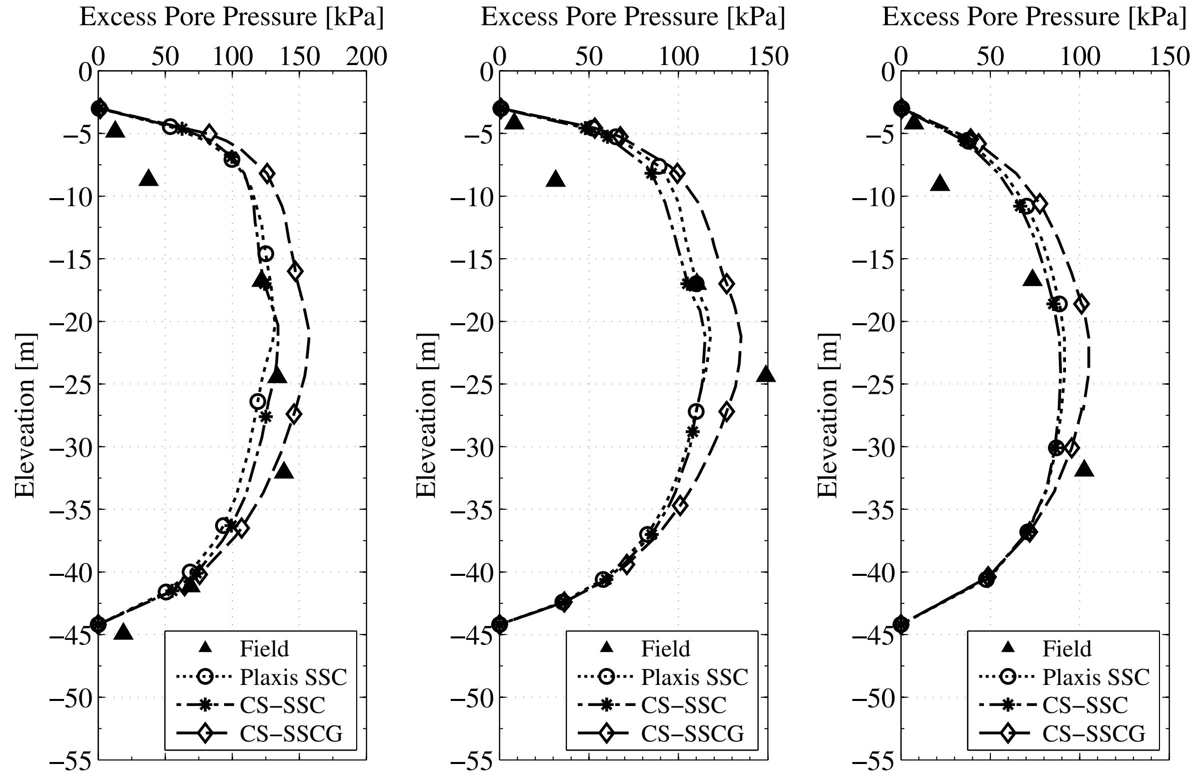

(a) P5P11-CD620 (b) P20P24-CD620 (c) P25P28-CD620

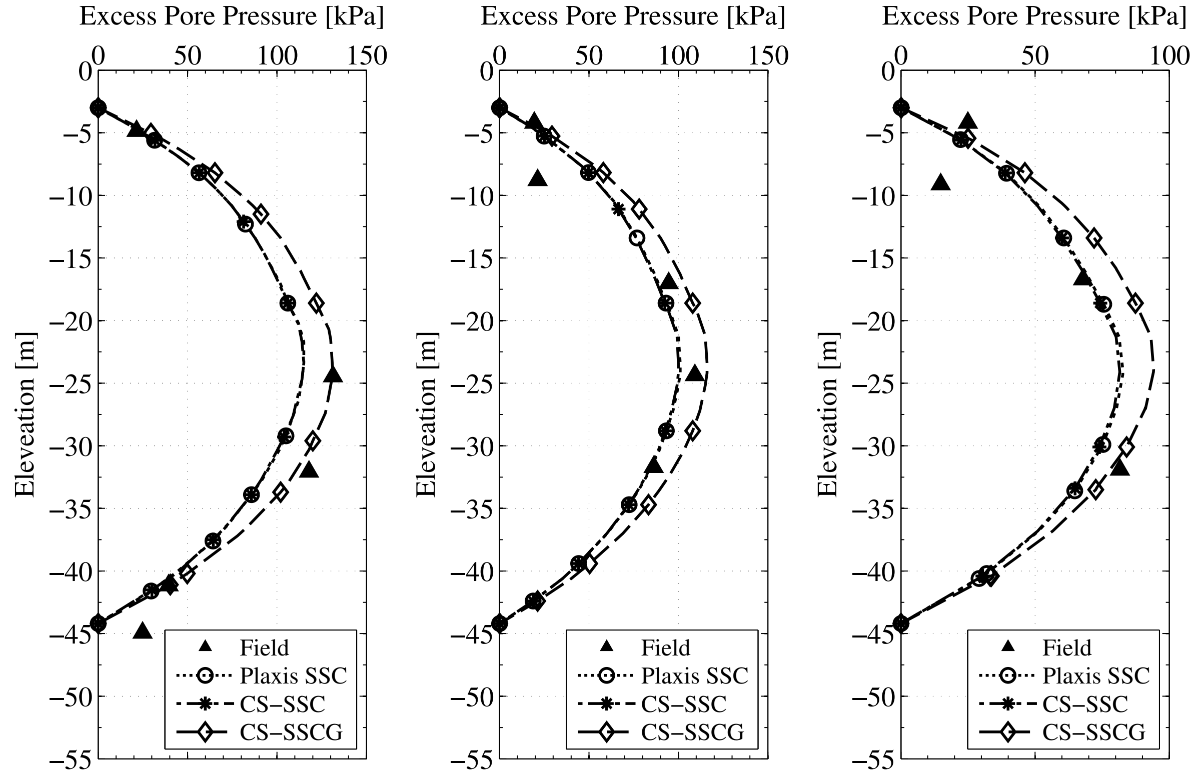

(d) P5P11-CD2053 (e) P20P24-CD2053 (f) P25P28-CD2053

Figure 4.17: Calculated and measured excess pore pressure at day 620 and 2053

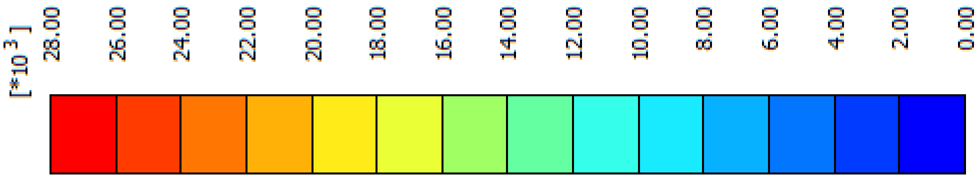

(a) G$_M$ [kPa]

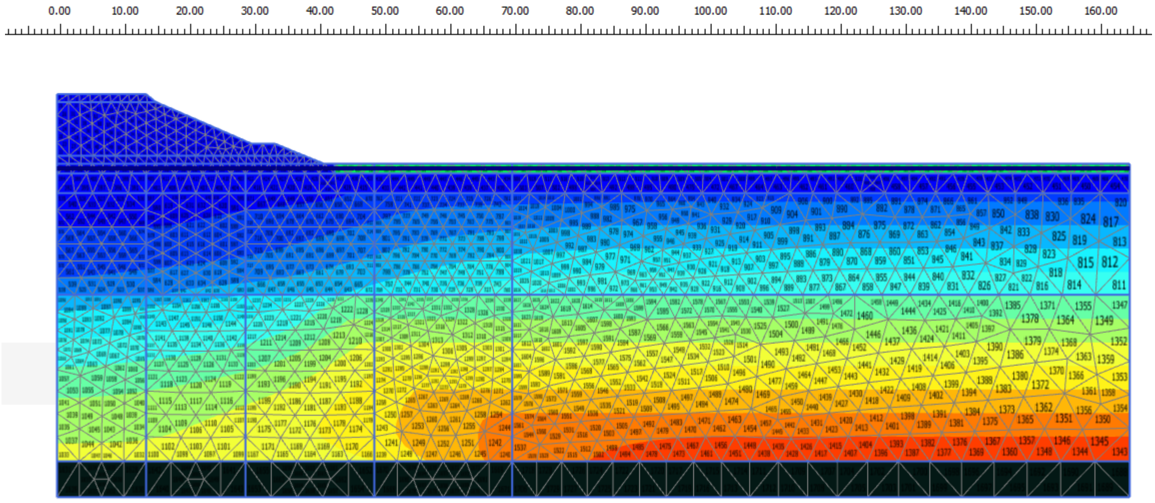

(b) G_M-CD620

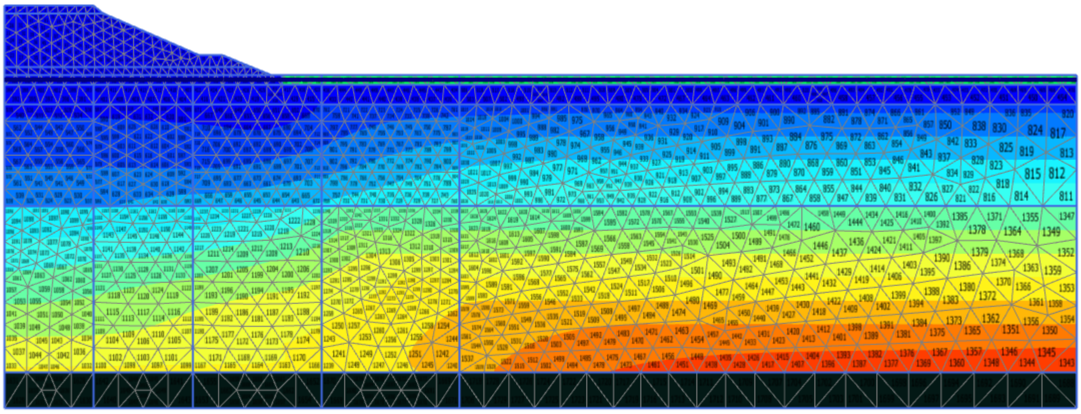

(c) G_M-CD2053

Figure 4.18: Mobilised shear stiffness contours at day 620 and 2053

Chapter 5

Conclusions and Recommendations for Further Work

5.1 Conclusions and discussion

A critical state soft soil creep model (CS-SSC) is implemented and verified against Plaxis SSC. Results from simulation of tests at element level in Chapter 3 shows that the model performance is very similar to the Plaxis SSC model before failure. In Chapter 4 the CS-SSC model was used as basis to develop and implement a new critical state soft soil creep model with mobilised shear stiffness (CS-SSCG). In this model the initial shear stiffness of the soil will be degraded with respect to the mobilisation degree. Results from the simulation of the MIT-MDPW embankment show that the CS-SSCG model were successful to reproduce the horizontal displacements that fits better to the field measurements compared to Plaxis SSC and CS-SSC. At the same it can capture the vertical displacements and the pore pressure response well.

In Plaxis SSC and CS-SSC two elasticity input parameters are Poisson's ratio ν and modified swelling index κ^*. The bulk modulus is mean stress dependent and its value will be given by κ^*. Therefore, with a specific Poisson's ratio the initial shear stiffness G_0 can be implicitly determined. Figure 5.1 shows the ratio of shear stiffness to bulk modulus. As can be seen from the figure for $\nu = 0.1$, the initial shear stiffness $G_0 \approx 1.1K$ and it will not be degraded under the construction of the embankment. However, DSS tests show that the initial shear stiffness of BBC are significantly higher at the deeper levels. For instance at BBC2 mid-layer $G_0 \approx 4.3K$. In other words the initial shear stiffness that is explicitly used in CS-SSCG is approximately four times as high as the one that is implicitly used in Plaxis SSC or CS-SSC. It implies that at the beginning of the creep settlement effective Poisson's ratio is negative $\nu \approx -0.4$. Thermodynamically the Poisson's ratio is valid in the range: $-1 < \nu < 0.5$

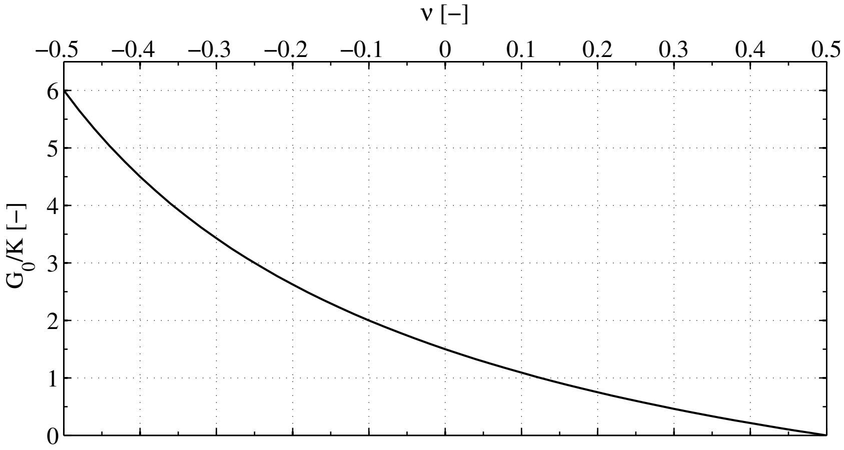

Figure 5.1: The ratio of shear stiffness to bulk modulus with varying Poisson's ratio

The degradation of initial shear stiffness is more important under the embankment and in BBC1 layer where mobilisation is higher. In CS-SSCG the initial shear stiffness will not be degraded for elements far from the embankment where mobilisation degree is negligible. Therefore in contrast to Plaxis CS-SSC and CS-SSC, simulation of horizontal displacement with the CS-SSCGM is not sensitive to the extension of the boundary.

Moreover, the prediction of vertical displacement for deeper layers has been improved. The first part of the curves predicted by Plaxis SSC and CS-SSCG have higher slope than the field measurements. This indicates that the stiffness of the clay is underestimated in the beginning of the creep settlement where elasticity dominates (OC-region). Figure 5.2 shows inclination of stress path in oedometer test in a $p-q$ plot. In NC-region the inclination of the stress path will be determined by K_0^{NC} which is similar for all the models, see Figure 5.2a. In OC-region, however, this inclination is significantly higher in CS-SSCG - for $\nu = 0.1$ this ratio is 2.2 while for $\nu = -0.4$ this ratio is 9.0, see Figure 5.2b. This can be similarly explained by higher initial shear stiffness used in CS-SSCG as discussed in Section 4.4.1.

The pore pressure response predicted by CS-SSCG was slightly higher than the other models which fits better to the field data in the clay mid-layer. However, all the models simulate

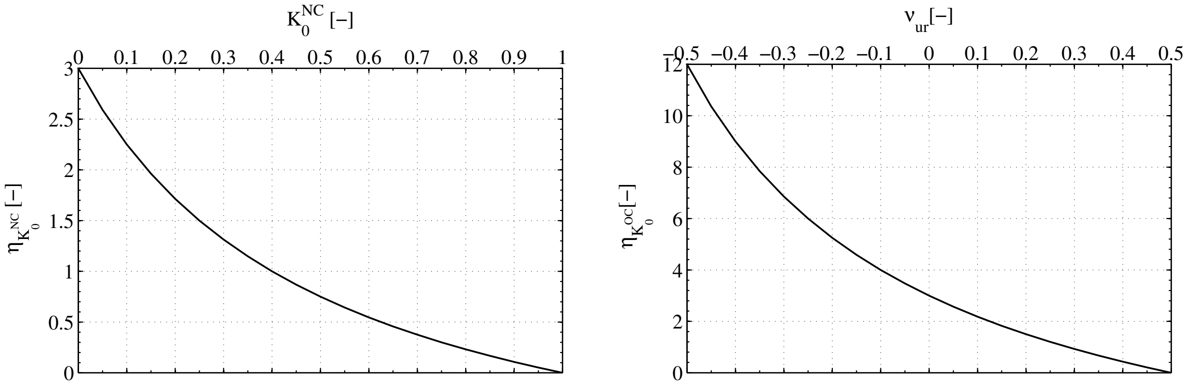

(a) NC-region (b) OC-region

Figure 5.2: Inclination of stress path in oedometer test in p-q plot

less accurate pore pressure response at the drainage boundaries. This could be resolved by a more refined layering at these areas.

The shear stiffness parameters used in CS-SSCG (G_0 and η) can be interpreted from standard geotechnical tests. The initial inclination in deviatoric stress versus strain diagram ($q-\varepsilon$) from an undrained triaxial test is equal to $3G_0$. The initial inclination in a shear stress versus shear strain diagram (τ - γ) from a direct simple shear test indicates G_0. The degradation factor η is a curve fitting parameter that controls the decay of initial shear stiffness.

In geotechnical engineering usually stress dependent moduli K and G are obtained from curve fitting of laboratory tests and not from a corresponding strain energy function. This may cause thermodynamic incompatibility of the model e.g. energy generation in a closed cyclic loop (Nordal, 2010). The models used in this study should not be used in a cyclic or an excavation problem. However, this issue is not relevant for a monotonic static compression loading as studied in this work e.g. settlement under the embankment. A simple solution to make the CS-SSCG model thermodynamically compatible is to set $\zeta = 0$ and use G_{50} instead of G_0. For $\zeta = 0$ nonlinear elasticity (hypoelasticiy) will be deactivated and G will be constant (neither mean stress dependent nor shear stress dependent). It may also result in more robust numerical calculation.

All the models used in this study use elastic volumetric strain $d\varepsilon^e_{vol}$ and elastic shear strain $d\varepsilon^e_q$ that are uncoupled. In triaxial test condition this formulation is given by Equation (5.1). In Plaxis SSC and CS-SSC the bulk modulus and the shear modulus are only mean stress dependent: $K = \Gamma_1(p)$ and $G = \Gamma_2(p)$. In the CS-SSCG model the shear modulus is also dependent on the deviatoric stress: $G = \Gamma_2(q, p)$, but similar to Plaxis SSC and CS-SSC the bulk modulus is only mean stress dependent: $K = \Gamma_1(p)$. In reality, however, shear and volumetric strains are coupled and K and G are both mean stress and deviatoric stress dependent: $K = \Gamma_1(p, q)$ and $G = \Gamma_2(q, p)$. To reflect this more complex formulation (5.2) should be used, where J is the coupling term.

$$\begin{pmatrix} dp \\ dq \end{pmatrix} = \begin{pmatrix} K & 0 \\ 0 & 3G \end{pmatrix} \begin{pmatrix} d\varepsilon^e_{vol} \\ d\varepsilon^e_q \end{pmatrix} \tag{5.1}$$

$$\begin{pmatrix} dp \\ dq \end{pmatrix} = \begin{pmatrix} K & J \\ J & 3G \end{pmatrix} \begin{pmatrix} d\varepsilon^e_{vol} \\ d\varepsilon^e_q \end{pmatrix} \tag{5.2}$$

5.2 Recommendations for further work

The recommendations for further work are as follows:

- Introducing better mobilization formula: In this thesis the focus was on monotonic static compressive loading problems. For unloading problems e.g. excavation or cyclic loading, introducing better mobilization formula that distinguishes between loading and unloading is required. It can be achieved by formulating mobilization f as a vector quantity.

- Adding more plasticity features: (1) rotating the reference surface to account for anisotropy and (2) accounting for unstable structure by associating the reference surface with a destructuration formulation. For more details about the development of a constitutive model with anisotropy and destructuration see e.g. Grimstad (2009).

  Note that in this work soil strength anisotropy is considered by using lode angle dependent M_θ. Therefore, the potential surface in CS-SSCG is dynamic compared to Plaxis SSC. In other words height of the ellipse is dynamically changing based on the lode angle. This feature improved significantly the results from the simulation of the boundary value problem in hand with the same parameters used in Plaxis SSC.

- Adding explicit failure criteria: The models in this study use the following approaches to include failure: Plaxis SSC: M is constant with Mohr Coulomb failure criteria; CS-

SSC: M is constant with no explicit failure criteria; CS-SSCG: M is lode angle dependent with no explicit failure criteria. The implemented models in this study do not include an explicit failure criteria. In these models failure will be reached by critical state. In order to include failure one more residual should be defined. Reaching to failure surface will result in plastic strains. Therefore the total strain is the sum of elastic strain, viscoplastic strain and plastic strain due to failure.

- Adding substeppping scheme: For large strain increments or large time increments the Jacobian matrix may become close to a singular matrix. Thus, the iteration procedure might diverge for some of the elements within the mesh. For the implementation purpose it is advantageous to use substeppping in the constitutive model.
- Testing the CS-SSCG model performance in more boundary value problems.

Bibliography

Aboshi, H. (1973). An experimental investigation on the similitude in the consolidation of a soft clay, including the secondary creep settlement. In *8th International Conference on Soil Mechanics and Foundation Engineering*, volume 4, page 88, Moscow.

Adachi, T., Oka, F., and Tange, Y. (1982). Finite element analysis of two dimensional consolidation using an elasto-viscoplastic constitutive equation. *International Journal for Numerical and Analytical Methods in Geomechanics*, 1:287–296.

Atkinson, H. and Sällfors, G. (1991). Experimental determination of soil properties. In *10th ECSMFE.*, volume 3 of *General Report to Session 1.*, pages 915–956, Florence.

Barden, L. (1969). Time dependent deformation of normally consolidated clays and peats. *Journal of the Soil Mechanics and Foundations Division, ASCE*, 95(1):1–32.

Benz, T. (2007). *Small-Strain Stiffness of Soils and its Numerical consequences.* PhD thesis, Stuttgart University.

Benz, T. (2010). Soil modelling, integration and numerical implementation of elastoplastic soil models. Norwegian University of Science and Technology (NTNU).

Bjerrum, L. (1967). 7th rankine lecture : Engineering geology of norwegian normally-consolidated marine clays as related to settlements of buildings. *Géotechnique*, 17(2):81–118.

Brinch Hansen, J. (1969). A mathematical model for creep phenomena in clay. In *7th International Conference on Soil Mechanics and Foundation Engineering*, volume Speciality session 12, pages 12–18, Mexico City, Mexico.

Buisman, K. (1936). Results of long duration settlement tests. In *1st International Conference on Soil Mechanics and Foundation Engineering*, volume 1, pages 103–107, Cambridge, Massachusetts, USA.

Burland, J. B. (1990). On the compressibility and shear strength of natural clays. *Géotechnique*, 40(3):329–378.

Casagrande, A. (1936). The determination of the preconsolidation load and its practical significance. In *1st International Conference of Soil Mechanics and and Foundation Engineering*, volume 3, page 60, Cambridge, Massachusetts, USA.

Casagrande, A. and Carillo, N. (1944). Shear failure of anisotropic materials. *Boston Society of Civil Engineers*, 31(4):74–87.

Coombs, W., , Crouch, R., and Augarde, C. (2009). Influence of lode angle dependency on the critical state for rotational plasticity. In *International Conference on Computational Plasticity*, Barcelona.

Dafalias, Y. F. (1986). An anisotropic critical state soil plasticity model. *Mechanics Research Communications*, 13(6):341–347.

Degago, S. A. (2011). *On Creep during Primary Consolidation of Clays.* comprehensive summary, Norwegian University of Science and Technology, Trondheim, Norway.

den Haan, E. (2014). Crebs-iv. Delft, The Netherlands.

Fatahi, B., Le, T. M., Le, M. Q., and Khabbaz, H. (2012). Soil creep effects on ground lateral deformation and pore water pressure under embankments. *Geomechanics and Geoengineering*, 8(2):107–124.

Gens, A. and Nova, R. (1993). Conceptual bases for a constitutive model for bonded soils and weak rocks. In Anagstopoulos, editor, *Geotech Eng of hard soils—soft rocks*. Balkema, Rotterdam.

Gibson, R.E. & Lo, K. (1961). A theory of consolidation for soils exhibiting secondary compression. Technical report, Norwegian Geotechnical Instituten (NGI), Oslo, Norway.

Gray, H. (1936). Progress report on research on the consolidation of fine-grained soils. In *1st International Conference on Soil Mechanics and Foundation Engineering*, volume 2, pages 138–141, Cambridge, Massachusetts, USA.

Grimstad, G. (2009). *Development of effective stress based anisotropic models for soft clays.* PhD thesis, Norwegian University of Science and Technology (NTNU).

Grimstad, G. and Degago, S. (2010). A non-associated creep model for structured anisotropic clay (n-sac). In Benz, T. and Nordal, S., editors, *Numerical Methods in Geotechnical Engineering*. Taylor & Francis Group.

Grimstad, G., Haji Ashrafi, M. A., Degago, S. A., Emdal, A., and Nordal, S. (2013). Discussion of 'soil creep effects on ground lateral deformation and pore water pressure under embankments'. *Geomechanics and Geoengineering: An International Journal*.

Haji Ashrafi, M. A. (2013). Modelling of time dependent settlement of mit-mdpw trial embankment. Project work, Norwegian University of Science and Technology (NTNU).

Hansen, B. (1969). A mathematical model for creep phenomena in clay. In *7th International Conference on Soil Mechanics and Foundation Engineering, Speciality Session*, volume 12, Mexico City, Mexico.

Havel, F. (2004). *Creep in soft soils*. PhD thesis, Norwegian University of Science and Technology (NTNU), Trondheim, Norway.

Hinchberger, S. D., Qu, G., and Lo, K. Y. (2010). Constitutive approach for rate-sensitive anisotropic structured clays. *International Journal for Numerical and Analytical Methods in Geomechanics*, 34(17):1797–1830.

Imai, G. and Tang, Y. (1992). A constitutive equation of one-dimensional consolidation derived from inter-connected tests. *SOILS AND FOUNDATIONS*, 32(2):83–96.

Jamiolkowski, M., Ladd, C., Germaine, J., and Lancellotta, R. (1985). New developments in field and laboratory testing of soils. In *11th International Conference on Soil Mechanics and Foundation Engineering*, volume 1, San Francisco.

Janbu, N. (1969). The resistance concept applied to deformations of soils. In *7th International Conference Soil Mechanics Foundation Engineering*, volume 1, page 191–196, Mexico city.

Janbu, N. (1998). Sediment deformation. In *Norwegian University of Science and Technology*, volume Bulletin 35, Trondheim, Norway.

Jostad, H. P. (2006). Crebs i. Oslo, Norway.

Kabbaj, M., Tavenas, F., and Leroueil, S. (1988). In situ and laboratory stress–strain relationships. *Géotechnique*, 38(1):83–100.

Karlsrud, K. (1969). *Evaluation and interpretation of the performance of an embankmenton clay*. PhD thesis, Massachusetts Institute of Technology (MIT).

Kim, Y.T. & Leroueil, S. (2001). Modeling the viscoplastic behaviour of clays during consolidation: application to berthierville clay in both laboratory and field conditions. *Canadian Geotechnical Journal*, 38(3):484–497.

Koppejan, A. W. (1948). A formula combining the terzaghi load compression relationship and the buisman secular time effect. In *Proceedings 2nd International Conference Soil Mechanics and Foundation Engineering*, volume 3, Rotterdam.

Ladd, C., Whittle, A., and Legaspi, D. (1994). Stress-deformation behavior of an embankment on boston blue clay. American Society of Civil Engineers.

Ladd, C. C. (1973). Settlement analysis for cohesive soils. Technical report, Massachusetts Inst. of Technology (MIT), Cambridge, MA, USA.

Ladd, C. C., Foott, R., Ishihara, K., Schlosser, F., and Poulos, H. G. (1977). Stress-deformation and strength characteristics. state-of-the-art report. In *9th International Conference on Soil Mechanics and Foundation Engineering*, volume 2, pages 421–494, Tokyo.

Lade, P. and Duncan, J. (1973). Cubical triaxial tests on cohensionless soil. *ASCE*, 99.

Leoni, M., Karstunen, M., and Vermeer, P. (2009). Anisotropic creep model for soft soils. *Geotechnique*, 58(3):215–266.

Leroueil, Serge & Marques, M. E. S. (1996). Importance of strain rate and temperature effects in geotechnical engineering. *Geotechnical Special Publication, ASCE*, 61(Session on Measuring and Modeling Time Dependent Soil Behavior):1–60.

Leroueil, S. (2006). The isotache approach. where are we 50 years after its development by professor Šuklje?

Leroueil, S. and Kabbaj, M. (1987). Discussion of "settlement analysis of embankments on soft clays" by g. mesri and y. k. choi (april, 1985, vol. 111, no. 4). *Journal of Geotechnical Engineering*, 113(9):1067–1070.

Leroueil, S., Kabbaj, M., Tavenas, F., and Bouchard, R. (1985). Stress–strain–strain rate relation for the compressibility of sensitive natural clays. *Géotechnique*, 35(2):159–180.

leroueil, S., Kabbaj, M., Tavenas, F., and Bouchard, R. (1986). Closure to "stress-strain-strain rate relation for the compressibility of sensitive natural clay. *Géotechnique*, 36(2):288–290.

Leroueil, S. and Vaughan, P. (1990). The general and congruent effects of structure in natural soils and weak rocks. *Géotechnique*, 40(3):467–488.

Lo, K. Y. and Morin, J. P. (1972). Strength anisotropy and time effects of two sensitive clays. *Canadian Geotechnical Journal*, 9(3):261–277.

Mair, R. (1993). Developments in geotechnical engineering research: application to tunnels and deep excavations. In *Proceedings of Institution of Civil Engineers, Civil Engineering*, pages 27–41. Unwin Memorial Lecture 1992.

Mesri, G. & Rokhsar, A. (1974). Theory of consolidation for clays. *Journal of the Geotechnical Engineering Division, ASCE*, 100, GT8:889–904.

Mesri, G. and Choi, Y. K. (1985). Settlement analysis of embankments on soft clays. *Journal of Geotechnical Engineering*, 111(4):441–464.

Mesri, G., Shahien, M., and Feng, T. (1995). Compressibility parameters during primary consolidation. In *International Symposium on Compression and Consolidation of Clayey Soils*, volume 2, Hiroshima.

Mesri, G. & Feng, T. (1986). Discussion of "stress strain-strain rate relation for the compressibility of sensitive natural clays". *Géotechnique*, 36(2):283.

Neher, H. P., Wehnert, M., and Bonnier, P. G. (2001). An evaluation of soft soil models based on trial embankments. In Desai, C. S., editor, *Computer Methods and Advances in Geomechanics*, pages 373–378, Rotterdam. Balkema.

Nordal, S. (2010). *Soil Modelling, Phd course BA.* Department og Civil and Transport Engineering, Norwegian University of Science and Technology (NTNU).

PLAXIS (2012). *PLAXIS 2D.* Plaxis bv, Delft, The Netherlands.

Plaxis (2014). *Plaxis User-Defined Soil Models.* Plaxis.

Plaxis2DManual (2012). Plaxis 2d manual. Plaxis bv.

Roscoe, K. H. and Burland, J. B. (1968). On the generalized stress–strain behaviour of wet clay. In *Engineering Plasticity*, pages 535–609. Cambridge.

Schädlich, B. and Schweiger, H. (2012). Influence of non-local strain regularization on the evolution of shear bands. *Institute for Soil Mechanics and Foundation Engineering, Graz University of Technology, Austria.*

Sivasithanparam, N. (2012). Modelling creep behaviour of soft soils. PLAXIS B.V. and University of Strathcyle.

Sällfors, G. (1975). *Preconsolidation pressure of soft high plastic clays.* PhD thesis, Chalmers University of Technology, Gothenburg, Sweden.

Stolle, D. F. E., Vermeer, P. A., and Bonnier, P. G. (1999a). A consolidation model for a creeping clay. *Canadian Geotechnical Journal*, 36(4):754–759.

Stolle, D. F. E., Vermeer, P. A., and Bonnier, P. G. (1999b). Time integration of a constitutive law for soft clays. *COMMUNICATIONS IN NUMERICAL METHODS IN ENGINEERING*, 15:603–609.

Tavenas, F. and Leroueil, S. (1977). Effects of stresses and time on yielding of clays.

Taylor, D. and Merchant, W. (1940). A theory of clay consolidation accounting for secondary compression. *Journal of Mathematical Physics*, 19:167–185.

Taylor, D. W. (1942). Research on consolidation of clays. Technical report, Massachusetts Institute of Technology (MIT), Cambridge, MA, USA.

Terzaghi, K. (1923). Die berechnung der durchla Èssigkeitsziffer des tones aus dem verlauf der hydrodynamischen spannungserscheinungen. akademie der wisenschaften in wien. mathematisch- naturwissenschaftliche klasse. *Abteilung II a.*, 132:125–138.

Šuklje, L. (1957). The analysis of the consolidation process by the isotaches method. In *4th Int. Conf. Soil Mech. Found. Engng*, pages 200–206, London.

Vermeer, P.A. & Neher, H. (1999). A soft soil model that accounts for creep. *Beyond 2000 in Computational Geotechnics – 10 Years of PLAXIS International © 1999 Balkema, Rotterdam.*

Wesley, L. (2013). Residual soils and the teaching of soil mechanics. In *Proceedings of the 18th International Conference on Soil Mechanics and Geotechnical Engineering*, pages 3479–3482, Paris.

Wheeler, S. J., Näätänen, A., Karstunen, M., and Lojander, M. (2003). An anisotropic elastoplastic model for soft clays. *Canadian Geotechnical Journal*, 40(2):403–418.

Whittle, J. F. (1974). Consolidation behavior of an embankment on boston blue clay. Master's thesis, MIT.

Appendix A

List of Symbols

λ^*	modified compression index
κ^*	modified swelling index
μ^*	modified creep index
C_α $(C_{\alpha e})$	secondary compression index or creep index
C_c	compression index
C_s	recompression index or swelling index
r_s (r)	resistance number or creep number
m_{nc}	clay stiffness number for normally consolidated region
m_{oc}	clay stiffness parameter for over consolidated region
Λ	plastic multiplier
ν	Poisson's ratio
ν_{ur}	Poisson's ratio for unloading-reloading
$\boldsymbol{\varepsilon}$	strain
$\dot{\boldsymbol{\varepsilon}}$	total strain rate or strain rate
ε_1	major principal strain
ε_a	axial strain

ε_r	radial strain
ε_{vol}^{vp}	volumetric viscoplastic strain
$\dot{\varepsilon}_{vol}^{vp}$	volumetric viscoplastic strain rate
ε_q^{vp}	deviatoric viscoplastic strain
$\dot{\varepsilon}_q^{vp}$	deviatoric viscoplastic strain rate
ε_{vol}^{e}	volumetric elastic strain
ε_q^{e}	deviatoric elastic strain
$\boldsymbol{\sigma}_d$	deviatoric stress vector
σ_{vc} (P_c)	vertical preconsolidation stress
σ_a	axial stress
σ_r	radial stress
p	mean stress or isotropic stress
q	deviatoric stress invariant
p^{eq}	equivalent mean stress or equivalent isotropic stress
p_p^{eq}	equivalent mean preconsolidation stress or equivalent isotropic preconsolidation stress
OCR	vertical overconsolidation ratio
POP	preoverburden pressure
τ	reference time
OCR_τ	overconsolidation ratio at the reference time
OCR_τ^{eq}	equivalent overconsolidation ratio corresponding to reference time
p_{p0}^{eq}	equivalent mean initial preconsolidation stress or equivalent isotropic initial preconsolidation stress
$p_{p_0^{NC}}$	initial isotropic preconsolidation stress at normally consolidation region
$q_{p_0^{NC}}$	initial deviatoric preconsolidation stress at normally consolidation region

y_{ref}	reference depth
G_{ref}	shear stiffness at reference depth
G_{inc}	shear stiffness increment per unit of depth
G_0	initial shear stiffness
G_M	mobilised shear stiffness
ζ	initial shear stiffness degradation factor
$\boldsymbol{J}$	Jacobian matrix
J_3	third deviatoric stress invariant
$\boldsymbol{D}$	elastic stiffness matrix
$\boldsymbol{D}_G$	elastic stiffness matrix with mobilised shear stiffness
E	Young's modulus
K	Bulk modulus
G	shear modulus
f	degree of mobilisation
e	void ratio
v	specific volume
K_0	lateral earth pressure at rest
K_0^{NC}	horizontal to vertical stress ratio at NC-region
K_0^{OC}	horizontal to vertical stress ratio at OC-region
k_0	initial hydraulic conductivity (permeability)
k_x	horizontal hydraulic conductivity
k_y	vertical hydraulic conductivity
M or M_{cs}	stress ratio at critical state
M_C	stress ratio at critical state in triaxial compression test

M_E	stress ratio at critical state in triaxial extension test
M_θ	lode angle dependent M
c	cohesion
ϕ	friction angle
ψ	dilatancy angle
γ	soil unit weight
θ	Lode angle
τ	reference time
t	time
t_r or t_c	intrinsic time
η	stress ratio (q/p)
η_{K_0}	stress ratio corresponding to K_0-condition
$\eta_{K_0^{NC}}$	stress ratio corresponding to normally consolidated region
$\eta_{K_0^{OC}}$	stress ratio corresponding to overconsolidated region
E_{oed}	oedometer stiffness modulus
E_{oed}^{ref}	reference oedometer stiffness modulus
E_{50}^{ref}	reference drained triaxial compression stiffness modulus
E_{ur}^{ref}	reference drained triaxial unloading-reloading stiffness modulus

List of Acronyms

SSC	Soft Soil Creep
CS	Critical State
CSL	Critical State Line
CS-SSC	Critical State Soft Soil Creep

CS-SSCG	Critical State Soft Soil Creep with Shear stiffness
MCCM	Modified Cam-Clay Model
MC	Mohr Coulomb
UDSM	User Defined Soil Model
IL	Incremental Loading
CRS	Constant Rate of Strain
$\mathrm{UTK_0TC}$	Untrained K_0-consolidated Triaxial Compression
$\mathrm{UTK_0TE}$	Untrained K_0-consolidated Triaxial Extension
DLL	Dynamic Link Library
EOP	End of Primary
DSS	Direct Simple Shear
NC	Normally Consolidated
OC	Over Consolidated
BBC	Boston Blue Clay
CD	Construction Day
ESP	Effective Stress Path
FEM	Finite Element Method
DOF	Degree of Freedom
GWL	Ground Water Level

Appendix B

CS-SSCG Fortran Pseudo Code

```
!23456789!23456789!23456789!23456789!23456789!23456789!23456789!23456789
      Subroutine User_Mod ( IDTask, iMod, IsUndr,
     *                      iStep, iTer, iEl, Int,
     *                      X, Y, Z,
     *                      Time0, dTime,
     *                      Props, Sig0, Swp0, StVar0,
     *                      dEps, D, BulkW,
     *                      Sig, Swp, StVar, ipl,
     *                      nStat, NonSym, iStrsDep, iTimeDep,iTang,
     *                      iPrjDir, iPrjLen, iAbort )
!!!!!!!!!!!!!!!!!!!!!!!!!!!!!!!!!!!!!!!!!!!!!!!!!!!!!!!!!!!!!!!
!      Title: CS-SSCG PLAXIS UDSM
!      Author: Mohammad Ali Haji Ashrafi <mohammha@stud.ntnu.no>
!!!!!!!!!!!!!!!!!!!!!!!!!!!!!!!!!!!!!!!!!!!!!!!!!!!!!!!!!!!!!!!
!  Depending on IDTask, 1 : Initialize state variables
!                       2 : Calculate stresses
!                       3 : Calculate elastic stiffness matrix
!                       4 : Return number of state variables
!                       5 : Inquire matrix properties
!                       6 : Calculate elastic stiffness matrix
!                           Return switch for non-symmetric D-matrix
!                             stress/time dependent matrix
! Arguments:
!           I/O  Type
!  IDTask    I    I     : see above
!  iMod      I    I     : Model number (1..10)
!  IsUndr    I    I     : =1 for undrained, 0 otherwise
!  iStep     I    I     : Global step number
!  iter      I    I     : Global iteration number
!  iel       I    I     : Global element number
!  Int       I    I     : Global integration point number
!  X         I    R     : X-Position of integration point
!  Y         I    R     : Y-Position of integration point
!  Z         I    R     : Z-Position of integration point
!  Time0     I    R     : Time at start of step
!  dTime     I    R     : Time increment
!  Props     I    R()   : List with model parameters
!  Sig0      I    R()   : Stresses at start of step
!  Swp0      I    R     : Excess pore pressure start of step
!  StVar0    I    R()   : State variable at start of step
!  dEps      I    R()   : Strain increment
!  D        I/O   R(,)  : Material stiffness matrix
!  BulkW    I/O   R     : Bulkmodulus for water (undrained only)
!  Sig       O    R()   : Resulting stresses
!  Swp       O    R     : Resulting excess pore pressure
!  StVar     O    R()   : Resulting values state variables
!  ipl       O    I     : Plasticity indicator
!  nStat     O    I     : Number of state variables
!  NonSym    O    I     : Non-Symmetric D-matrix ?
!  iStrsDep O    I     : =1 for stress dependent D-matrix
!  iTimeDep O    I     : =1 for time dependent D-matrix
!  iAbort    O    I     : =1 to force stopping of calculation
!
```

```
      Implicit Double Precision (A-H, O-Z)
!
      Dimension Props(*), Sig0(*), StVar0(*), dEps(*), D(6,6),
     *          Sig(*),   StVar(*), iPrjDir(*)
      Character*255 PrjDir, Dbg_Name

      Select Case (iMod)
        Case (1)   !CS-SSCG
          Call CS-SSCG( IDTask, iMod, IsUndr, iStep, iTer, iEl, Int,
     *             X, Y, Z, Time0, dTime,
     *             Props, Sig0, Swp0, StVar0,
     *             dEps, D, BulkW, Sig, Swp, StVar, ipl,
     *             nStat, NonSym, iStrsDep, iTimeDep, iTang,
     *             iAbort )

               Return
      End Select ! iMod
      Return
      End ! User_Mod

      Subroutine CS-SSCG(IDTask, iMod, IsUndr,
     *                iStep, iTer, iEl, Int,
     *                X, Y, Z,
     *                Time0, dTime,
     *                Props, Sig0, Swp0, StVar0,
     *                dEps, D, BulkW,
     *                Sig, Swp, StVar, ipl,
     *                nStat,
     *                NonSym, iStrsDep, iTimeDep, iTang,
     *                iAbort )

      Implicit Double Precision (A-H, O-Z)
      Dimension Props(*), Sig0(*), StVar0(*), dEps(*), D(6,6),
     *          Sig(*), StVar(*)
      Dimension dV(8), Res(8), A0(8,8), B(8,8)    ! Local Variables
      nStatV = 15

      if (IDTask .Eq. 1) Then
          CALL SetProps() ! Set Input Parametres
          CALL ppeq0()

          if (StVar0(10) .NE. 12347d-1 ) then ! Initialize State Variables
              StVar0(1:6) = - Sig0(1:6)
              StVar0(7) = - ppeq0
              StVar0(8) = 0d0
              StVar0(9) = xGref + Max ((xYref-Y)* xGinc , 0d0 )
              StVar0(10) = 12347d-1
          End if
      End if  ! IDTask = 1

      If (IDTask .Eq. 2) Then ! Calculate stresses
          CALL SetProps()  ! Assign material parameters

          If (IsUndr.Eq.1) Then   ! Undrained Calculation
          dEpsV = dEps(1) + dEps(2) + dEps(3)
          dSwp  = BulkW * dEpsV
          Swp   = Swp0 + dSwp
          Else
          Swp = Swp0
          End If
      ! Implicit Iteration scheme
          Call MZeroR(A0,64)
          Call MZeroR(Res,8)
          Call MZeroR(dV,8)
          DotRes = 100d0
          ii = 1
          DO
          CALL ReMap()     ! Return Mapping
          CALL Debug()     ! Debug Printing
          if (DotRes .LT. TOL**2  )  EXIT ! Check Tolerance
              ii = ii + 1
          if (ii .GT. maxiter)  EXIT   ! Limit Number of iterations
          ENDDO
         Sig(1:6) = - StVar(1:6) ! Update Stresses
      End If ! IDTask = 2

      If ( IDTask .Eq. 3 .Or.
     *     IDTask .Eq. 6     ) Then    ! Calculate D-Matrix
          CALL SetProps()
          Call MZeroR(D,36)
          CALL Lode()       ! Calculate Lode Angle
          xM = xMtheta      ! Update M
          CALL Dmatrix()    ! Calculate Elastic Matrix
      End If  ! IDTask = 3, 6

      If (IDTask .Eq. 4) Then ! Number of State Variables
          nStat = nStatV
      End If  ! IDTask = 4

      If (IDTask .Eq. 5) Then ! Matrix Type
          NonSym    = 0  ! 1 for non-symmetric D-matrix
          iStrsDep  = 1  ! 1 for stress dependent D-matrix
          iTang     = 0  ! 1 for tangent D-matrix
          iTimeDep  = 0  ! 1 for time dependent D-matrix
      End If  ! IDTask = 5

```

```
        Return
        End ! CS–SSCG
```

Appendix C

Paper Abstract to be Submitted

A Critical State Soft Soil Creep Model with Shear Stiffness

The existing creep constitutive models do not include directly shear stiffness of the soil that can be easily obtained by standard geotechnical tests. These models do not account for high shear stiffness of the soil at small mobilisation degree. In this respect, they do not distinguish between soil elements that undergo lower mobilisation in the far field and the ones that undergo higher mobilisation close to the embankment. This may result in overprediction of horizontal displacements under the field and the result of the finite element analysis is sensitive to the extension of the model boundary. To address this model deficiency, a new critical state soft soil creep model with shear stiffness (CS-SSCG) is implemented. In the CS-SSCG model, shear stiffness of the soil will be explicitly given by the engineer instead of commonly used Poisson’s ratio.

Keywords: constitutive soil model, creep, shear stiffness

Appendix D

Curriculum Vitae

First Name:	**Mohammad Ali**
Last Name:	**Haji Ashrafi**
Date of birth:	14. July 1986
Email (1):	mohammha@stud.ntnu.no
Email (2):	moashrafi@engineer.com
Telephone:	+47 45177927

Language Skills

- Persian (Farsi): Native Language
- English: IELTS overall band score 7.0
- Norwegian: NTNU Norwegian for Foreigners Level 2 with Grade B

Education

- **MSc student in Geotechnics & Geohazards**: Norwegian University of Science and Technology (NTNU), Trondheim, Aug 2012 - present
- **BSc in Civil Engineering**: Iran University of Science and Technology (IUST), Tehran, Iran, Sep 2004 - May 2009

Computer Skills

- PLAXIS 2D 2012/AE: Good knowledge
- FORTRAN: Good knowledge
- MATLAB: Good knowledge
- Phase 2: Fair knowledge
- LaTeX: Good knowledge

Job Experience

- Research assistant in Geotechnics, NTNU, Sep 2013 - present

Hobbies and Other Activities

- Reading, Participating in group works, Watching TV-series
- Sports: Jogging